NASA Contractor Report 4506

Coupled 2-Dimensional Cascade Theory for Noise and Unsteady Aerodynamics of Blade Row Interaction in Turbofans

Volume 1–Theory Development and Parametric Studies

Donald B. Hanson
United Technologies Corporation
Pratt and Whitney Division
East Hartford, Connecticut

Prepared for the
Lewis Research Center
Under Contract NAS3–25952
January 1994

National Aeronautics and
Space Administration

Office of Management

**Scientific and Technical
Information Program**

1994

FOREWORD

This report reveals a feature of the noise generation process in turbofans described herein as "mode trapping". As with most physical phenomena, its understanding developed on more than one front and several people contributed to the evolution of the idea. Test data characteristic of mode trapping and elements of its physical explanation were first identified in a paper by Topol, Holhubner, and Mathews entitled "A Reflection Mechanism for Aft Fan Tone Noise" (AIAA Paper No. 87-2699, October 1987). At that time, the author of this report (Hanson) was employed at the Hamilton Standard division of United Technologies and working on noise associated with unsteady coupling between rotors of a counter rotation prop-fan. While consulting to Hamilton Standard, also in 1987, Professor Mårten Landahl of MIT recognized the possibility of trapping a wave between 2 rotors and proposed a method for computing the effect via an impedance model. In conjunction with Landahl's work, Professor Kenneth Hall, then at UTRC and now at Duke University, originated the idea of using the S. N. Smith's unsteady cascade code to represent the coupling and developed a model for the interaction of 2 unloaded rotors at a single harmonic.

In 1990, at the request of the Pratt and Whitney division of United Technologies, Hanson continued work on the reflection mechanism to put it on a firmer analytical basis for ducted fans. His work was funded by NASA-Lewis in 1991 as part of Contract NAS3-25952, during the course of which the author transferred to Pratt and Whitney. NASA project management was provided originally by Dr. Christopher Miller and finally by Mr. Dennis Huff. The author owes thanks to all of the individuals named above for their support and technical assistance. Thanks are also due to Professor Edward Kerschen of the University of Arizona who provided valuable encouragement on use of the actuator disk model employed herein and on the matrix method finally used to solve the coupled equations.

TABLE OF CONTENTS

SUMMARY

Typical analytical models for interaction between rotor and stator in a turbofan analyze the effect of wakes from the rotor impinging on the stator, producing unsteady loading, and thereby generating noise. Reflection/transmission characteristics of the rotor are sometimes added in a separate calculation. In those models, there is a one-to-one relationship between wake harmonics and noise harmonics; that is, the BPF (blade passing frequency) wake harmonic causes only the BPF noise harmonic, etc. This report presents a more complete model in which flow tangency boundary conditions are satisfied on 2 cascades in relative motion for several harmonics simultaneously. By an extension of S. N. Smith's code for 2D flat plate cascades, the noise generation/frequency scattering/blade row reflection problem is solved in a single matrix inversion. It is found that the BPF harmonic excitation of the stator scatters considerable energy into the higher BPF harmonics due to relative motion between the blade rows. Furthermore, when swirl between the rotor and stator is modeled, a "mode trapping" effect occurs which explains observations on fans operating at rotational speeds below BPF cuton: the BPF mode amplifies between blade rows by multiple reflections but cannot escape to the inlet and exit ducts. However, energy scattered into higher harmonics does propagate and dominates the spectrum at 2 and 3 times BPF.

This report presents the complete derivation of the theory, comparison with a previous (more limited) coupled rotor/stator interaction theory due to Kaji and Okazaki, exploration of the mode trapping phenomenon, and parametric studies showing the effects of vane/blade ratio and rotor/stator interaction. For generality, the analysis applies to stages where the rotor is either upstream or downstream of the stator and to counter rotation stages. The theory has been coded in a FORTRAN program called CUP2D, documented in Volume II of this report.

It is concluded that the new features of this analysis - unsteady coupling, frequency scattering, and flow turning between rotor and stator - have a profound effect on noise generation caused by rotor/stator interaction. Treating rotors and stators as isolated cascades is not adequate for noise analysis and prediction.

SECTION 1
INTRODUCTION

Rotor/stator interaction is undoubtedly the oldest and most frequently treated subject in turbofan noise research. Countless reports and journal articles have appeared over the past three decades analyzing the complex aerodynamic interference and acoustic reflection effects that contribute to noise at blade passing frequency and its harmonics. Geometry of interest shown in figure 1 is representative of modern engines where the rotor is upstream of the stator. The first major insight into the acoustics of this kind of fan was provided by Tyler and Sofrin (ref.1) and then Sofrin and McCann (ref. 2) who revealed the link from number of blades, number of vanes, and tip speed to the duct modes and their propagation/decay behavior. Methods to compute the strength of these modes via unsteady aerodynamic calculations at first used crude representations of unsteady loading response at the stators. Then Ventres, Theobald, and Mark (ref. 3) at Bolt Beranek and Newman developed a computer code (herein called the BBN code) that linked a 2D flat plate cascade theory for the unsteady aerodynamics to the 3D annular duct acoustic modes via a strip analysis. Their theory included axial flow and non-compact treatment of a stator that could be leaned, tapered, or swept. The unsteady aerodynamic model in the BBN code can be explained with reference to figure 2. Rotor blades trail viscous wakes producing an upwash distribution on the stator. The stator responds with the lift response calculated to produce an equal and opposite upwash so as to satisfy the flow tangency boundary conditions on the vanes. The computed loading then acts as a dipole distribution in the ensuing coupling to the duct modes. In figure 2, the rotor blades are shown with dashes to emphasize that their role is only to generate the wakes; any reflection effect that they might have on the acoustics or unsteady aerodynamics is ignored in the BBN code.

Nevertheless, the BBN model includes much of the important physics of the problem and has been exercised extensively by Topol (ref. 4) in comparison with test data. However, in another study, Topol, Holhubner, and Mathews (ref. 5) found that the method failed to predict observed phenomena, even qualitatively at some RPM's, for a fan designed for BPF cutoff. These authors noted that BPF modes could cut on in the swirl flow region between the rotor and stator at speeds considerably lower than in the inlet and exit flow. In this intermediate speed range (between BPF cut-on in the swirl region and cuton in the aft duct flow), 2xBPF and 3xBPF harmonics (which are cut on) in the aft region were found to increase to levels far above those predicted by the BBN code. Aft-radiated sound power behavior for the first 3 BPF harmonics is shown in figure 3 for a typical, current day, high bypass ratio fan engine with 38 blades and 72 vanes. The revealing behavior to note in figure 3 is the rapid onset of 2xBPF and 3xBPF at the RPM where BPF cuts on in the swirl region. Reference 5 concluded that the increase in higher harmonics in the aft region was due to the following sequence of events. The rotor wake excites the stator predominately at BPF; this sends a BPF wave to the rotor that scatters it into higher harmonics; these harmonics are cut on and propagate through the stator to the far field. This hypothesis was supported by analytical modeling that included various simple models for the source strength and for reflection and transmission coefficients at the rotor and stator.

The BBN code cannot be used to check this reflection/scattering hypothesis because it includes neither the frequency scattering mechanism nor reflections from the rotor. In the present paper, the model depicted in figure 2 is refined to include the rotor in the aerodynamic calculations via a fully coupled unsteady analysis satisfying the flow tangency boundary condition on both blade rows simultaneously for several harmonics. Thus, noise generation, frequency

scattering, and reflections from both rotor and stator are solved simultaneously via a single matrix inversion. Furthermore, swirl between the rotor and stator is modeled via a simplistic system that turns the flow at the rotor leading edge and straightens it at the stator trailing edge. (This is a first approximation to including blade mean loading in the analysis by concentrating it at actuator disks.) Modal jump conditions across these disks are derived to satisfy continuity of mass and momentum. It should be pointed out that Kaji and Okazaki developed a coupled rotor/stator method (ref. 6) in 1970; however, this model was confined to one frequency and did not include the swirl effect. Correlation with their work is shown later in this paper.

This work is an extension of the Smith code (ref. 7), which is an industry-standard 2D, compressible, linearized, unsteady flat plate cascade method. The coupled cascade theory has been coded in FORTRAN 77 as CUP2D and developed on UNIX™ workstations. The theory applies to counter-rotation stages and to rotor/stator stages with the rotor either upstream or downstream of the stator. Applications herein are primarily to rotor/EGV combinations, but comparisons are given with the Kaji and Okazaki results for IGV/rotor interaction.

SECTION 2
REVIEW OF SMITH'S CASCADE METHOD

Since this paper is an extension of Smith's theory (ref. 7), we start with an overview of his method. Further description can be found in a survey paper by Whitehead (ref. 8) and, of course, in the original Smith paper. Figure 4 shows the basic geometry to be a single cascade of flat plates aligned with the mean flow direction. The objective is to find the unsteady loading distribution on the cascade (and the resulting output waves) for a specified velocity disturbance input to the system. Smith's approach is to derive an integral equation for the upwash on the cascade caused by the unknown load distribution, discretize the equation, and solve for the loads by matrix inversion.

Smith's analysis starts with the linearized differential equations for continuity and momentum. He finds solutions for velocity and pressure disturbances in the form

$$\begin{bmatrix} u \\ v \\ p \end{bmatrix} = \begin{bmatrix} \overline{u} \\ \overline{v} \\ \overline{p} \end{bmatrix} e^{i(\alpha x + \beta y + \omega t)} \tag{1}$$

where the space, time behavior is given by the exponential and the overbarred quantities are complex amplitude coefficients. The kernel of the integral equation is expressed as a Fourier series in the y coordinate with terms counted by an index k (r in Smith's notation), which corresponds to the circumferential spinning mode index in the Tyler-Sofrin theory. Transverse wavenumber β can take on all values given by

$$\beta = \frac{\sigma - 2\pi k}{s}, \qquad -\infty < k < +\infty \tag{2}$$

where σ is the interblade phase angle which will be discussed later. σ and frequency ω are inputs to the problem.

Substitution of equation 1 into the original continuity and momentum equations leads to a characteristic equation with two families of solutions, each having a different form for the axial wavenumbers. In one family are the vorticity waves which are carried at the mean flow speed in the downstream direction only. Components of these waves are denoted by the subscript 3 as in u_3, v_3, and p_3. Axial wavenumbers for the vorticity waves are

$$\alpha_3 = -\frac{(\omega + V\beta)}{U} \tag{3}$$

The second family are the pressure waves, which propagate at the speed of sound. Upstream- and downstream-going pressure waves are denoted by the subscripts 1 and 2, respectively and their axial wavenumbers are given by

$$\alpha_{1,2} = \frac{U(\omega + V\beta) \pm a\sqrt{(\omega + V\beta)^2 - (a^2 - U^2)\beta^2}}{a^2 - U^2} \tag{4}$$

where a is the speed of sound and the square root contains the cutoff information critical in fan acoustics. When the argument of the square root is positive, the axial wavenumber is real and

the wave propagates at constant amplitude in the duct; in this case, the ± choice is made to give a shorter wavelength upstream and a longer wavelength downstream. When the argument of the square root is negative, the wave decays exponentially; the ± choice is made to guarantee vanishing disturbance for $x \to \infty$. The cuton criterion can be simply stated: a wave with transverse wavenumber β will propagate if the frequency is "large enough", that is if $(\omega+V\beta)^2 > (a^2-U^2)\beta^2$. The higher the mode order, the higher the frequency required for propagation.

Blade loading is in terms of the vorticity distribution $\Gamma(z_o)$ over the source coordinate z_o (along the chord). With this notation, Smith wrote the following for the transverse velocity in the pressure wave anywhere upstream of the cascade

$$v_1 = \int_o^c \frac{\Gamma(z_o)}{s} \sum_{k=-\infty}^{\infty} v_1' \, e^{i(\alpha_1 x + \beta y + \omega t)} \, e^{-i(\alpha_1 \cos\theta + \beta \sin\theta) z_o} \, dz_o \tag{5}$$

where c is the airfoil chord. v_1' is a function of ω, β, θ, and W given by Smith and defined in Appendix C. Expressions for the downstream velocity components are obtained by replacing the 1 subscripts with 2's and 3's. Axial velocity and pressure are linked to the v''s as follows

$$u_{1,2}' = \alpha_{1,2} \frac{v_{1,2}'}{\beta} \tag{6}$$

and

$$p_{1,2}' = -(\omega + U\alpha_{1,2} + V\beta)\rho_o \frac{v_{1,2}'}{\beta} \tag{7}$$

for pressure waves and

$$u_3' = -\beta \frac{v_3'}{\alpha_3} \tag{8}$$

for the vorticity waves (which do not produce a pressure disturbance).

Finally, to discretize equation 5, the load distribution is divided into N_p panels and the integral is converted to a sum according to

$$\frac{1}{c} \int_0^c \frac{\Gamma(z_o)}{W} \, dz_o \to \sum_{j=1}^{N_p} L(j) \tag{9}$$

The result is

$$v_1 = \frac{W}{s/c} \sum_{j=1}^{N_p} \sum_{k=-\infty}^{\infty} v_1' \, e^{i(\alpha_1 x + \beta y + \omega t)} \, e^{-i(\alpha_1 \cos\theta + \beta \sin\theta) z_{oj}} \times L(j) \tag{10}$$

where z_{oj} is the normalized chordwise coordinate.

The next section shows in general terms how this type of expression can be adapted to the blade row interaction problem.

SECTION 3
DEVELOPMENT OF THEORY FOR LOADING AND ACOUSTICS OF COUPLED CASCADES

The previous section described the mechanics of finding waves generated by the unsteady loading distribution on an isolated, infinite (in the y direction) 2-dimensional cascade. Geometry to be analyzed for the coupled cascade problem is sketched in figure 5. The analysis is kept general so that either blade row can rotate in either direction; thus, counter-rotation cases and IGV/rotor combinations are included. In spite of this generality, the upstream blade row will be called the rotor and the downstream blade row will be called the "stator" to simplify the terminology in the lengthy derivation that follows. The typical case of interest herein is for an upstream rotor and a downstream stator. In this case, the downstream blade row would be fixed and θ_1 would have a negative value. If the downstream blade row is moving, its tangential speed is input as a negative number.

3.1 DUCT COORDINATES AND MULTIPLE HARMONICS

The 2-dimensional geometry of figure 5 will be adapted to annular geometry (annulus radius R) for the case of a "stator" with B_2 rotating at angular speed Ω_2 and a rotor with B_1 blades rotating at angular speed Ω_1. The stator is fixed in the x,y_2 coordinates with inflow angle θ_2 defined by its rotational speed $\Omega_2 R$ and the swirl velocity V_s, as shown by the velocity triangle. The rotor is fixed in its x,y_1 system which is moving up at speed $\Omega_1 R$. The relative air speed in the tangential direction is $\Omega_1 R - V_s$ which defines the inflow angle θ_1.
In this section we adapt Smith's formulas to the notation of duct acoustics and account for a general periodic waveform rather than a single harmonic. This is done by examination of the term in equation 10 that we call the kinematic phase

$$\psi = \beta y + \omega t \tag{11}$$

which is discussed in some detail in appendix A. Frequencies of stator excitation, of course, are the blade passing harmonics, $\omega = nB_1\Omega$, where we have defined the relative angular velocity $\Omega=\Omega_1-\Omega_2$. We normalize the transverse coordinate y_2 by the radius of the annulus R, effectively converting to cylindrical coordinates with $y_2 = R\phi_2$ for the stator. Appendix A shows that the normalized transverse wavenumber can then be written as

$$\beta R = \beta_{nk} = -(nB_1 - kB_2) \tag{12}$$

so that for the stator

$$\psi \rightarrow \psi_{nk} = \beta_{nk}\phi_2 + nB_1\Omega t \tag{13}$$

This is the exponential already familiar from the Tyler-Sofrin spinning mode theory (ref. 1). Equations 12 and 13 represent a mode with nB_1-kB_2 lobes spinning at angular speed $nB_1\Omega/(nB_1-kB_2)$, as viewed in the stator frame of reference.

Given this notation, equation 10 can be generalized immediately for stator waves with multiple harmonics:

$$\frac{v_1}{a} = \frac{M_{r2}}{SC_2} \sum_{n=1}^{\infty} \sum_{j=1}^{N_p} \sum_{k=-\infty}^{\infty} v_1' \, e^{i[\alpha_{1nk}(\bar{x}-\bar{x}_s)+\psi_{nk}]} \, e^{-i(\alpha_{1nk}\cos\theta_2 + \beta_{nk}\sin\theta_2)\bar{c}_2 z_{oj}} \times L(n,j) \qquad (14)$$

Overbars denote normalization by R, the dimensionless axial wavenumber is $\alpha_1 R = \alpha_{1nk}$, M_{r2} is the relative Mach number W_2/a, and SC_2 is the spacing to chord ratio for the stator. Working forms for the ψ's are given in appendix A, for the α's in Appendix B, and for the v''s in appendix C.

As a preview of the frequency scattering phenomenon, note that ψ_{nk} for the *stator* waves can be viewed in *rotor* frame of reference via the transformation $\phi_2 = \phi_1 + \Omega t$. The result is

$$\psi_{nk} = \beta_{nk}\phi_1 + kB_2\Omega t \qquad (15)$$

This shows that the waves caused by any one stator loading harmonic n appear at all multiples of *vane passing frequency* in the rotor coordinate system.

3.2 ACCOUNTING FOR FLOW TURNING AT THE ROTOR AND STATOR

The model discussed so far includes swirl in the flow entering the stator but no turning of the flow by the rotor and stator loading. Since swirl was fundamental to the mechanism proposed by Topol *et al* (ref. 5), a method was developed to represent turning of the flow that could be combined easily with elements of the Smith code. The scheme is to use actuator disks to turn the mean flow at the rotor leading edge and at the stator trailing edge as sketched at the top of figure 6. Since the mean flow properties (tangential and axial velocity, density, speed of sound) jump across the inlet and exit interfaces, the unsteady quantities jump also. This is handled by deriving reflection and transmission coefficients for each type of wave to maintain continuity of mass and momentum (linearized) on a mode-by-mode basis. Derivation of these coefficients is given in appendix D.

Since the actuator disk representation of the mean loading effect seems to be new in this context, a few more words are in order. We consider the blade loading to be the sum of a steady part and an unsteady part. The unsteady loading is distributed over the blade chords via panels as in the original Smith method and is considered small enough to be treated as a perturbation of the mean flow. The steady loading is concentrated at the rotor leading edge and at the stator trailing edge and may be large enough to have a significant influence on the mean flow. In fact, this is its main role in the analysis; it provides the background flow that is perturbed by the unsteady loading and controls the propagation properties for the various types of waves. Thus, we can think of building up the loading as follows. First, turn on the mean loading. The mean flow enters the stage axially, turns at the rotor leading edge, and straightens out again at the stator trailing edge. The mean flow is thus divided into three regions by the two actuator disks. Mean flow properties in the three regions are considered known from a separate analysis. Next, the unsteady loading is activated; the waves behave according to Smith's theory in each region with jumps across the actuator disks to preserve continuity and momentum.

Smith's analysis was based on the assumption of sources generating waves in an infinite

uniform medium so that there were only outgoing waves. These waves were solutions to a set of inhomogeneous equations with blade vorticity representing the loading source. Now we must include waves that are solutions to the homogeneous equations to account for the reflections from the inlet and exit interfaces. The situation is sketched in figure 6 where we show the loading source *LS(n,j)* sending out the direct source waves *KS1*, *KS2*, and *KS3* from Smith's analysis. The reflected waves *VS1*, *VS2*, and *VS3* will be derived in the next section in terms of the inlet and exit reflection coefficients. With the *KS*'s and *VS*'s as known functions proportional to the loading source, the entire wave field is still driven by the unknown loading elements *LS(n,j)* as with the original Smith method.

For the reflection and transmission coefficients, three interactions had to be considered, as shown in figure 7: upstream-going pressure waves v_1 could transmit a pressure wave v_4 and reflect a pressure wave v_2 and a vorticity wave v_3. Downstream-going pressure v_2 and vorticity v_3 waves could each transmit pressure and vorticity waves (v_8 and v_9) and reflect pressure waves (v_1). It was most convenient to derive the coefficients in terms of the modal transverse velocity components as follows.

Upstream-going pressure waves at inlet

$$\begin{aligned}
\bar{v}_2/a_b\beta_{nk} &= R_{12}(n,k)\,\bar{v}_1/a_b\beta_{nk} \\
\bar{v}_3/a_b\alpha_{3nk} &= R_{13}(n,k)\,\bar{v}_1/a_b\beta_{nk} \\
\bar{v}_4/a_a\beta_{nk} &= T_{14}(n,k)\,\bar{v}_1/a_b\beta_{nk}
\end{aligned} \tag{16}$$

Downstream-going pressure waves at exit

$$\begin{aligned}
\bar{v}_1 e^{i\alpha_{1nk}\bar{x}_e}/a_b\beta_{nk} &= R_{21}(n,k)\,\bar{v}_2 e^{i\alpha_{2nk}\bar{x}_e}/a_b\beta_{nk} \\
\bar{v}_8 e^{i\alpha_{8nk}\bar{x}_e}/a_c\beta_{nk} &= T_{28}(n,k)\,\bar{v}_2 e^{i\alpha_{2nk}\bar{x}_2}/a_b\beta_{nk} \\
\bar{v}_9 e^{i\alpha_{9nk}\bar{x}_e}/a_c\alpha_{9nk} &= T_{29}(n,k)\,\bar{v}_2 e^{i\alpha_{2nk}\bar{x}_e}/a_b\beta_{nk}
\end{aligned} \tag{17}$$

Vorticity waves at exit

$$\begin{aligned}
\bar{v}_1 e^{i\alpha_{1nk}\bar{x}_e}/a_b\beta_{nk} &= R_{31}(n,k)\,\bar{v}_3 e^{i\alpha_{3nk}\bar{x}_e}/a_b\alpha_{3nk} \\
\bar{v}_8 e^{i\alpha_{8nk}\bar{x}_e}/a_c\beta_{nk} &= T_{38}(n,k)\,\bar{v}_3 e^{i\alpha_{3nk}\bar{x}_e}/a_b\alpha_{3nk} \\
\bar{v}_9 e^{i\alpha_{9nk}\bar{x}_e}/a_c\alpha_{9nk} &= T_{39}(n,k)\,\bar{v}_3 e^{i\alpha_{3nk}\bar{x}_e}/a_b\alpha_{3nk}
\end{aligned} \tag{18}$$

Smith's subscripting convention has been continued so that 4 denotes the pressure wave upstream of the rotor and 8 and 9 denote the pressure and vorticity waves downstream of the stator. Derivation of the reflection and transmission coefficients is given in appendix D. It will be shown later that reflections are small at interfaces between regions where a mode is cut on. However, for modes passing from a cut on region to a cut off region, the reflection coefficient is of order unity. Thus, modes can become trapped between the rotor and stator and can be amplified, as will be seen.

3.3 EQUATIONS FOR COUPLING

The wave field between the rotor leading edge and the stator trailing edge can now be constructed in terms of direct waves from the load elements (via Smith's methodology) plus the waves reflected from the inlet and exit interfaces as sketched in figure 6. Equations coupling the rotor and stator will be derived in 4 arrays of influence coefficients as follows.

KSS - Stator on Stator
KSR - Stator on Rotor
KRR - Rotor on Rotor
KRS - Rotor on Stator

Later, these will be assembled into a large matrix to represent the entire coupled system and the system of equations will be solved by inverting the large matrix. The difficult parts of *KRR* and *KSS* have been taken care of by existing subroutines from Smith's original code. In particular, all issues of singularities that occur as source and field points approach each other are handled by these routines. *KRS* and *KSR* and the parts of *KRR* and *KSS* associated with the reflected waves are new and their derivation is described below.

Waves Caused by Stator Unsteady Loading

Consider first the direct waves caused by the stator loading. In terms of a kernel *KS1* defined below, we can write for the upstream wave of equation 14

$$v_{1\mathrm{dir}} = a_b \sum_{n=1}^{\infty} \sum_{k=-\infty}^{\infty} \beta_{nk}\, e^{i[\alpha_{1nk}(\bar{x}-\bar{x}_s)+\psi_{nk}]} \sum_{j=1}^{N_p} KS1(n,k,j)\times LS(n,j) \tag{19}$$

Similarly, the downstream waves are

$$v_{2\mathrm{dir}} = a_b \sum_{n=1}^{\infty} \sum_{k=-\infty}^{\infty} \beta_{nk}\, e^{i[\alpha_{2nk}(\bar{x}-\bar{x}_s)+\psi_{nk}]} \sum_{j=1}^{N_p} KS2(n,k,j)\times LS(n,j) \tag{20}$$

$$v_{3\mathrm{dir}} = a_b \sum_{n=1}^{\infty} \sum_{k=-\infty}^{\infty} \alpha_{3nk}\, e^{i[\alpha_{3nk}(\bar{x}-\bar{x}_s)+\psi_{nk}]} \sum_{j=1}^{N_p} KS3(n,k,j)\times LS(n,j) \tag{21}$$

where the kernels are defined by

$$KS1 = \frac{M_{r2}}{SC_2}\frac{v_1'}{\beta_{nk}} e^{-i(\alpha_{1nk}\cos\theta_2 + \beta_{nk}\sin\theta_2)\bar{c}_2 z_{oj}}$$

$$KS2 = \frac{M_{r2}}{SC_2}\frac{v_2'}{\beta_{nk}} e^{-i(\alpha_{2nk}\cos\theta_2 + \beta_{nk}\sin\theta_2)\bar{c}_2 z_{oj}} \qquad (22)$$

$$KS3 = \frac{M_{r2}}{SC_2}\frac{v_3'}{\alpha_{3nk}} e^{-i(\alpha_{3nk}\cos\theta_2 + \beta_{nk}\sin\theta_2)\bar{c}_2 z_{oj}}$$

(Use of v_1'/β_{nk}, v_2'/β_{nk}, and v_3'/α_{3nk} avoids problems later with divisions by 0.) The reflected waves are written in parallel form in terms of the coefficients *VS1*, *VS2*, and *VS3* which will be found in terms of the reflection coefficients derived in appendix D:

$$v_{1ref} = a_b \sum_{n=1}^{\infty}\sum_{k=-\infty}^{\infty} \beta_{nk}\, e^{i(\alpha_{1nk}\bar{x} + \psi_{nk})} \sum_{j=1}^{N_p} VS1(n,k,j)\times LS(n,j) \qquad (23)$$

$$v_{2ref} = a_b \sum_{n=1}^{\infty}\sum_{k=-\infty}^{\infty} \beta_{nk}\, e^{i(\alpha_{2nk}\bar{x} + \psi_{nk})} \sum_{j=1}^{N_p} VS2(n,k,j)\times LS(n,j) \qquad (24)$$

$$v_{3ref} = a_b \sum_{n=1}^{\infty}\sum_{k=-\infty}^{\infty} \alpha_{3nk}\, e^{i(\alpha_{3nk}\bar{x} + \psi_{nk})} \sum_{j=1}^{N_p} VS3(n,k,j)\times LS(n,j) \qquad (25)$$

Now, by applying the definitions of the reflection coefficients in equations 16-18, 3 equations can be written for the 3 *VS* coefficients:

$$\begin{aligned} VS1\, e^{i\alpha_{1nk}\bar{x}_e} &= (KS2\, e^{-i\alpha_{2nk}\bar{x}_s} + VS2)\, e^{i\alpha_{2nk}\bar{x}_e} R_{21}(n,k) \\ &\quad + (KS3\, e^{-i\alpha_{3nk}\bar{x}_s} + VS3)\, e^{i\alpha_{3nk}\bar{x}_e} R_{31}(n,k) \\ VS2 &= (KS1\, e^{-i\alpha_{1nk}\bar{x}_s} + VS1)\, R_{12}(n,k) \\ VS3 &= (KS1\, e^{-i\alpha_{1nk}\bar{x}_s} + VS1)\, R_{13}(n,k) \end{aligned} \qquad (26)$$

This set of equations can be solved for *VS1*, *VS2*, and *VS3* in terms of *KS1*, *KS2*, and *KS3* and the reflection coefficients, effectively determining the entire wavefield generated by any stator loading element *LS(n,j)*. The results upstream and downstream of the stator are

$$v_{up} = a_b \sum_{n=1}^{\infty}\sum_{k=-\infty}^{\infty}\sum_{j=1}^{N_p} e^{i\psi_{nk}} [\, \beta_{nk}(KS1\, e^{i\alpha_{1nk}(\bar{x}-\bar{x}_s)} + VS1\, e^{i\alpha_{1nk}\bar{x}} + VS2\, e^{i\alpha_{2nk}\bar{x}}) + \alpha_{3nk} VS3\, e^{i\alpha_{3nk}\bar{x}}\,] \times LS(n,j) \qquad (27)$$

and

$$v_{dn} = a_b \sum_{n=1}^{\infty} \sum_{k=-\infty}^{\infty} \sum_{j=1}^{N_p} e^{i\psi_{nk}} [\, \beta_{nk}(KS2\, e^{i\alpha_{2nk}(\bar{x}-\bar{x}_s)} + VS1\, e^{i\alpha_{1nk}\bar{x}} + VS2\, e^{i\alpha_{2nk}\bar{x}}) + \alpha_{3nk}(KS3\, e^{i\alpha_{3nk}(\bar{x}-\bar{x}_s)} + VS3\, e^{i\alpha_{3nk}\bar{x}}\,] \times LS(n,j) \tag{28}$$

These velocity fields have only to be evaluated at control points on the stator and rotor to find the effect of the stator on itself, *KSS*, and the effect of the stator on the rotor, *KSR*. This is treated in the next two sections.

Effect of Stator on Stator

We place one control point on each stator loading panel to give the values for $\bar{x}$ and ϕ_2 for use in equations 27 and 28. Control points, counted by i from 1 to N_p, are at the same chordwise locations z_i used by Smith and lead to the following:

$$\begin{aligned} \bar{x} &\rightarrow \bar{x}_s + \bar{c}_2 z_i \cos\theta_2 \\ \phi_2 &\rightarrow \quad \bar{c}_2 z_i \sin\theta_2 \end{aligned} \tag{29}$$

In examining equations 27 and 28, note that the terms with the *KS*'s are the direct waves that Smith already accounts for in his method. The remaining terms, with the *VS*'s are common to both equations and can be evaluated at the control points. To find the upwash (normal to the stator chord), we add the transverse component times $\cos\theta_2$ and minus the axial component times $\sin\theta_2$, the latter requiring Equations 6 and 8. For control point i the result can be written

$$\frac{w'_{ssi}}{W_2} = \sum_{n=1}^{\infty} \sum_{j=1}^{N_p} KSS'(n,i,j) \times LS(n,j)\, e^{inB_1\Omega t} \tag{30}$$

where the primes on w_{ssi} and *KSS* are a reminder that this part of the stator upwash is due to the reflected waves and is to be added to matrices from the original Smith method. The array of influence functions is

$$\begin{aligned} KSS'(n,i,j) = \sum_{k=-\infty}^{\infty} \frac{1}{M_{r2}} \times \\ [(\beta_{nk}\cos\theta_2 - \alpha_{1nk}\sin\theta_2)\, VS1\, e^{i\alpha_{1nk}\bar{x}_s} e^{i(\alpha_{1nk}\cos\theta_2 + \beta_{nk}\sin\theta_2)\bar{c}_2 z_i} \\ + (\beta_{nk}\cos\theta_2 - \alpha_{2nk}\sin\theta_2)\, VS2\, e^{i\alpha_{2nk}\bar{x}_s} e^{i(\alpha_{2nk}\cos\theta_2 + \beta_{nk}\sin\theta_2)\bar{c}_2 z_i} \\ + (\alpha_{3nk}\cos\theta_2 + \beta_{nk}\sin\theta_2)\, VS3\, e^{i\alpha_{3nk}\bar{x}_s} e^{i(\alpha_{3nk}\cos\theta_2 + \beta_{nk}\sin\theta_2)\bar{c}_2 z_i}\,] \end{aligned} \tag{31}$$

Equation 30 gives the waveform of the upwash at the stator control points z_i as an infinite Fourier series. For a matrix solution, we can satisfy the flow tangency requirement simultaneously for only a finite number of harmonics, N_h. (By adopting the Smith code, we have already accepted tangency at only a finite number of control points, N_p, along the chord.) Since each of the loading harmonics on each blade row induces upwash at the other blade row

in all harmonics, it is not clear *a priori* that truncating the harmonic series will lead to acceptable results. It does turn out, however, that the computed results for the lower harmonics are not strongly influenced by higher harmonics. A demonstration of this is given later in Section 4. Based on the above argument, the upwash waveform can be written

$$\frac{w'_{ssi}}{W_2} = \sum_{n=1}^{N_h} WSS'(n,i)\; e^{inB_1\Omega t} \tag{32}$$

where

$$WSS'(n,i) = \sum_{j=1}^{N_p} KSS'(n,i,j) \times LS(n,j) \tag{33}$$

When KSS' is added to the matrix from the direct waves computed with the Smith subroutines, that matrix is called KSS and the net effect of the stator loading elements at the stator control points is

$$WSS(n,i) = \sum_{j=1}^{N_p} KSS(n,i,j) \times LS(n,j) \tag{34}$$

This is the first of the coupling equations. It can be seen that, for the effect of the stator on itself, each loading harmonic n couples only to the same harmonic in the upwash.

Effect of Stator on Rotor

For this effect, we proceed in a similar fashion. But in this case, we will find that each loading harmonic on the stator couples to all of the upwash harmonics on the rotor. In the rotor coordinate system the control points are

$$\begin{aligned} \bar{x} &= \bar{c}_1 z_i \cos\theta_1 \\ \phi_1 &= \bar{c}_1 z_i \sin\theta_1 \end{aligned} \tag{35}$$

which can be applied to the form for ψ_{nk} given by equation 15 or A-17. These apply to waves caused by stator loads as viewed in the rotor system and explicitly shows the scattering from loading harmonic n into the other harmonics counted by k. The result, written for a finite number of harmonics, is

$$\frac{w_{sri}}{W_1} = \sum_{n=1}^{N_h} \sum_{k=-N_h}^{N_h} \sum_{j=1}^{N_p} KSR(n,k,i,j) \times LS(n,j)\; e^{ikB_2\Omega t} \tag{36}$$

where

$$\begin{aligned} KSR(n,k,i,j) = \\ \frac{1}{M_{r1}} [\, & (\beta_{nk}\cos\theta_1 - \alpha_{1nk}\sin\theta_1)(VS1 + KS1\, e^{-i\alpha_{1nk}\bar{x}_s})\, e^{i(\alpha_{1nk}\cos\theta_1 + \beta_{nk}\sin\theta_1)\bar{c}_1 z_i} \\ & + (\beta_{nk}\cos\theta_1 - \alpha_{2nk}\sin\theta_1)\, VS2\, e^{i(\alpha_{2nk}\cos\theta_1 + \beta_{nk}\sin\theta_1)\bar{c}_1 z_i} \\ & + (\alpha_{3nk}\cos\theta_1 + \beta_{nk}\sin\theta_1)\, VS3\, e^{i(\alpha_{3nk}\cos\theta_1 + \beta_{nk}\sin\theta_1)\bar{c}_1 z_i} \,] \end{aligned} \tag{37}$$

Note in equation 36 that negative frequencies have appeared as a result of viewing stator waves in the rotor coordinate system. To obtain a form parallel to equation 30 with only positive frequencies, we rewrite equation 36 using the following strategy. The k-summation can be written as a single sided series:

$$\frac{w_{sri}}{W_1} = \sum_{k=1}^{N_h} \sum_{n=1}^{N_h} \sum_{j=1}^{N_p} [KSR(n,k,i,j) \times LS(n,j)\, e^{ikB_2\Omega t} + KSR(n,-k,i,j) \times LS(n,j)\, e^{-ikB_2\Omega t}] \quad (38)$$

But only the real part of this expression has meaning so we are free to take the complex conjugate of any term. Applying this to the second term above and denoting conjugate by a *, we find

$$\frac{w_{sri}}{W_1} = \sum_{k=1}^{N_h} \sum_{n=1}^{N_h} \sum_{j=1}^{N_p} \{KSR(n,k,i,j) \times LS(n,j) + [KSR(n,-k,i,j) \times LS(n,j)]^* \}\, e^{ikB_2\Omega t} \quad (39)$$

which is in terms of positive frequencies, as desired. Now, in parallel with Equation 30 for the stator upwash, we can write the upwash waveform as

$$\frac{w_{sri}}{W_1} = \sum_{k=1}^{N_h} WSR(k,i)\; e^{ikB_2\Omega t} \quad (40)$$

where the k^{th} upwash harmonic on the i^{th} rotor panel is given by

$$WSR(k,i) = \sum_{n=1}^{N_h} \sum_{j=1}^{N_p} \{ KSR(n,k,i,j) \times LS(n,j) + [\, KSR(n,-k,i,j) \times LS(n,j)]^* \} \quad (41)$$

This is the second set of coupling equations. Again, note that each stator loading harmonic n contributes to all upwash harmonics k on the rotor.

Waves Caused by Rotor Unsteady Loading

The derivation for the effect of the rotor loading on the rotor and stator proceeds along similar lines; the procedure is only outlined here but the working equations are presented in detail. The main differences between the formulas for rotor and stator loading waves is permutation of the 1 and 2 indices, permutation of the n's and k's, exchange of R's and S's in some of the symbols, and the appearance of exponentials containing $\bar{x}_s$, which relate to the position of the leading edge of the stator along the x axis. For instance, the direct rotor wave upstream is analogous to equation 19 above for the stator

$$v_{1\text{dir}} = a \sum_{n=1}^{\infty} \sum_{k=-\infty}^{\infty} \beta_{kn}\, e^{i(\alpha_{1kn}\bar{x} + \psi_{kn})} \sum_{j=1}^{N_p} KR1(n,k,j) \times LR(n,j) \quad (42)$$

The direct waves downstream are analogous to equations 20 and 21 and the three coefficients corresponding to equation 22 are

$$KR1 = \frac{M_{r1}}{SC_1}\frac{v_1'}{\beta_{kn}} e^{-i(\alpha_{1kn}\cos\theta_1 + \beta_{kn}\sin\theta_1)\bar{c}_1 z_{oj}}$$

$$KR2 = \frac{M_{r1}}{SC_1}\frac{v_2'}{\beta_{kn}} e^{-i(\alpha_{2kn}\cos\theta_1 + \beta_{kn}\sin\theta_1)\bar{c}_1 z_{oj}} \tag{43}$$

$$KR3 = \frac{M_{r1}}{SC_1}\frac{v_3'}{\alpha_{3kn}} e^{-i(\alpha_{3kn}\cos\theta_1 + \beta_{kn}\sin\theta_1)\bar{c}_1 z_{oj}}$$

Reflections from the actuator disks are handled with the same reflection coefficients derived for the stator waves. Note the permutation of the n's and k's in comparison with equation 26

$$\begin{aligned} VR1\, e^{i\alpha_{1kn}\bar{x}_e} &= (KR2 + VR2)\, e^{i\alpha_{2kn}\bar{x}_e} R_{21}(k,n) \\ &\quad + (KR3 + VR3)\, e^{i\alpha_{3kn}\bar{x}_e} R_{31}(k,n) \\ VR2 &= (KR1 + VR1)\, R_{12}(k,n) \\ VR3 &= (KR1 + VR1)\, R_{13}(k,n) \end{aligned} \tag{44}$$

where, as for the stator loading case, the VR's can be solved for in terms of the KR's.

Effect of Rotor on Rotor

Upwash caused by the reflected waves on the rotor due to the rotor loading is given by the analog of equation 30 for the control points already defined for the stator-on-rotor effect in equation 35.

$$\frac{w_{rri}'}{W_1} = \sum_{n=1}^{\infty}\sum_{j=1}^{N_p} KRR'(n,i,j) \times LR(n,j)\, e^{inB_2\Omega t} \tag{45}$$

where the array of influence coefficients is given by

$$\begin{aligned} KRR'(n,i,j) = &\sum_{k=-\infty}^{\infty} \frac{1}{M_{r1}} \times \\ &[(\beta_{kn}\cos\theta_1 - \alpha_{1kn}\sin\theta_1)\, VR1\, e^{i(\alpha_{1kn}\cos\theta_1 + \beta_{kn}\sin\theta_1)\bar{c}_1 z_i} \\ &+(\beta_{kn}\cos\theta_1 - \alpha_{2kn}\sin\theta_1)\, VR2\, e^{i(\alpha_{2kn}\cos\theta_1 + \beta_{kn}\sin\theta_1)\bar{c}_1 z_i} \\ &+(\alpha_{3kn}\cos\theta_1 + \beta_{kn}\sin\theta_1)\, VR3\, e^{i(\alpha_{3kn}\cos\theta_1 + \beta_{kn}\sin\theta_1)\bar{c}_1 z_i}\ ] \end{aligned} \tag{46}$$

As before, we truncate the infinite Fourier series in equation 43 to the following form in analogy with equation 32

$$\frac{w_{rri}'}{W_1} = \sum_{n=1}^{N_h} WRR'(n,i)\, e^{inB_2\Omega t} \tag{47}$$

where

$$WRR'(n,i) = \sum_{j=1}^{N_p} KRR'(n,i,j) \times LR(n,j) \tag{48}$$

When the terms for the effects of the direct wave are added from the original Smith formulas, the primes are dropped and equation 46 becomes

$$WRR(n,i) = \sum_{j=1}^{N_p} KRR(n,i,j) \times LR(n,j) \tag{49}$$

This is the desired coupling equation for the upwash on the rotor caused by the rotor loading.

Effect of Rotor on Stator

Here the waveform, including only a finite number of harmonics, is

$$\frac{w_{rsi}}{W_2} = \sum_{n=1}^{N_h} \sum_{k=-N_h}^{N_h} \sum_{j=1}^{N_p} KRS(n,k,i,j) \times LR(n,j)\, e^{ikB_1\Omega t} \tag{50}$$

where

$$\begin{aligned} KRS(n,k,i,j) = & \\ & \frac{1}{M_{r2}} [(\beta_{kn}\cos\theta_2 - \alpha_{1kn}\sin\theta_2)\, VR1\; e^{i\alpha_{1kn}\bar{x}_s} e^{i(\alpha_{1kn}\cos\theta_2 + \beta_{kn}\sin\theta_2)\bar{c}_2 z_i} \\ & + (\beta_{kn}\cos\theta_2 - \alpha_{2kn}\sin\theta_2)(KR2 + VR2)\, e^{i\alpha_{2kn}\bar{x}_s} e^{i(\alpha_{2kn}\cos\theta_2 + \beta_{kn}\sin\theta_2)\bar{c}_2 z_i} \\ & + (\alpha_{3kn}\cos\theta_2 + \beta_{kn}\sin\theta_2)(KR3 + VR3) e^{i\alpha_{3kn}\bar{x}_s} e^{i(\alpha_{3kn}\cos\theta_2 + \beta_{kn}\sin\theta_2)\bar{c}_2 z_i}] \end{aligned} \tag{51}$$

As with the stator loading formulas, we rewrite equation 50 in terms of positive frequencies, preserving only the real part of the equation

$$\frac{w_{rsi}}{W_2} = \sum_{k=1}^{N_h} \sum_{n=1}^{N_h} \sum_{j=1}^{N_p} \{ KRS(n,k,i,j) \times LR(n,j) + [KRS(n,-k,i,j) \times LR(n,j)]^* \}\, e^{ikB_1\Omega t} \tag{52}$$

To define *WRS(k,i)*, this can be written

$$\frac{w_{rsi}}{W_2} = \sum_{k=1}^{N_h} WRS(k,i)\; e^{ikB_1\Omega t} \tag{53}$$

where

$$WRS(k,i) = \sum_{n=1}^{N_h} \sum_{j=1}^{N_p} \{ KRS(n,k,i,j) \times LR(n,j) + [KRS(n,-k,i,j) \times LR(n,j)]^* \} \tag{54}$$

which is the last of the coupling equations.

3.4 SOLVING THE COUPLED EQUATIONS

Equations 34, 41, 49, and 54 are four sets of linear equations giving the upwash velocities at the stator and rotor control points as functions of the unknown loading on the rotor and stator panels. The upwash components are considered known from the requirement of flow tangency on the blades and vanes. Specifically, the condition to be satisfied on the rotor is

$$WR(n,i) = WRR(n,i) + WSR(n,i) = 0\,, \qquad \text{all n,i} \tag{55}$$

This states that the sum of the upwash at the rotor due to the rotor and stator waves is zero for all harmonics and at all control points. For the stator, the condition is different because it is excited by the viscous wake, as indicated in figure 2. If we call the wake upwash harmonics $WWS(n,i)$, then the stator boundary condition is

$$WS(n,i) = WSS(n,i) + WRS(n,i) = -WWS(n,i), \qquad \text{all n,i} \tag{56}$$

indicating that the net effect of the waves from the stator and rotor must be equal and opposite to the wake upwash for flow tangency. Formulas for the wake are given in appendix E.

The preceding equations can be put into a matrix form written schematically as follows

$$\begin{bmatrix} KRR & KSR \\ KRS & KSS \end{bmatrix} \times \begin{bmatrix} LR \\ LS \end{bmatrix} = \begin{bmatrix} WR \\ WS \end{bmatrix} \tag{57}$$

which indicates that the rotor and stator loading each cause upwash at both the rotor and stator. To find the loading, the matrix equation is inverted subject to the boundary conditions in equations 52 and 53. The method to find the sound pressure and sound power from the unsteady loading is described in Section 3.5.

As indicated above, equation 57 only gives the form of the matrix equation schematically. To understand the details, we must look down two levels deeper into the matrix structure. Equation 57 shows that rotor and stator are both coupled to themselves and to each other but it does not show the frequency scattering explicitly. This can be seen at the next level by examining equation 58 where the harmonic dependence is stated explicitly for the special case of N_h=3. Loading harmonics are counted by n and upwash harmonics are counted by k. From the empty submatrices, it can be seen that there is no frequency scattering for each blade row acting on itself. However, for each blade row acting on the other, each loading harmonic produces upwash at all harmonics.

There is a problem which prevents equation 58 from being used directly. Examination of equations 41 and 54 reveals that two of the coupling equations do not express a simple linear relationship from loading to upwash because of the appearance of the loading complex conjugates. This is dealt with by expressing the equations in pure real terms and is explained below first for the rotor-on-rotor submatrices and then for the rotor-on-stator submatrices. The stator loading submatrices then follow immediately.

$$
\begin{bmatrix}
\begin{bmatrix} KRR \\ n=1 \\ k=1 \end{bmatrix} & \begin{bmatrix} 0 \end{bmatrix} & \begin{bmatrix} 0 \end{bmatrix} & | & \begin{bmatrix} KSR \\ n=1 \\ k=1 \end{bmatrix} & \begin{bmatrix} KSR \\ n=2 \\ k=1 \end{bmatrix} & \begin{bmatrix} KSR \\ n=3 \\ k=1 \end{bmatrix} \\
\begin{bmatrix} 0 \end{bmatrix} & \begin{bmatrix} KRR \\ n=2 \\ k=2 \end{bmatrix} & \begin{bmatrix} 0 \end{bmatrix} & | & \begin{bmatrix} KSR \\ n=1 \\ k=2 \end{bmatrix} & \begin{bmatrix} KSR \\ n=2 \\ k=2 \end{bmatrix} & \begin{bmatrix} KSR \\ n=3 \\ k=2 \end{bmatrix} \\
\begin{bmatrix} 0 \end{bmatrix} & \begin{bmatrix} 0 \end{bmatrix} & \begin{bmatrix} KRR \\ n=3 \\ k=3 \end{bmatrix} & | & \begin{bmatrix} KSR \\ n=1 \\ k=3 \end{bmatrix} & \begin{bmatrix} KSR \\ n=2 \\ k=3 \end{bmatrix} & \begin{bmatrix} KSR \\ n=3 \\ k=3 \end{bmatrix} \\
\text{-----} & \text{-----} & \text{-----} & - & \text{-----} & \text{-----} & \text{-----} \\
\begin{bmatrix} KRS \\ n=1 \\ k=1 \end{bmatrix} & \begin{bmatrix} KRS \\ n=2 \\ k=1 \end{bmatrix} & \begin{bmatrix} KRS \\ n=3 \\ k=1 \end{bmatrix} & | & \begin{bmatrix} KSS \\ n=1 \\ k=1 \end{bmatrix} & \begin{bmatrix} 0 \end{bmatrix} & \begin{bmatrix} 0 \end{bmatrix} \\
\begin{bmatrix} KRS \\ n=1 \\ k=2 \end{bmatrix} & \begin{bmatrix} KRS \\ n=2 \\ k=2 \end{bmatrix} & \begin{bmatrix} KRS \\ n=3 \\ k=2 \end{bmatrix} & | & \begin{bmatrix} 0 \end{bmatrix} & \begin{bmatrix} KSS \\ n=2 \\ k=2 \end{bmatrix} & \begin{bmatrix} 0 \end{bmatrix} \\
\begin{bmatrix} KRS \\ n=1 \\ k=3 \end{bmatrix} & \begin{bmatrix} KRS \\ n=2 \\ k=3 \end{bmatrix} & \begin{bmatrix} KRS \\ n=3 \\ k=3 \end{bmatrix} & | & \begin{bmatrix} 0 \end{bmatrix} & \begin{bmatrix} 0 \end{bmatrix} & \begin{bmatrix} KSS \\ n=3 \\ k=3 \end{bmatrix}
\end{bmatrix}
\times
\begin{bmatrix}
\begin{bmatrix} LR \\ n=1 \end{bmatrix} \\
\begin{bmatrix} LR \\ n=2 \end{bmatrix} \\
\begin{bmatrix} LR \\ n=3 \end{bmatrix} \\
\text{----} \\
\begin{bmatrix} LS \\ n=1 \end{bmatrix} \\
\begin{bmatrix} LS \\ n=2 \end{bmatrix} \\
\begin{bmatrix} LS \\ n=3 \end{bmatrix}
\end{bmatrix}
=
\begin{bmatrix}
\begin{bmatrix} WR \\ k=1 \end{bmatrix} \\
\begin{bmatrix} WR \\ k=2 \end{bmatrix} \\
\begin{bmatrix} WR \\ k=3 \end{bmatrix} \\
\text{----} \\
\begin{bmatrix} WS \\ k=1 \end{bmatrix} \\
\begin{bmatrix} WS \\ k=2 \end{bmatrix} \\
\begin{bmatrix} WS \\ k=3 \end{bmatrix}
\end{bmatrix}
\tag{58}
$$

Equation 49 for the rotor-on-rotor coupling can be written in terms of real and imaginary parts as follows

$$
\begin{aligned}
W_R + iW_I &= \sum_j (K_R + iK_I) \times (L_R + iL_I) \\
&= \sum_j (K_R L_R - K_I L_I) + i(K_I L_R + K_R L_I)
\end{aligned}
\tag{59}
$$

which can be expressed in matrix form

$$
\begin{bmatrix} W_R \\ W_I \end{bmatrix} = \begin{bmatrix} K_R & -K_I \\ K_I & K_R \end{bmatrix} \times \begin{bmatrix} L_R \\ L_I \end{bmatrix}
\tag{60}
$$

which is all real, as desired. This breakdown into real and imaginary parts is applied to each submatrix of equation 58. If we write the entire coupling system from equation 58 simply as

$$
\sum_{\nu} K(\mu,\nu)\, L(\nu) = W(\mu)
\tag{61}
$$

then we place the real parts of KRR into K as follows

$$
\begin{aligned}
&\text{Real}[KRR(n,i,j)] \rightarrow K[\,(2n-2)N_p + i\,,\ (2n-2)N_p + j\,] \\
&\text{and} \\
&\text{Real}[KRR(n,i,j)] \rightarrow K[\,(2n-1)N_p + i\,,\ (2n-1)N_p + j\,]
\end{aligned}
\tag{62}
$$

and the imaginary parts

$$\begin{aligned} -\mathrm{Imag}[KRR(n,i,j)] &\rightarrow K[\,(2n-2)N_p+i\,,\;(2n-1)N_p+j\,] \\ \text{and} \\ \mathrm{Imag}[KRR(n,i,j)] &\rightarrow K[\,(2n-1)N_p+i\,,\;(2n-2)N_p+j\,] \end{aligned} \tag{63}$$

The corresponding locations for the stator-on-stator elements in the lower right hand corner of the K matrix for the real parts are

$$\begin{aligned} \mathrm{Real}[KSS(n,i,j)] &\rightarrow K[\,2N_pN_h+(2n-2)N_p+i\,,\;2N_PN_h+(2n-2)N_p+j\,] \\ \text{and} \\ \mathrm{Real}[KSS(n,i,j)] &\rightarrow K[\,2N_pN_h+(2n-1)N_p+i\,,\;2N_pN_h+(2n-1)N_p+j\,] \end{aligned} \tag{64}$$

and for the imaginary parts

$$\begin{aligned} -\mathrm{Imag}[KSS(n,i,j)] &\rightarrow K[\,2N_pN_h+(2n-2)N_p+i\,,\;2N_pN_h+(2n-1)N_p+j\,] \\ \text{and} \\ \mathrm{Imag}[KSS(n,i,j)] &\rightarrow K[\,2N_pN_h+(2n-1)N_p+i\,,\;2N_pN_h+(2n-2)N_p+j\,] \end{aligned} \tag{65}$$

The situation for the rotor-on-stator elements is slightly more complicated. First, we rewrite equation 54, noting that the conjugate of a product is the product of the conjugates in the second term

$$WRS(k,i)=\sum_{n=1}^{N_h}\sum_{j=1}^{N_p}\left[KRS(n,k,i,j)\times LR(n,j)+KRS^{*}(n,-k,i,j)\times LR^{*}(n,j)\right] \tag{66}$$

Then, using the shorthand notation $KRS(n,k,i,j)=K_R(k)+iK_I(k)$, this can be written in terms of real and imaginary parts

$$WRS(k,i)=\sum_{n=1}^{N_h}\sum_{j=1}^{N_p}\left[K_R(k)+iK_I(k)\right](L_R+iL_I)+\left[K_R(-k)-iK_I(-k)\right](L_R-iL_I) \tag{67}$$

Separating the real and imaginary parts leads to submatrices of the form

$$\begin{bmatrix} W_R \\ W_I \end{bmatrix}=\begin{bmatrix} [K_R(k)+K_R(-k)] & [-K_I(k)-K_I(-k)] \\ [K_I(k)-K_I(-k)] & [K_R(k)-K_R(-k)] \end{bmatrix}\times\begin{bmatrix} L_R \\ L_I \end{bmatrix} \tag{68}$$

The result of the above development is that the KRS real and imaginary parts are placed into the lower left corner of K as follows

$$\begin{aligned} \mathrm{Real}[KRS(n,k,i,j)]+\mathrm{Real}[KRS(n,-k,i,j)] &\rightarrow K[\,2N_pN_h+(2k-2)N_p+i\,,\;(2n-2)N_p+j\,] \\ -\mathrm{Imag}[KRS(n,k,i,j)]-\mathrm{Imag}[KRS(n,-k,i,j)] &\rightarrow K[\,2N_pN_h+(2k-2)N_p+i\,,\;(2n-1)N_p+j\,] \\ \mathrm{Imag}[KRS(n,k,i,j)]-\mathrm{Imag}[KRS(n,-k,i,j)] &\rightarrow K[2N_pN_h+(2k-1)N_p+i,\;(2n-2)N_p+j] \\ \mathrm{Real}[KRS(n,k,i,j)]-\mathrm{Real}[KRS(n,-k,i,j)] &\rightarrow K[2N_pN_h+(2k-1)N_p+i,\;(2n-1)N_p+j] \end{aligned} \tag{69}$$

The development for the KSR terms proceeds exactly the same way to place these elements in the upper right corner of the matrix in equation 58. The result is given below

$$
\begin{aligned}
\text{Real}[KSR(n,k,i,j)] + \text{Real}[KSR(n,-k,i,j)] &\rightarrow K[(2k-2)N_p + i,\ 2N_pN_h + (2n-2)N_p + j] \\
-\text{Imag}[KSR(n,k,i,j)] - \text{Imag}[KSR(n,-k,i,j)] &\rightarrow K[(2k-2)N_p + i,\ 2N_pN_h + (2n-1)N_p + j] \\
\text{Imag}[KSR(n,k,i,j)] - \text{Imag}[KSR(n,-k,i,j)] &\rightarrow K[(2k-1)N_p + i,\ 2N_pN_h + (2n-2)N_p + j] \\
\text{Real}[KSR(n,k,i,j)] - \text{Real}[KSR(n,-k,i,j)] &\rightarrow K[(2k-1)N_p + i,\ 2N_pN_h + (2n-1)N_p + j]
\end{aligned}
\tag{70}
$$

Finally, for inversion of equation 58 (or 61), we need to describe the construction of the upwash vector $W(\mu)$ in terms of the rotor and stator upwash boundary conditions in equations 55 and 56 and the interpretation of the rotor and stator loading components $LR(n,j)$ and $LS(n,j)$ in terms of the loading vector $L(\nu)$. The upwash vector is constructed as follows

$$
\begin{aligned}
\text{Real}[WR(k,i)] &\rightarrow W[(2k-2)N_p + i] \\
\text{Imag}[WR(k,i)] &\rightarrow W[(2k-1)N_p + i] \\
\text{Real}[WS(k,i)] &\rightarrow W[2N_pN_h + (2k-2)N_p + i] \\
\text{Imag}[WS(k,i)] &\rightarrow W[2N_pN_h + (2k-1)N_p + i]
\end{aligned}
\tag{71}
$$

and inverting the matrix and computing the L vector, the rotor and stator loads are constructed from $L(\nu)$ according to

$$
\begin{aligned}
LR(n,j) &= L[(2n-2)N_p + j] + i\,L[(2n-1)N_P + j] \\
LS(n,j) &= L[2N_PN_h + (2n-2)N_p + j] + i\,L[2N_PN_h + (2n-1)N_p + j]
\end{aligned}
\tag{72}
$$

If we only needed unsteady blade loading, we could stop here. However, for acoustic application, we are interested in the upstream and downstream pressure waves and their sound power. This is the subject of the next section.

3.5 SOUND PRESSURE AND SOUND POWER FORMULAS

The preceding sections showed how to find the unsteady rotor and stator loading in a coupled fan stage and gave expressions for the transverse velocity components of the waves caused by this loading. For acoustic purposes, we need to derive the expressions for sound pressure as well. Furthermore, acoustic power desired as a fundamental measure of sound generation independent of time and axial and transverse position in the duct. To develop formulas for acoustic power, we also need formulas for the axial component of acoustic velocity. The expressions for pressure and axial velocity are developed next and then power formulas are developed later in the section.

Sound Pressure and Axial Velocity

The theory of this report develops expressions for acoustic disturbances in three regions: Region A extends from the rotor leading edge to upstream infinity. Region B lies between the rotor leading edge to the stator trailing edge. Region C extends from the stator trailing edge to downstream infinity. Section 3 developed expressions for the transverse components of the disturbance velocities in Region B. To find the acoustic pressure and velocity in Region A, the required steps are to 1) find the transverse velocity at the upstream boundary of Region B, 2)

apply the transmission coefficients developed in appendix D to jump to the transverse velocity in Region A, 3) apply Smith's equations (equations 6 and 7 herein) relating pressure and axial velocity to transverse velocity to find the desired quantities. Acoustic pressure and velocity in Region C are found by the same method.

Waves in Upstream Region

We start with the stator waves given by equation 27. We select only the upstream-going waves since definition of the transmission coefficients is based on them. At the rotor leading edge, $\bar{x}=0^+$,

$$v_1 = a_b \sum_{n=1}^{\infty} \sum_{k=-\infty}^{\infty} \sum_{j=1}^{N_p} e^{i\psi_{nk}} \beta_{nk} (KS1\, e^{-i\alpha_{1nk}\bar{x}_s} + VS1) \times LS(n,j) \tag{73}$$

To find the corresponding value just across the inlet actuator disk at $\bar{x}=0^-$, we apply the definition of the transmission coefficient in equation 16 (and in appendix D) to find

$$v_4 = a_a \sum_{n=1}^{\infty} \sum_{k=-\infty}^{\infty} \sum_{j=1}^{N_p} e^{i\psi_{nk}} \beta_{nk} (KS1\, e^{-i\alpha_{1nk}\bar{x}_s} + VS1)\, T_{14}(n,k) \times LS(n,j) \tag{74}$$

Now we define

$$KSUP(n,k,j) = (KS1\, e^{-i\alpha_{1nk}\bar{x}_s} + VS1)\, T_{14}(n,k) \tag{75}$$

and insert the axial wavenumber exponential to find v_4 at any upstream location

$$v_4 = a_a \sum_{n=1}^{\infty} \sum_{k=-\infty}^{\infty} \sum_{j=1}^{N_p} \beta_{nk}\, e^{i(\psi_{nk} + \alpha_{4nk}\bar{x})} KSUP(n,k,j) \times LS(n,j) \tag{76}$$

The working form for this is obtained by performing the j-sum and defining

$$LSUP(n,k) = \sum_{j=1}^{N_p} KSUP(n,k,j) \times LS(n,j) \tag{77}$$

so that

$$v_4 = a_a \sum_{n=1}^{\infty} \sum_{k=-\infty}^{\infty} \beta_{nk}\, e^{i(\psi_{nk} + \alpha_{4nk}\bar{x})} LSUP(n,k) \tag{78}$$

As mentioned above, equations 6 and 7 provide the connection from the transverse velocity component to the axial component and the pressure. When these are applied, we find

$$\left[u_4\right]_{\text{stator}} = a_a \sum_{n=1}^{\infty} \sum_{k=-\infty}^{\infty} \alpha_{4nk}\, e^{i(\psi_{nk} + \alpha_{4nk}\bar{x})} LSUP(n,k) \tag{79}$$

and

$$\left[p_4\right]_{\text{stator}} = \rho_{oa}\, a_a^2 \sum_{n=1}^{\infty} \sum_{k=-\infty}^{\infty} \gamma_{4nk}\, e^{i(\psi_{nk} + \alpha_{4nk}\bar{x})}\, LSUP(n,k) \tag{80}$$

where we have defined

$$\gamma_{4nk} = -\left(\frac{a_b}{a_a}\,\Omega_{nk} + M_{xa}\alpha_{4nk}\right) \tag{81}$$

Equations 79 and 80 are the desired forms for the axial velocity and pressure in the upstream region caused by stator loading. Derivation of the corresponding forms for waves from rotor loading is similar and leads to the following results.

$$\left[u_4\right]_{\text{rotor}} = a_a \sum_{n=1}^{\infty} \sum_{k=-\infty}^{\infty} \alpha_{4kn}\, e^{i(\psi_{kn} + \alpha_{4kn}\bar{x})}\, LRUP(n,k) \tag{82}$$

and

$$\left[p_4\right]_{\text{rotor}} = \rho_{oa}\, a_a^2 \sum_{n=1}^{\infty} \sum_{k=-\infty}^{\infty} \gamma_{4kn}\, e^{i(\psi_{kn} + \alpha_{4kn}\bar{x})}\, LRUP(n,k) \tag{83}$$

Permutation of the n and k indices (in comparison with equations 79 and 80) arises from viewing the rotor waves in the stator coordinate system. This is an important aspect of the kinematics of blade row interaction and is discussed in detail in appendix A. The definitions of *LRUP* and *KRUP* are similar to those for *LSUP* and *KSUP* above:

$$LRUP(n,k) = \sum_{j=1}^{N_p} KRUP(n,k,j) \times LR(n,j) \tag{84}$$

and

$$KRUP(n,k,j) = (KR1 + VR1)\, T_{14}(k,n) \tag{85}$$

The total acoustic pressure in the upstream region, of course, is the sum of equations 80 and 83. By noting that $\bar{x}_s$ appears in equation 75 but not in equation 85, it can be seen that the phase difference between the rotor and stator waves associated with axial spacing is accounted for and thus that interference effects associated with rotor/stator spacing are included in the theory.

Waves in Downstream Region

This derivation is similar to the one just presented, but slightly more complicated because the jump between regions is not at $\bar{x}=0$ and because both pressure and vorticity waves impinge on the downstream actuator disk. From equation 28, the downstream-going waves from the stator are

$$\begin{aligned} v_2 + v_3 = a_b \sum_{n=1}^{\infty} \sum_{k=-\infty}^{\infty} \sum_{j=1}^{N_p} e^{i\psi_{nk}} \left[\beta_{nk} (KS2\, e^{-i\alpha_{2nk}\bar{x}_s} + VS2)\, e^{i\alpha_{2nk}\bar{x}_e} \right. \\ \left. + \alpha_{3nk} (KS3\, e^{-i\alpha_{3nk}\bar{x}_s} + VS3)\, e^{i\alpha_{3nk}\bar{x}_e} \right] \times LS(n,j) \end{aligned} \tag{86}$$

at the exit plane $\bar{x} = \bar{x}_e^-$. The definitions for the transmissions coefficients T_{28} and T_{38} from Equations 17 and 18 are applied to find the transverse velocity in the pressure wave at $\bar{x} = \bar{x}_e^+$ and the x-wavenumber exponentials are added to find the velocity anywhere downstream of the stator actuator disk.

$$v_8 = a_c \sum_{n=1}^{\infty} \sum_{k=-\infty}^{\infty} \sum_{j=1}^{N_p} e^{i\psi_{nk}} \beta_{nk} [(KS2\, e^{-i\alpha_{2nk}\bar{x}_s} + VS2)\, e^{i\alpha_{2nk}\bar{x}_e} T_{28}(n,k) + (KS3\, e^{-i\alpha_{3nk}\bar{x}_s} + VS3)\, e^{i\alpha_{3nk}\bar{x}_e} T_{38}(n,k)]\, e^{i\alpha_{8nk}(\bar{x}-\bar{x}_e)} \times LS(n,j) \tag{87}$$

Now, by defining

$$KSDN(n,k,j) = (KS2\, e^{-i\alpha_{2nk}\bar{x}_s} + VS2)\, e^{i\alpha_{2nk}\bar{x}_e} T_{28}(n,k) + (KS3\, e^{-i\alpha_{3nk}\bar{x}_s} + VS3)\, e^{i\alpha_{3nk}\bar{x}_e} T_{38}(n,k)] \tag{88}$$

and

$$LSDN(n,k) = \sum_{j=1}^{N_p} KSDN(n,k,j) \times LS(n,j) \tag{89}$$

the transverse velocity for the pressure wave in the downstream region can be written

$$v_8 = a_c \sum_{n=1}^{\infty} \sum_{k=-\infty}^{\infty} \beta_{nk}\, e^{i[\psi_{nk} + \alpha_{8nk}(\bar{x}-\bar{x}_e)]} LSDN(n,k) \tag{90}$$

Again by applying equations 7 and 8, the axial component of the acoustic velocity and the acoustic pressure in the downstream region are found to be

$$[u_8]_{\text{stator}} = a_c \sum_{n=1}^{\infty} \sum_{k=-\infty}^{\infty} \alpha_{8nk}\, e^{i[\psi_{nk} + \alpha_{8nk}(\bar{x}-\bar{x}_e)]} LSDN(n,k) \tag{91}$$

and

$$[p_8]_{\text{stator}} = \rho_{oc} a_c^2 \sum_{n=1}^{\infty} \sum_{k=-\infty}^{\infty} \gamma_{8nk}\, e^{i[\psi_{nk} + \alpha_{8nk}(\bar{x}-\bar{x}_e)]} LSDN(n,k) \tag{92}$$

where γ_{8nk} is given by

$$\gamma_{8nk} = -\left(\frac{a_b}{a_c} \Omega_{nk} + M_{xc} \alpha_{8nk} \right) \tag{93}$$

For the rotor waves the procedure is similar and leads to the following forms for axial velocity and pressure

$$\left[u_8\right]_{\text{rotor}} = a_c \sum_{n=1}^{\infty} \sum_{k=-\infty}^{\infty} \alpha_{8kn}\, e^{i[\psi_{kn} + \alpha_{8kn}(\bar{x} - \bar{x}_e)]}\, LRDN(n,k) \tag{94}$$

and

$$\left[p_8\right]_{\text{rotor}} = \rho_{oa} a_c^2 \sum_{n=1}^{\infty} \sum_{k=-\infty}^{\infty} \gamma_{8kn}\, e^{i[\psi_{kn} + \alpha_{8kn}(\bar{x} - \bar{x}_e)]}\, LRDN(n,k) \tag{95}$$

where

$$LRDN(n,k) = \sum_{j=1}^{N_p} KRDN(n,k,j) \times LR(n,j) \tag{96}$$

and

$$\begin{aligned} KRDN(n,k,j) = {} & (KR2 + VS2)\, e^{i\alpha_{2kn}\bar{x}_e}\, T_{28}(k,n) \\ & + (KR3 + VR3)\, e^{i\alpha_{3kn}\bar{x}_e}\, T_{38}(k,n) \end{aligned} \tag{97}$$

The above equations for pressure are coded in CUP2D for output on a modal basis and as a sum over the modes at each frequency. The pressure formulas and those for the axial velocity components are used in the next section to derive equations for acoustic power.

Sound Power

Formulas for sound power are derived from Goldstein's (ref. 9) equation for acoustic energy flux vector

$$\boldsymbol{I} = (p/\rho_o + \boldsymbol{u}\cdot\boldsymbol{v}_o)(\rho_o \boldsymbol{u} + \rho \boldsymbol{v}_o) \tag{98}$$

where p , ρ , and $\boldsymbol{u}$ are the acoustic pressure, density, and velocity and $\boldsymbol{v}_o$ is the mean velocity of the background flow. We are interested in Regions A and B, where the flow is axial, so that $\boldsymbol{u}\cdot\boldsymbol{v}_o = uU$. Then, with $\rho = p/a^2$, the flux becomes

$$\boldsymbol{I} = (p/\rho_o + Uu)\left(\rho_o \boldsymbol{u} + \frac{p}{a^2}\boldsymbol{v}_o\right) \tag{99}$$

Since we are interested in the flux in the axial direction, we form

$$I_x = \boldsymbol{I}\cdot\boldsymbol{i}_x = (p/\rho_o + Uu)\left(\rho_o u + \frac{p}{a^2}U\right) \tag{100}$$

or

$$I_x = (1+M_x^2)pu + \frac{M_x}{\rho_o a}p^2 + \rho_o a M_x u^2 \tag{101}$$

This is the instantaneous energy per unit time crossing a unit area element that is normal to the x-axis. The power is the time average of I_x integrated over the duct cross-sectional area. Since the concept of area in a 2D duct is nebulous, we will simply compute a non-dimensional quantity equal to the average power per unit area normalized by the ambient value of $\rho_o a^3$. The average power is then

$$II_x = \frac{1}{2\pi}\int_0^{2\pi}\frac{1}{T}\int_0^T I_x \, dt \, d\phi \tag{102}$$

Since this is defined to be positive for flux in the x direction, computed values for our problem must be positive downstream of the source and negative upstream to represent energy propagating away from the source region.

Upstream Power

To begin operations with equations 101 and 102, we need convenient forms for u and p. As stated above, the axial velocity in Region A is given by the sum of the stator and rotor contributions expressed by equations 79 and 82.

$$\begin{aligned} u_4 = a_a \,\text{Real} \sum_{n=1}^{\infty}\sum_{k=-\infty}^{\infty} \alpha_{4nk}\, LSUP(n,k)\, e^{i(\psi_{nk}+\alpha_{4nk}\bar{x})} \\ + a_a \,\text{Real} \sum_{n=1}^{\infty}\sum_{k=-\infty}^{\infty} \alpha_{4kn}\, LRUP(n,k)\, e^{i(\psi_{kn}+\alpha_{4kn}\bar{x})} \end{aligned} \tag{103}$$

The declaration "Real" has been implicit all along but is shown here explicitly because of the need to eliminate it for the manipulations that follow. This is done by changing to double sided series in n as follows

$$\begin{aligned} u_4 = \frac{a_a}{2} \sum_{n=-\infty}^{\infty}\sum_{k=-\infty}^{\infty} \alpha_{4nk}\, LSUP(n,k)\, e^{i(\psi_{nk}+\alpha_{4nk}\bar{x})} \\ + \frac{a_a}{2} \sum_{n=-\infty}^{\infty}\sum_{k=-\infty}^{\infty} \alpha_{4kn}\, LRUP(n,k)\, e^{i(\psi_{kn}+\alpha_{4kn}\bar{x})} \end{aligned} \tag{104}$$

The reader can verify that equations 103 and 104 are equivalent by noting that ψ_{nk} and α_{4nk} simply change sign when both indices change sign and by defining $LSUP(-n,-k)=LSUP^*(n,k)$. The "Real" declaration in no longer needed since the imaginary parts of the upper and lower halves of the n-series cancel identically. The key step now is to switch the dummy k and n indices in the second line of the equation, yielding

$$u_4 = \frac{a_a}{2} \sum_{n=-\infty}^{\infty}\sum_{k=-\infty}^{\infty} \alpha_{4nk}\,[LSUP(n,k) + LRUP(k,n)]\, e^{i(\psi_{nk}+\alpha_{4nk}\bar{x})} \tag{105}$$

or, by defining

$$LUP(n,k) = LSUP(n,k) + LRUP(k,n) \tag{106}$$

we obtain the simpler form

$$u_4 = \frac{a_a}{2} \sum_{n=-\infty}^{\infty} \sum_{k=-\infty}^{\infty} \alpha_{4nk}\, LUP(n,k)\, e^{i(\psi_{nk} + \alpha_{4nk}\bar{x})} \tag{107}$$

which will be seen to be convenient for manipulation later.

By a similar argument, the desired form for the upstream pressure is

$$p_4 = \frac{\rho_o a_a^2}{2} \sum_{n=-\infty}^{\infty} \sum_{k=-\infty}^{\infty} \gamma_{4nk}\, LUP(n,k)\, e^{i(\psi_{nk} + \alpha_{4nk}\bar{x})} \tag{108}$$

Now, consider the expression for the product $p_4 u_4 = p_4 u_4^*$ (because u_4 is real) which has be averaged over ϕ and t. This requires the quadruple summation

$$p_4\, u_4 = \frac{\rho_{oa}\, a_a^3}{4} \sum_n \sum_m \sum_k \sum_q \alpha_{4nk}\, \gamma_{4mq}\, LUP(n,k)\, LUP^*(m,q) e^{i(\alpha_{4nk} - \alpha_{4,-m,-q})\bar{x}} \times e^{-i[(n-m)B_1 - (k-q)B_2]\phi}\; e^{i[(n-m)B_1\Omega_1 + (k-q)]B_2\Omega_2]t} \tag{109}$$

Averaging over ϕ involves only the second exponential. That average is zero for each term in the series except for the cases where $(n\text{-}m)B_1 = (k\text{-}q)B_2$, when the average value is unity. When this expression is substituted into the time exponential in equation 109, the result is $\exp[i(n\text{-}m)B_1(\Omega_1+\Omega_2)t]$. When this is averaged over time, the result is unity for $n=m$ and zero otherwise. Thus, when the m and q sums are performed in equation 109, the exponentials vanish and the result is

$$\overline{\overline{p_4\, u_4}} = \frac{\rho_{oa}\, a_a^3}{4} \sum_{n=-\infty}^{\infty} \sum_{k=-\infty}^{\infty} \alpha_{4nk}\, \gamma_{4nk}\, LUP(n,k)\, LUP^*(n,k) \tag{110}$$

where the double overline denotes the average over ϕ and t. From the symmetry properties of the α's, γ's, and LUP's, it can be shown upper and lower halves of the n-series are identical so that

$$\overline{\overline{p_4\, u_4}} = \frac{\rho_{oa}\, a_a^3}{2} \sum_{n=1}^{\infty} \sum_{k=-\infty}^{\infty} \alpha_{4nk}\, \gamma_{4nk}\, LUP(n,k)\, LUP^*(n,k) \tag{111}$$

where the $n=0$ term is omitted because it makes no noise. This is the working form for the average of the first term in equation 101. It exhibits the usual behavior that the total power is the sum of the modal powers. Also, as required, the result is independent of $\bar{x}$ and ϕ. Averages of the remaining terms in equation 101 can now be written down by inspection. The final form for the sound power in Region A is

$$\Pi_{xa} = \frac{\rho_{oa}\, a_a^3}{2} \sum_{n=1}^{\infty} \sum_{k=-\infty}^{\infty} [(1 + M_{xa}^2)\alpha_{4nk}\, \gamma_{4nk} + M_{xa}(\alpha_{4nk}^2 + \gamma_{4nk}^2)]\, |LUP(n,k)|^2 \tag{112}$$

This is the form used in the computer code except that the factor $\frac{1}{2}\rho_{oa}a_a^3$ is omitted via the following normalization.

$$\bar{\Pi}_{xa} = \frac{\Pi_{xa}}{\frac{1}{2}\rho_{oa}\, a_a^3} \tag{113}$$

For a decibel output, the value is divided by 10^{-13}, arbitrarily, to give positive values for plotting purposes

$$PWL = 10\log_{10}\left[\frac{\bar{\Pi}_{xa}}{10^{-13}}\right] \tag{114}$$

Downstream Power

The derivation for power in Region C follows along identical lines. The result is

$$\Pi_{xc} = \frac{\rho_{oc}\, a_c^3}{2}\sum_{n=1}^{\infty}\sum_{k=-\infty}^{\infty}\left[(1+M_{xc}^2)\alpha_{8nk}\,\gamma_{8nk} + M_{xc}(\alpha_{8nk}^2+\gamma_{8nk}^2)\right]|LDN(n,k)|^2 \tag{115}$$

where

$$LDN(n,k) = LSDN(n,k) + LRDN(k,n) \tag{116}$$

Normalization for this in the code is the same as for the upstream power, except that the downstream conditions ρ_{oc} and a_c are used.

The theory of this section is coded in program CUP2D. Documentation for CUP2D can be found in Volume 2 of this report and includes a source listing, user instructions, and a test case. Typical cases for 3 harmonics and 30 panels on each blade row run a few minutes on a workstation computer or a 386 PC.

SECTION 4
COMPARISON WITH OTHER THEORIES

The theory of the present paper adds three effects not included in the Smith theory: blade row coupling, frequency scattering, and flow turning. For verification of the theory, it was possible to check only two of these effects by comparison with previous work.

Comparison with Kaji and Okazaki

Kaji and Okazaki developed a method (ref. 6) to compute the coupled interaction between a downstream rotor and an inlet guide vane (IGV) cascade with viscous wakes. Their method could treat one harmonic only and did not account for turning of the flow. Since the present analysis treats rotor/EGV, rotor/rotor, and IGV/rotor interaction, it was possible to make comparisons with the earlier Kaji/Okazaki results. (The wake model used here is equivalent to that of Kaji and Okazaki and is developed in appendix E.) A sample is shown in figure 8 for a case where $B_1=B_2$ and the gap/chord ratio is the same for both rotor and stator. The geometry and flow condition are such that the relative Mach number is the same for both blade rows. The curves show the upstream and downstream sound pressure for two rotor spacings as relative Mach number varies. Agreement of the two theories is excellent. This provides confidence in the coupling part of the new theory, which is handled differently in the Kaji and Okazaki work.

Simulation of the Kaji/Okazaki case was as follows. The IGV and rotor blade angles were both 30 deg., gap/chord ratios were both 1.0, and the interblade phase angle was zero. Since theirs was an unloaded model, this corresponds to a stage with an inlet (and exit) flow angle of 30 deg. The model of this report does not permit swirl in the exit flow and therefore the Kaji and Okazaki configuration was simulated by running both blade rows as rotors with equal and opposite RPMs. By using $-M_{y2} = M_{y1} = M_x \tan 30$ deg. , the geometry and flow angles were correctly represented. The blade numbers had to be equal and were chosen to be equal to 10. Conditions were taken to be sea level standard for density and sound speed.

Comparison with Kousen and Verdon

For single cascades, a much more sophisticated method has been developed at the United Technologies Research Center by Verdon and his co-workers (ref. 10). Their code, called LINFLO, starts with a steady flow field from a compressible potential flow calculation and computes an unsteady perturbation field due to input waves or blade motions based on a linearized, inviscid, unsteady analysis. In a recent paper, Kousen and Verdon (ref. 11) showed calculations that provided an opportunity to establish how well the present method represents the effect of flow turning. In figure 9 the cascade is excited by a vorticity wave with an interblade phase angle and frequency such that it is cut on upstream of the cascade and cut off downstream. Kousen and Verdon compared this to a no turning, flat plate calculation (equivalent to a Smith code calculation) and found that the case with turning increased the upstream response wave by a factor of 8.4, or 18.5 dB. Some alterations to the present method were made to represent a single flat plate cascade with (or without) turning at the exit. When the Kousen/Verdon case was simulated, it was found that the reflected wave was amplified by 19.7 dB by the turning. It was concluded for this case that the primary effect of the real blades (beyond the flat plate results) is reflection of the waves from a region where they cannot propagate and that the simplistic

actuator disk model did a reasonably good job of representing the effect.

Simulation of the Kousen/Verdon case was as follows. In the upstream/downstream regions the axial Mach numbers were 0.476/0.450, the swirl Mach numbers were 0.275/0.000, the sound speeds were 1116/1128 ft/sec, and the densities were 0.07631/0.080185 lbm/ft^3. Use of B_1 =36, B_2=57, chord/radius = 0.131, and rotor rotational Mach number = 0.478 produced the correct reduced frequency (4.106) and interblade phase angle (2.31). To eliminate wave reflections from the rotor and inlet actuator disk, *KR1, KR2, KR3,* R_{12}, and R_{13} were set to zero. Finally, reflections from the exit actuator disk (representing the mean flow turning) could be turned off by setting R_{21} and R_{31} equal to zero.

SECTION 5
BEHAVIOR OF THE COUPLED CASCADE THEORY & THE MODE TRAPPING PHENOMENON

In this section, behavior of the new theory is examined using a format similar to that of the test data in figure 3 to find to what extent the features of coupling, frequency scattering, and flow turning explain the observed behavior. Since the theory is 2-dimensional, we are only looking for qualitative behavior at this point; absolute level predictions will have to await a 3D analysis. The calculations lead to the conclusion that the high levels of noise at 2x and 3xBPF are caused by a mode that reflects back and forth between the rotor and stator, amplifying in level and coupling to the upper harmonics. The final part of this section verifies the assertion made during derivation of the theory that valid results can be obtained by including only a small number of loading harmonics in the coupling equations.

The cases presented in this section are all in the form of RPM sweeps with mean flow conditions representative of the 85 percent radius in the turbofan of figure 3. The mean flow values used for the computations, which are given in Table I, were obtained by running a standard streamline curvature code. Each column corresponds to one operating condition. For the curves to be presented below, M_{y1} (the first row) is treated as the independent variable and values of the other parameters are found by straight line interpolation on M_{y1}.

TABLE I - MEAN FLOW CONDITIONS
a) Upstream of rotor, b) Between rotor and stator, and c) Downstream of stator

M_{y1}	0.672	0.908	0.974	1.017
M_{xa}	0.269	0.418	0.467	0.496
M_{xb}	0.321	0.440	0.469	0.480
M_{xc}	0.382	0.519	0.544	0.546
M_s	0.205	0.285	0.334	0.359
ρ_{oa}	.02978	.02837	.02767	.02738
ρ_{ob}	.03222	.03407	.03525	.03592
ρ_{oc}	.03201	.03381	.03539	.03647
a_a	1041	1031	1027	1025
a_b	1065	1080	1091	1098
a_c	1065	1081	1094	1104

ρ_o - density - lbm/ft^3, a - speed of sound - ft/sec

In particular, the reflection and transmission coefficients are computed from the jumps in mean flow properties from regions *a* to *b* (across the rotor) and from regions *b* to *c* (across the stator). For comparison with figure 3, note that M_{y1} is taken as 85 percent of the fan tip rotational Mach number. In addition to conditions given by the table, the rotor and stator gap/chord ratios were 0.763 and 0.957 and the spacing from the rotor trailing edge to the stator leading edge was two rotor chords. There were 38 blades and 72 vanes. Stagger angles follow the mean flow according to figure 5 but were generally about 55 deg. for the rotor and 32 deg. for the stator. Furthermore, all were run with a wake model equivalent to that in the Kaji/Okazaki work (derived herein in appendix E) with a drag coefficient of 0.02 but with all of the wake harmonics above BPF set to 0. Thus, excitation of the coupled system is exclusively at BPF and any appearance of higher harmonics must be caused by frequency scattering. These conditions apply to all cases discussed in this section.

5.1 EFFECTS OF COUPLING, FREQUENCY SCATTERING, AND SWIRL

Four RPM sweeps are shown in figure 10 to demonstrate the effects of the new theoretical features. The plot at the upper left presents a baseline case and then various effects are "turned on" to illustrate their influence. For the cases without swirl, all the mean flow conditions are set to the values for the aft duct in the table above. Thus, without swirl, all of the reflection coefficients associated with turning of the mean flow are 0.

Figure 10a shows calculations without swirl for one harmonic only. BPF cuton in the aft duct is at a rotor rotational Mach number of 0.80. The first mode to cut on at BPF has order m=-34, which is computed from $m=nB_1-kB_2$ with B_1=38, B_2=72, n=1, k=1. The uncoupled curve corresponds to results from the original Smith theory (KRS and KSR were set to zero). The case with coupling uses theory equivalent to that of Kaji and Okazaki. It can be seen that the coupling effect is very weak for this case and could easily be ignored for acoustic purposes.

Figure 10b was generated without swirl but with coupling and scattering to 2 and 3 times BPF included. This is the first case showing excitation at BPF producing noise at higher harmonics. Also, note that there is a small amount of noise in the higher harmonics at speeds below BPF cuton. This figure does not look at all like figure 3 with its high levels of 2xBPF and 3xBPF below BPF cuton. However, above cuton, the scattering effect is not negligible. For example, a spectrum at a rotor rotational Mach number M_{y1} = 0.82 would show 2xBPF and 3xBPF only 5 dB below BPF.

Figure 10c shows coupled calculations for one harmonic only, with and without swirl. The change here is due mostly to the fact that, in the theoretical model, the cascade stagger angles follow the mean flow as indicated by figure 5. Thus, for the case without swirl, the stator angle is 0 deg. and the rotor stagger is typically 60 deg. The extended range of rotational speeds with swirl is due to the fact that swirl reduces the relative Mach number at the rotor fig. 5) and permits a higher RPM before the rotor relative Mach number reaches unity. The rapid rise in the curve for the "with swirl" results from cuton of a second propagating mode (n,k = 1,0) at M_{y1} = 0.87.

Finally, figure 10d shows calculations with all of the theoretical features included. We see that the combination of swirl and coupling produces a substantial increase in levels of the higher harmonics, particularly below BPF cuton. In comparing this with the plot of engine data in figure 3, we see that, although the plots are not exactly the same, there are some striking similarities. At the RPM where BPF cuts on in the interstage area, 2xBPF and 3xBPF rise rapidly and are actually higher than BPF when it cuts on in the aft duct. When BPF cuts on in the aft duct, the higher harmonics drop substantially. In the intermediate speed range, 3xBPF is higher than 2xBPF by about the same amount as in the engine data. These similarities suggest that the 2D model embodies the correct physical features to explain the experimental behavior.

5.2 INTERPRETATION OF RESULTS

To interpret the results presented in figure 10, it is necessary to understand behavior of the reflection coefficients associated with the inlet and exit actuator disks and how they are related to modal cutoff ratios. The 1,1 mode is the first to cut on and we show its behavior in figure 11. The upper panel relates to the inlet interface and shows $R_{12}(1,1)$ and $R_{13}(1,1)$, which are the coefficients for an upstream going pressure wave reflecting into downstream going pressure and vorticity waves. Point b indicates cuton between rotor and stator and point a indicates cuton in the inlet duct. It can be seen that reflection into the vorticity wave is always weak. However, for the pressure wave, the coefficient is of order unity between a and b and is small outside. This indicates that a wave travelling from a region where it is cut on to a region where it is cut off is reflected with little change in amplitude. The lower panel in figure 11 relates to the exit interface and shows $R_{21}(1,1)$ and $R_{31}(1,1)$, the coefficients for the upstream going pressure wave reflected from the downstream going pressure and vorticity waves. Again, there is strong reflection for waves traveling from a region where they are cut on to one where they are cut off. This is believed to be the dominant reason for the strong reflections shown in the Kousen/Verdon[11] calculations in figure 9.

The explanation for the behavior of the upper harmonics shown in figure 10d can be explained pictorially with the sketch in figure 12. The top panel relates to the speed range from cuton between blade rows to cuton in the aft duct. In this range, the 1,1 mode can bounce back and forth freely between rotor and stator, *but it cannot escape*. It effectively is trapped in the interstage area and builds to high levels as it couples to the higher harmonics. The higher harmonics then *can* escape to the aft duct. Thus, in this speed range, the excitation of the system is BPF of the rotor wakes, but the only noise escaping from the system is at higher harmonics. The lower panel in figure 12 relates to speeds where BPF can propagate in the aft duct. The 1,1 mode is no longer trapped so that the BPF levels between rotor and stator do not amplify as strongly and the coupling to the higher harmonics produces lower levels.

Finally, note that figure 10 shows that the combination of coupling *and* swirl was required to produce the effect. Swirl or coupling by itself produced much less dramatic results.

5.3 CONVERGENCE WITH INCREASING NUMBER OF HARMONICS

In the theory derivation of Section 3, the coupling equations were initially written as waveforms of upwash with an infinite number of harmonics. Since the coupled system of equations is solved numerically, flow tangency can be guaranteed simultaneously at only a finite number of harmonics. Thus, the summation over loading harmonic order was truncated at N_h rather than running to infinity. Since each loading harmonic on the stator produces an infinite number of upwash harmonics on the rotor and *vice versa*, it was not known *a priori* that this truncation would produce acceptable results. The only way to verify correct behavior was to run a series of calculations with increasing values of N_h. It was hoped that as more and more harmonics are included in the coupling, the influence on the lower harmonics would be minimal.

Verification of this convergence is shown in figure 13, which is based on the same conditions used for figure 10. The top panel shows predicted aft PWL at BPF for separate calculations where 1, 2, 3, 4, and 5 harmonics were included in the coupling. It can be seen that near cuton the number of harmonics does influence results but that levels tend to converge for larger N_h. When the next mode cuts on near rotational Mach number $M_{yI} = 0.87$, the sensitivity to number of harmonics disappears. It seems that the upper harmonics are taking energy from only the $m = 38\text{-}72 = -34$ mode.

The second panel from the top in figure 13 shows results for 2xBPF. Here the sensitivity to N_h is minimal. The lower panels in the figure indicate that the situation improves at higher harmonics. Thus, we have given an example where results for the lower harmonics are not strongly affected by the number of harmonics included in the coupling. Although all of the cases checked so far exhibit this behavior, this does not constitute proof of convergence. A probable explanation for the convergence is that loading response diminishes with increasing frequency. Also, interference between waves from adjacent panels increases with increasing frequency. However, until a more rigorous theoretical explanation can be provided, we cannot be sure that convergence will always occur.

SECTION 6
PARAMETRIC STUDIES

The calculations of the previous section were chosen to provide a physical understanding of noise generation in a coupled environment. Geometry and operating conditions were the same for all of the figures and are representative of modern turbofan design; in particular, there were more vanes than blades. In this section, we explore the new theory via additional computations.

First, in figure 14 we compare upstream and downstream harmonic powers from the same calculation. The top panel in the figure is the same as in figure 10d and is the "base case" for variations in the remaining figures. The forward PWL's shown in the lower panel exhibit behavior similar to the aft noise but with cuton of BPF at a slightly higher rotor speed because of differences in inlet and exit mean flow conditions. Note that the forward noise levels are much lower than the aft noise. This is believed to be due to the fact that the basic noise source is the stator and its noise must propagate upstream through the rotor. Note also that the forward levels are so low that they are likely to be masked by other sources, such as inlet distortion/rotor interaction in a real engine environment.

The top part of figure 14 also indicates the cuton speed for relevant modes via the arrows along the bottom grid line. For example, the notation 1,1 b at rotational Mach number M_{y1} = 0.665 indicates that the n,k = 1,1 mode cuts on at this speed in region b (between rotor and stator). In the figure it can also be seen that the same mode doesn't cut on in the aft duct (region c) until M_{y1} reaches 0.800. Thus, the 1,1 mode is trapped between these rotor speeds. The figure also shows that mode 1,0 cuts on at M_{y1} = 0.870, accounting for the rapid rise in BPF at this speed.

Because of the motivation to understand the importance of frequency scattering, all of the computed noise so far in this report has been excited by the BPF harmonic (fundamental) of the rotor wake; the upper wake harmonics have been set to zero. In the lower portion of figure 15, the wake harmonics are computed in the normal way from the wake formulas in appendix E. Thus, there are three wake harmonics and three harmonics in the coupling calculation. By comparing with the base case in the upper portion of the figure, it can be seen that BPF and 3xBPF are only slightly affected, however, 2xBPF changes considerably. Since this is a linear analysis, superposition applies: the 2xBPF oscillations must be caused by interference between noise caused by the wake upper harmonics and noise caused by scattering from the fundamental. Note that the overall noise is not increased much by including the upper wake harmonics; that is, the upper noise harmonics are caused primarily by the scattering phenomenon and not by the better known process whereby each wake harmonic couples only to the same noise harmonic. This behavior, of course, depends on the wake properties so that no universal conclusions can be drawn.

The cases above were all for geometry with 38 rotor blades and 72 stator vanes, that is for a typical cut off design. For these, the first mode to cut on at BPF has order m=-34, (computed from $m=nB_1-kB_2$ with n=1, for BPF, and k=1, for the first wake spatial harmonic). The significance of the negative mode order is that this mode spins counter to the rotor direction, and the swirl direction, and therefore cuts on earlier in the swirl region than in the aft region. Thus,

the typical behavior that we have seen above is high levels of 2xBPF and 3xBPF when BPF is cut off. In figure 16, we compare this base case for 38 blades and 72 vanes with calculations for the same blade count but 38 and 26 vanes. Blade row solidity and rotor/stator spacing are the same for all three vane counts. For B_2=38 and 26, BPF is cut on throughout the speed range of interest and we do not find any speed range where the upper harmonics dominate, however, there is considerable frequency scattering. (All portions of figure 16 were computed with only the wake fundamental harmonic for excitation.) Now, for the 38-vane case, note the rapid rise in the 3xBPF harmonic near M_{y1}=0.72. This is caused by the 1,2 mode which cuts on at a rotor rotational Mach number of 0.72 between blade rows and at 0.87 in the aft region. As denoted by the *'s above the 1,2 b and 1,2 c notations, this is another trapped mode. Here is a case where BPF noise is cut on, for k=1, but there is considerable influence on a higher harmonic due to another BPF mode which is cut off and counter rotating. For the 26-vane case at the bottom of figure 16, similar remarks apply for the 2xBPF and 3xBPF harmonics. In this case the 1,3 mode is trapped between rotor speeds 0.750 and 0.915. Thus, we find that frequency scattering and mode trapping can have a significant impact on the noise even for cut on designs.

The final set of calculations is for variations in rotor/stator spacing. Figure 17 compares aft power levels for axial spacings of 1.0, 1.5, and 2.0 rotor chords between the rotor trailing edge and the stator leading edge. There is very little difference in the three sets of curves except for a slight decrease for increased spacing. Since all of the curves go down as a family, this appears to be due simply to the weaker wake excitation as spacing increases. (The wake formulas are given in appendix E.) At the low speed end of the curves, note that the slope is steeper for the greater spacing. Noise at rotor speeds below 0.675 rotational Mach number is caused by excitation of the rotor by a cut off mode from the stator. Thus, at a given RPM in this low range, noise will depend strongly on rotor/stator spacing because of the exponential decay of the cut off mode.

SECTION 7
CONCLUDING REMARKS

An analytical model has been developed for rotor/stator interaction by extending the industry-standard 2-dimensional unsteady cascade theory of S. N. Smith to include 1) unsteady coupling of rotor and stator, 2) frequency scattering due to relative motion between blade rows, and 3) turning of the flow due to the mean loading on the blade rows. Unsteady loading is handled rigorously by collocation at many panels simultaneously on each cascade for several harmonics. The effect of finite mean loading is treated simplistically via actuator discs that turn the flow at the rotor leading edge and straighten it at the stator trailing edge. For typical turbofans designed for cutoff, there is a speed range where the fundamental mode at BPF can bounce back and forth between the rotor and stator but cannot escape to the inlet or exit ducts. In this range, the mode amplifies and couples to the higher harmonics, producing a significant amount of noise at these frequencies. This mode trapping mechanism appears to explain observations in engine data where the source of excitation is at blade passing frequency but the spectrum is dominated by 2xBPF and 3xBPF.

The computational method requires truncating the Fourier series that represents the blade and vane loading. It was demonstrated that, when three or four harmonics are included in the coupling, noise at the lower harmonics is predicted with reasonable accuracy.

Limited verification of the theory was possible by comparison with earlier work of Kaji and Okazaki, although their analysis did not include frequency scattering or turning of the flow. By comparison with calculations from the LINFLO code for loaded, isolated cascades, it appears that turning of the mean flow is the major feature of real cascades (as opposed to flat plates) that influences noise.

Although unsteady coupling produces frequency scattering under any conditions, swirl is the critical ingredient that produces the mode trapping and amplification. Scattering into the upper harmonics can be significant for both cut off and cut on designs. It is concluded that any further modeling of rotor/stator interaction for noise calculations should include the features of coupling, frequency scattering, and flow turning.

SECTION 8
REFERENCES

1. Tyler, J. M.; and Sofrin, T. G.: Axial Flow Compressor Noise Studies. SAE Trans., vol. 70, 1962, pp. 309-332.

2. Sofrin, T. G.; and McCann, J. C.: Pratt and Whitney Experience in Compressor Noise Reduction. J. Acoust. Soc. Am., vol. 40, no. 5, Nov. 1966, pp. 1248-1249.

3. Ventres, C. S.; Theobald, M. A.; and Mark, W. D.: Turbofan Noise Generation, Vol. I: Analysis. NASA CR-167952, 1982.

4. Topol, D.: Rotor Wake/Stator Interaction Noise - Prediction Versus Data. AIAA Paper 90-3951, 1990.

5. Topol, D. A.; Holhubner, S. C.; and Mathews, D. C.: A Reflection Mechanism for Aft Fan Tone Noise. AIAA Paper 87-2699, 1987.

6. Kaji, S.; and Okazaki, T.: Generation of Sound by Rotor-Stator Interaction. J. Sound Vib., vol. 13, no. 3, 1970, pp. 281-307.

7. Smith, S. N.: Discrete Frequency Sound Generation in Axial Flow Turbomachines. Report R. & M. no. 3709, 1973.

8. Whitehead, D.: Classical Two-Dimensional Methods. AGARD Manual on Aeroelasticity in Axial-Flow Turbomachines, Vol. 1: Unsteady Turbomachinery Aerodynamics, ch. 3, M.F. Platzer and F.O. Carta, eds., AGARD-AG-298 Vol.1, Mar. 1987, 30 p.

9. Goldstein, M. E.: Aeroacoustics. McGraw-Hill, New York, 1976.

10. Verdon, J. M.: Linearized Unsteady Aerodynamics for Turbomachinery Aeroelastic Applications. AIAA Paper 90-2355, 1990.

11. Kousen, K. A.; and Verdon, J. M.: Aeroacoustics of Real Blade Cascades, presented at the sixth International Symposium on Unsteady Aerodynamics, Aeroacoustics, and Aeroelasticity of Turbomachinery and Propellers. Symposium proceedings to be published by Springer-Verlag, 1993.

12. Horlock, J. H.: Actuator Disc Theory. McGraw-Hill, New York, 1978.

13. Silverstein, A.; Katzoff, S.; and Bullivant, W. K.: Downwash and Wake Flow Behind Plain and Flapped Airfoils. NACA TP-651, 1939.

APPENDIX A
KINEMATICS OF ROTOR/STATOR INTERACTION

The objectives of this appendix are 1) to find, via a kinematic analysis, the form of all of the waves that can result from rotor/stator interaction, 2) to relate the interblade phase angle notation of cascade theory to the spinning mode order notation of duct acoustics, and 3) to develop one system of indices for the transverse wavenumbers that can be used for both rotor and stator waves.

Kinematics of the interaction are determined by a part of the exponential in equation 1 which we call the kinematic phase

$$\psi = \beta y + \omega t \tag{A-1}$$

In the following, we study the properties of ψ for the rotor and stator and relate it to the spinning mode notation of fan acoustics.

Consider the two blade rows shown in figure 5. For generality, it is assumed that both blade rows can rotate in either direction. To simplify the nomenclature, the front blade row will be called the "rotor" and the rear blade row will be called the "stator"; however, in reality, the analysis can treat IGV/rotor and rotor/rotor configurations as well as the rotor/EGV configuration indicated by the nomenclature. There are three coordinate systems with common values for x: the x,y system is fixed in the duct; the x,y_1 system is locked to the rotor; and the x,y_2 system is locked to the stator. The rotor is shown with positive stagger angle θ_1 in conformity with Smith's nomenclature, but for the rotor/EGV geometry emphasized in this report, the rotor stagger angle will be negative. Blades are aligned with the mean flow direction so that stagger angles are determined by the axial velocity U the swirl velocity V_s and the angular speeds according to the velocity triangles in figure 5. The constant R used below can be considered the effective radius of a thin annular duct and is the reference used throughout the paper for non-dimensionalizing wavenumbers, chords, and distances. The y's and the cylindrical coordinate angles are related by

$$\begin{aligned} y &= R\phi \\ y_1 &= R\phi_1 \\ y_2 &= R\phi_2 \end{aligned} \tag{A-2}$$

The coordinate systems are related to each other by

$$\begin{aligned} \phi &= \phi_1 + \Omega_1 t \\ \phi &= \phi_2 + \Omega_2 t \\ \phi_2 &= \phi_1 + \Omega t \end{aligned} \tag{A-3}$$

where

$$\Omega \equiv \Omega_1 - \Omega_2 \tag{A-4}$$

Because the Smith equations were developed in a coordinate system locked to a blade row, the discussion below will jump from stator coordinates to rotor coordinates and back again. Implications for frequencies in the duct-fixed system will be discussed afterwards. Starting in the stator frame, we can see that the relative motion of the rotor with B_1 blades will induce loading harmonics of order nB_1 with

frequencies $nB_1\Omega$. The resulting kinematic phase can thus be written

$$\psi_s = \beta_s y_2 + nB_1\Omega t \tag{A-5}$$

Inserting equation 2, the relation between blade gap and blade number, $S_2=2\pi R/B_2$, and the conversion to cylindrical coordinates via equation A-2 leads to

$$\psi_s = (\frac{\sigma_s}{2\pi}B_2 + kB_2)\phi_2 + nB_1\Omega t \tag{A-6}$$

Now, to find the interblade phase angle for the stator σ_s, compare the condition just analyzed with that when the rotor has advanced one stator vane gap, that is by angle $2\pi/B_2$ in time $2\pi/B_2\Omega$. It can be seen that the geometry will be identical to figure 5 but with the y_2 (or ϕ_2) axis shifted. We conclude that ψ_s, with $\phi_2 \rightarrow \phi_2 + 2\pi/B_2$ and $t \rightarrow t + 2\pi/B_2\Omega$, is the same as ψ_s in equation A-6. By equating these expressions for ψ_s, we find

$$\sigma_s = -2\pi n B_1/B_2 \tag{A-7}$$

for the interblade phase angle, that is the difference in loading phase on two adjacent stator vanes at harmonic n. Inserting this into equation A-6 gives the expression familiar from duct acoustics

$$\psi_s = -(nB_1 - kB_2)\phi_2 + nB_1\Omega t \tag{A-8}$$

which indicates modes of order nB_1-kB_2 (for all k) appearing at frequency $nB_1\Omega$ and spinning at speed $[nB_1/(nB_1-kB_2)]\Omega$ in stator coordinates.

A similar derivation for rotor loading harmonics of order n and frequency $nB_2\Omega$ leads to interblade phase angle

$$\sigma_r = +2\pi n B_2/B_1 \tag{A-9}$$

where the + sign appears because the relative motion of the stator is opposite that of rotor. With these results, the kinematic phases for rotor loading harmonic n are

$$\psi_r = -(kB_1 - nB_2)\phi_1 + nB_2\Omega t \tag{A-10}$$

for all k.

We now define the mode order notation for the stator

$$\beta_{nk} \equiv \beta_s R = -(nB_1 - kB_2) \tag{A-11}$$

and take advantage of the symmetry with the rotor waves to note that

$$\beta_r R = \beta_{kn} \tag{A-12}$$

Then the kinematic phases for the stator (in the stator coordinate system) can be written

$$\psi_s = \psi_{nk} = \beta_{nk}\phi_2 + nB_1\Omega t \tag{A-13}$$

and for the rotor (in the rotor coordinate system)

$$\psi_r = \beta_{kn}\phi_1 + nB_2\Omega t \tag{A-14}$$

A revealing step now is to find the *rotor* wave properties in the *stator* coordinates by substituting $\phi_1 = \phi_2 - \Omega t$ into equation A-14. The result is

$$\psi_r = \beta_{kn}\phi_2 + kB_1\Omega t \tag{A-15}$$

which is to say

$$\psi_r = \psi_{kn} \tag{A-16}$$

Since indices n and k take on all integer values, comparison of equations A-13 and A-16 shows that the set of rotor waves and the set of stator waves are the same set. Thus, we have found all waves generated by coupled rotor/stator interaction (equation A-13); they are the same set found in uncoupled analyses such as that of Tyler and Sofrin (ref. 1)! Furthermore, comparison of equations A-14 and A-15 shows that the roles of the n and k indices switch when the same wave is viewed in different frames. In the rotor frame, k is the cascade index and, in the stator frame, it is the time harmonic index.

Study of the above equations also shows the origin of frequency scattering. equation A-14 gives the form in the rotor frame of the waves caused by rotor loading. A single loading harmonic n produces the waves indicated where k takes on all integer values. That is, one loading harmonic produces waves at the same frequency but with many mode orders. Equation A-15 represents these same waves in the stator frame and shows that the waves caused by a single harmonic (n) of rotor loading appear at all harmonics $(kB_1\Omega)$ of blade passing frequency in the stator frame.

Kinematic phases for rotor and stator waves can also be expressed in duct-fixed coordinates via equation A-3. This result plus the other results derived above are summarized below.

Waves due to stator load harmonic n and cascade index k

$$\psi_s = \psi_{nk} = \begin{cases} \beta_{nk}\phi_2 + nB_1\Omega t & \text{in stator frame} \\ \beta_{nk}\phi_1 + kB_2\Omega t & \text{in rotor frame} \\ \beta_{nk}\phi + (nB_1\Omega_1 - kB_2\Omega_2)t & \text{in fixed frame} \end{cases} \tag{A-17}$$

Waves due to rotor load harmonic n and cascade index k

$$\psi_r = \psi_{kn} = \begin{cases} \beta_{kn}\phi_1 + nB_2\Omega t & \text{in rotor frame} \\ \beta_{kn}\phi_2 + kB_1\Omega t & \text{in stator frame} \\ \beta_{kn}\phi + (kB_1\Omega_1 - nB_2\Omega_2)t & \text{in fixed frame} \end{cases} \tag{A-18}$$

In code CUP2D the β_{nk}'s are computed in subroutine ALFBET.

APPENDIX B
AXIAL WAVENUMBERS AND THE CUTON CRITERION

The general 2-dimensional waves studied in this report are in the form of complex coefficients multiplied by the exponential $\exp[i(\alpha x+\beta y+\omega t)]$. Appendix A showed how the frequency ω and transverse wavenumber β are related to the kinematics of the problem, that is to the numbers of blades and the rotational speeds. The axial wavenumber α was derived by Smith from aerodynamic analysis as a function of β and ω. Its form determines whether waves propagate or decay in the axial direction. In this appendix, we find non-dimensional forms for the axial wavenumbers that can be used for both rotor and stator waves. We also evaluate the cuton criterion and deal with a sign choice for the upstream and downstream going pressure waves.

In appendix A we saw that the kinematic phase, $\psi = \beta y + \omega t$ took on different forms in the duct-fixed and rotating coordinate systems. The axial wavenumbers, however, must be the same in any of these coordinate systems. We choose to evaluate them as related to stator waves in the duct-fixed frame. The form for the rotor waves will be found simply by permuting indices using the principles derived in appendix A. Consider first the wavenumbers for the pressure waves given by equation 4 of the main text

$$\alpha_{S\,1,2} = \frac{U(\omega + V\beta) + a\sqrt{(\omega + V\beta)^2 - (a^2 - U^2)\beta^2}}{a^2 - U^2} \tag{B-1}$$

From equation A-17, the frequency in the duct-fixed system is $\omega=nB_1\Omega_1-kB_2\Omega_2$. We define a non-dimensional form of this as

$$\Omega_{nk} = (nB_1\Omega_1 - kB_2\Omega_2)R/a = nB_1M_{y1} - kB_2M_{y2} \tag{B-2}$$

where M_{y1} and M_{y2} are the rotational Mach numbers of the two blade rows. We further define the axial and swirl Mach numbers to be

$$\begin{aligned} M_x &= U/a \\ M_s &= V_s/a \end{aligned} \tag{B-3}$$

Substituting these plus the mode order definition from equation A-11 into equation B-1 gives results in the following form for α_{1nk} and α_{2nk} for the stator pressure waves

$$\alpha_{1,2nk} = \alpha_{S\,1,2}R = \frac{M_x(\Omega_{nk} + M_s\beta_{nk}) \pm \sqrt{(\Omega_{nk} + M_s\beta_{nk})^2 - (1 - M_x^2)\beta_{nk}^2}}{1 - M_x^2} \tag{B-4}$$

The sign choice is discussed below. For the rotor, it is easily shown that $\alpha_r R = \alpha_{1,2nk}$ permitting the forms for α_{1nk} and α_{2nk} defined in equation B-4 to be used for both the rotor and stator.

Equation B-4 contains the desired information regarding cuton. When the square root is real, the wavenumbers (upstream and downstream) are real and the waves propagate undiminished. When the square root is imaginary, $i\alpha x$ in the exponential has a negative real part and the waves decay. Thus, the argument of the square root supplies the cuton criterion

$$(\Omega_{nk} + M_s\beta_{nk})^2 > (1 - M_x)^2\beta_{nk}^2 \quad \text{for cuton} \tag{B-5}$$

This is more conveniently expressed in terms of the cutoff ratio ξ, which is defined as follows

$$\xi = \frac{\left|\Omega_{nk} + M_s \beta_{nk}\right|}{\beta_{nk}\sqrt{1 - M_x^2}} \tag{B-6}$$

which must be greater than zero for a mode to be cut on. This means that, for a mode with β_{nk} lobes, the frequency, that is Ω_{nk}, has to be "high enough", to satisfy equation B-6, for propagation. If β_{nk} is positive, then the effect of swirl is to lower the RPM for cuton (assuming $M_s > 0$). For fans designed for cutoff, that is with $B_2 > B_1$ this will be the case because the $k = 1$ mode is the first to propagate at BPF so that $\beta_{nk} = -(nB_1 - kB_2) = -(B_1 - B_2) = B_2 - B_1 > 0$. Study of equation A-8 and the following text reveals that this condition corresponds to the case where the mode is spinning in a direction *opposite* to the swirl, that is the velocity of the mode relative to the fluid is increased by the swirl.

The sign choice in equation B-4 is made from physical reasoning which is different for decaying and propagating waves. For decay, the requirement is simply that the waves diminish to 0 as $x \rightarrow \pm\infty$. For progagation, we require that the wavelength (reciprocal of α) in the upstream region be smaller than the wavelength in the downstream region. The working forms for the axial wavenumbers are summarized below using the definitions

$$\begin{aligned} F &= M_x(\Omega_{nk} + M_s\beta_{nk}) \\ E &= (1 - M_x^2)\beta_{nk}^2 - (\Omega_{nk} + M_s\beta_{nk})^2 \end{aligned} \tag{B-7}$$

which apply in the region between the rotor leading edge and the stator trailing edge. The wavenumbers for the vorticity waves are also given in terms of quantities already defined.

Propagating pressure waves ($E<0$)

$$F>0: \qquad \begin{aligned} \alpha_{1nk} &= \frac{1}{1 - M_x^2}\left[F + \sqrt{-E}\right] \\ \alpha_{2nk} &= \frac{1}{1 - M_x^2}\left[F - \sqrt{-E}\right] \end{aligned} \tag{B-8}$$

$$F<0: \qquad \begin{aligned} \alpha_{1nk} &= \frac{1}{1 - M_x^2}\left[F - \sqrt{-E}\right] \\ \alpha_{2nk} &= \frac{1}{1 - M_x^2}\left[F + \sqrt{-E}\right] \end{aligned} \tag{B-9}$$

Decaying pressure waves ($E>0$)

$$\alpha_{1nk} = \frac{1}{1-M_x^2}[F - i\sqrt{E}]$$
$$\alpha_{2nk} = \frac{1}{1-M_x^2}[F + i\sqrt{E}] \qquad \text{(B-10)}$$

Vorticity waves

$$\alpha_{3nk} = -\frac{\Omega_{nk} + M_s \beta_{nk}}{M_x} \qquad \text{(B-11)}$$

As a result of nomenclature developed in appendixes A and B, convenient forms can be used for the exponential $\exp[i(\alpha x+\beta y+\omega t)]$. For the upstream pressure wave caused by stator loading harmonic of order n, the exponential is $\exp[i(\alpha_{1nk}x+\psi_{nk})]$, where k is the cascade index that takes on all integer values. Formulas for ψ_{nk} valid in all coordinate systems of interest are given in equation A-17. For the upstream pressure waves caused by rotor loading harmonic of order n, the exponential is $\exp[i(\alpha_{1kn}x+\psi_{kn})]$, where ψ_{kn} is given in equation A-18. For downstream waves, change the 1 in the α subscripts to 2's.

The axial wavenumbers derived above apply directly to the swirl region between the rotor and stator. For the region upstream of the rotor, the notation is continued with α_{4nk} for the upstream- and downstream-going pressure waves. Downstream of the stator, α_{8nk} and α_{9nk} apply to the downstream going pressure and vorticity waves. To apply the formulas above, set $M_s=0$ and use the axial Mach number M_x appropriate for the region. Also, because Ω_{nk} is based on the speed of sound in region b, this must be adjusted for the other regions. The results are

$$F_a = M_{xa}\,\Omega_{nk}\,a_b/a_a$$
$$E_a = (1-M_{xa}^2)\beta_{nk}^2 - (\Omega_{nk}\,a_b/a_a)^2 \qquad \text{(B-12)}$$

for region a and

$$F_c = M_{xc}\,\Omega_{nk}\,a_b/a_c$$
$$E_c = (1-M_{xc}^2)\beta_{nk}^2 - (\Omega_{nk}\,a_b/a_c)^2 \qquad \text{(B-13)}$$

for region c.

In code CUP2D the α's are computed in subroutine ALFBET.

APPENDIX C
COMMON FORMS FOR TRANSVERSE VELOCITY COMPONENTS

In reference 7, Smith derives expressions for v_1', v_2', and v_3', the transverse velocity of the upstream-going pressure wave, downsteam-going pressure wave, and vorticity wave caused by a unit loading element. The axial velocity and pressure are then computed from the v''s. In this appendix, we apply the non-dimensionalizations of this report and derive forms for these transverse velocity components that can be applied in the coupled cascade code CUP2D to both the rotor waves and the stator waves.

Starting with pressure waves from the stator, we apply Smith's equations 23 and 28 to find

$$v'_{1,2} = \frac{\beta}{2A_2}\left(\mp\beta \mp \lambda_2 \sin\theta_2 + \frac{i\lambda_2\beta\cos\theta_2}{\sqrt{\beta^2 - M_{r2}^2 A_2}}\right) \tag{C-1}$$

which is written directly for decaying waves. The upper/lower signs apply to the up-/downstream-going wave. By reproducing Smith's derivation, it can be shown that the correct interpretation for the square root for propagating waves gives

$$v'_{1,2} = \frac{\beta}{2A_2}\left(\mp\beta \mp \lambda_2 \sin\theta_2 + \frac{\lambda_2\beta\cos\theta_2}{\sqrt{M_{r2}^2 A_2 - \beta^2}}\right) \tag{C-2}$$

where

$$A_2 = \lambda_2^2 + \beta^2 + 2\lambda_2\beta\sin\theta_2 \tag{C-3}$$

The subscripts on the right side have been added to identify waves caused by stator (blade row 2) loading waves. M_{r2} is the relative Mach number at the stator. The reduced frequency and transverse wavenumber are

$$\lambda_2 = \frac{nB_1(\Omega_1 - \Omega_2)c_2}{W_2} \tag{C-4}$$

and

$$\beta = \beta c_2 \tag{C-5}$$

In terms of the dimensionless quantities $\bar{c}_2 = c_2/R$ and $\beta_{nk} = \beta R$, the reduced frequency can be rewritten as

$$\lambda_2 = n\,\Lambda_2 \bar{c}_2 \tag{C-6}$$

where

$$\Lambda_2 = \frac{B_1(M_{y1} - M_{y2})}{M_{r2}} \tag{C-7}$$

and where $M_{y1}=\Omega_1 R/a$ and $M_{y2}=\Omega_2 R/a$ are the rotor and "stator" rotational Mach numbers. (Recall from appendix A that this analysis applies to counter rotation systems; however, for convenience, the downstream blade row is called the stator.) Now, the normalized velocity components for the upstream-going pressure waves can be written

$$V_1 \equiv \frac{v_1'}{\beta_{nk}} = \frac{1}{2\bar{A}_2}\left(-\beta_{nk} - n\Lambda_2 \sin\theta_2 + \frac{n\Lambda_2 \beta_{nk}\cos\theta_2}{ROOT}\right) \tag{C-8}$$

and for the downstream-going pressure waves

$$V_2 \equiv \frac{v_2'}{\beta_{nk}} = \frac{1}{2\bar{A}_2}\left(+\beta_{nk} + n\Lambda_2 \sin\theta_2 + \frac{n\Lambda_2 \beta_{nk}\cos\theta_2}{ROOT}\right) \tag{C-9}$$

Normalization by β_{nk} is needed for cases when $\beta_{nk} = 0$. In these cases, v_1'/β_{nk} is still defined and is needed to determine the axial component and the pressure from equations 7 and 8. In equations C-8 and C-9 the complex square root is defined by

$$ROOT = \begin{cases} \sqrt{-E_2} & \textit{for propagation} \\ -i\sqrt{E_2} & \textit{for decay} \end{cases} \tag{C-10}$$

and

$$E_2 = \beta_{nk}^2 - M_{r2}^2\,\bar{A}_2 \tag{C-11}$$

$$\bar{A}_2 \equiv \frac{A_2}{\bar{c}_2^2} = n^2\Lambda_2^2 + \beta_{nk}^2 + 2n\Lambda_2\beta_{nk}\sin\theta_2 \tag{C-12}$$

For the vorticity wave, Smith's equations 24 and 28 give

$$v_3' = \frac{\lambda_2^2 + \beta\lambda_2 \sin\theta_2}{A_2} \tag{C-13}$$

The same procedure used above leads to the normalized form

$$V_3 \equiv \frac{v_3'}{\alpha_{3nk}} = -\frac{n\Lambda_2}{\bar{A}_2}\cos\theta_2 \tag{C-14}$$

The above derivation applies to waves from the stator caused by loading harmonics of order n. For rotor waves associated with rotor loading harmonic n, the derivation proceeds along the same lines but with subscripts 2 (on the right hand sides of the equations above) replaced by 1's and β_{nk} replaced by β_{kn}. The result is that common forms can be writted for the V's as follows.

$$V_1 \equiv \frac{v_1'}{\bar{\beta}} = \frac{1}{2\bar{A}}\left(-\bar{\beta} - n\Lambda\sin\theta + \frac{n\Lambda\bar{\beta}\cos\theta}{ROOT}\right) \tag{C-15}$$

$$V_2 \equiv \frac{v_1'}{\bar{\beta}} = \frac{1}{2\bar{A}}\left(+\bar{\beta} + n\Lambda\sin\theta + \frac{n\Lambda\bar{\beta}\cos\theta}{ROOT}\right) \tag{C-16}$$

$$V_3 \equiv \frac{v_3'}{\bar{\alpha}} = -\frac{n\Lambda}{\bar{A}}\cos\theta \tag{C-17}$$

with

$$\bar{A} = n^2\Lambda^2 + \bar{\beta}^2 + 2\Lambda\bar{\beta}\sin\theta \tag{C-18}$$

$$E = \bar{\beta}^2 - \bar{A}\,(M_x/\cos\theta)^2 \tag{C-19}$$

$$ROOT = \begin{cases} \sqrt{-E} & \textit{for propagation} \quad (E<0) \\ -i\sqrt{E} & \textit{for decay} \quad (E>0) \end{cases} \tag{C-20}$$

Interpretation of the above notation for waves caused by either rotor and stator loading at harmonic n is given in the table below.

	STATOR	ROTOR
$\bar{\alpha}$:	α_{3nk}	α_{3kn}
$\bar{\beta}$:	β_{nk}	β_{kn}
θ:	θ_2	θ_1
Λ:	$\frac{B_1(M_{y1}-M_{y2})}{M_{r2}}$	$\frac{B_2(M_{y1}-M_{y2})}{M_{r1}}$

In code CUP2D, V_1, V_2, and V_3 are computed in subroutine GETVS using equations C-15, C-16, and C-17.

APPENDIX D
REFLECTION AND TRANSMISSION OF WAVES AT ACTUATOR DISKS

In this report the effects of mean blade and vane loading are to modify the mean flow environment in which the acoustic waves propagate. Thus, the rotor turns its axial inflow in the swirl direction and the stator straightens the flow. Blade loading is considered the superposition of a mean loading component and the unsteady loading. Unsteady loading is distributed over the blade chords and produces small flow perturbations; however, the steady loading can be large and affects the wave propagation properties. Since the steady loading by itself does not make noise with subsonic rotors, we consider only its effect on wave propagation. For simplicity, the mean loading is concentrated in two actuator disks; one at the rotor leading edge and the other at the stator trailing edge. Smith's theory can be applied in any region where the mean flow is constant.

To treat the environment sketched in figure 7, we need to establish the boundary conditions (or jump conditions) at the disks. This done in this appendix by deriving reflection and transmission coefficients for waves incident on the two disks. As shown in the figure, the upstream-going pressure wave, v_1 can transmit a pressure wave v_4, and can reflect pressure and vorticity waves v_2 and v_3. Similar comments apply at the exit actuator disk. Boundary conditions are derived by applying conservation of mass, axial momentum, and transverse momentum at the disks for each type of wave on a mode by mode basis. These lead to reflection and transmission coefficients as defined in equations 16, 17, and 18.

Horlock (ref. 12) in his book on actuator disk theory gives the (unlinearized) 2 dimensional conservation equations as follows

$$\rho_1 u_1 = \rho_2 u_2 \qquad \text{continuity} \qquad \text{(D-1)}$$

$$-L\cos\alpha_m + \rho_1 u_1 v_1 = \rho_2 u_2 v_2 \qquad \text{transverse momentum} \qquad \text{(D-2)}$$

$$L\sin\alpha_m + p_1 + \rho_1 u_1^2 = p_2 + \rho_2 u_2^2 \qquad \text{axial momentum} \qquad \text{(D-3)}$$

where the definitions for the ρ's, u's, and v's are standard. The subscripts 1 and 2 are Horlock's and apply to conditions on the two sides of the disk in the above equations only. They should not be mistaken for 1 and 2 subscripts elsewhere in this report. The terms with the L's represent axial and transverse mean loading on the disk. These terms will be seen to drop out of the analysis via the linearization that separates steady and unsteady effects. In the following, the procedure is to linearize the continuity and momentum and equations, express the fluctuating quantities in terms of pressure and velocity components, and then apply the notation from Smith's report to represent each wave by its transverse velocity component. As indicated by Figure 7, there are three interactions to be considered, each involving an input wave and three resulting waves. For instance, at the upstream interface, the input wave v_1 produces the reflected waves v_2 and v_3 and the transmitted wave v_4. Thus, for these four waves, linearized versions of the three equations above can be used to express the resulting three waves in terms of the input wave.

Upstream-going Pressure Waves

In figure 7 the flow field is divided into regions a, b, and c. In this section we consider the jump condition at the interface between region a and region b starting with the continuity equation.

Continuity Equation

Equation D-1 can be expressed in terms of the mean and fluctuating components as follows.

$$(\rho_a + \tilde{\rho}_a)(U_a + \tilde{u}_a) = (\rho_b + \tilde{\rho}_b)(U_b + \tilde{u}_b) \tag{D-4}$$

from which the first order unsteady terms give

$$\rho_a \tilde{u}_a + U_a \tilde{\rho}_a = \rho_b \tilde{u}_b + U_b \tilde{\rho}_b \tag{D-5}$$

The mean flow quantities ρ_a, ρ_b, U_a, and U_b are considered known constants for the analysis. In order to deal with pressure rather than density for the fluctuating quantities, we apply $p = \rho a^2$ with the result

$$\rho_a \tilde{u}_a + \frac{U_a}{a_a^2} \tilde{p}_a = \rho_b \tilde{u}_b + \frac{U_b}{a_b^2} \tilde{p}_b \tag{D-6}$$

In the upstream region, only the upstream-going wave exists. For axial velocity and pressure, this can be expressed in Smith's notation as follows.

$$\begin{aligned} \tilde{u}_a &= \bar{u}_4 e^{i\alpha_4 x} \\ \tilde{p}_a &= \bar{p}_4 e^{i\alpha_4 x} \end{aligned} \tag{D-7}$$

where the remainder of the exponential, $\exp[i(\omega t + \beta y)]$, is implied and is the same throughout the field for each mode/frequency. Between the disks, all 3 waves exist as expressed by

$$\begin{aligned} \tilde{u}_b &= \bar{u}_1 e^{i\alpha_1 x} + \bar{u}_2 e^{i\alpha_2 x} + \bar{u}_3 e^{i\alpha_3 x} \\ \tilde{p}_b &= \bar{p}_1 e^{i\alpha_1 x} + \bar{p}_2 e^{i\alpha_2 x} \end{aligned} \tag{D-8}$$

Substitution of equations D-7 and D-8 into equation D-5 gives the relation between the unsteady pressures and the unsteady axial velocities

$$\rho_a \bar{u}_4 + \frac{U_a}{a_a^2} \bar{p}_4 = \rho_b (\bar{u}_1 + \bar{u}_2 + \bar{u}_3) + \frac{U_b}{a_b^2} (\bar{p}_1 + \bar{p}_2) \tag{D-9}$$

at the inlet interface (x=0). Now equations 7 and 8 from the main text can be applied to express this in terms of complex amplitudes of the transverse velocity components as follows.

$$\rho_a[\alpha_4 - \frac{U_a}{a_a^2}(\omega + U_a\alpha_4)]\frac{\bar{\nu}_4}{\beta} = \rho_b[\alpha_1 - \frac{U_b}{a_b^2}(\omega + U_b\alpha_1 + V_s\beta)]\frac{\bar{\nu}_1}{\beta}$$
$$+\rho_b[\alpha_2 - \frac{U_b}{a_b^2}(\omega + U_b\alpha_2 + V_s\beta)]\frac{\bar{\nu}_2}{\beta} \qquad \text{(D-10)}$$
$$+\rho_b[-\beta]\frac{\bar{\nu}_3}{\alpha}$$

This can be non-dimensionalized by multiplying numerators and denominators by the effective radius R. The result is

$$C_4\bar{V}_4 = C_1\bar{V}_1 + C_2\bar{V}_2 + C_3\bar{V}_3 \qquad \text{(D-11)}$$

where we have defined

$$\begin{aligned}\bar{V}_1 &= \bar{\nu}_1/(a_b\beta_{nk})\\ \bar{V}_2 &= \bar{\nu}_2/(a_b\beta_{nk})\\ \bar{V}_3 &= \bar{\nu}_3/(a_b\alpha_{3nk})\\ \bar{V}_4 &= \bar{\nu}_4/(a_a\beta_{nk})\end{aligned} \qquad \text{(D-12)}$$

and

$$\begin{aligned}C_1 &= \rho_b a_b[(1-M_b^2)\alpha_{1nk} - M_b(\Omega_{nk} + M_s\beta_{nk})]\\ C_2 &= \rho_b a_b[(1-M_b^2)\alpha_{2nk} - M_b(\Omega_{nk} + M_s\beta_{nk})]\\ C_3 &= \rho_b a_b[-\beta_{nk}]\\ C_4 &= \rho_a a_a[(1-M_a^2)\alpha_{4nk} - M_a\frac{a_b}{a_a}\Omega_{nk}]\end{aligned} \qquad \text{(D-13)}$$

We define reflection and transmission coefficients as in equation 16 of the main text

$$\begin{aligned}\bar{V}_2 &= R_{12}\bar{V}_1\\ \bar{V}_3 &= R_{13}\bar{V}_1\\ \bar{V}_4 &= T_{14}\bar{V}_1\end{aligned} \qquad \text{(D-14)}$$

These allow equation D-11 to be written in the following 2 forms

$$C_4\bar{V}_4 = (C_1 + C_2R_{12} + C_3R_{13})\bar{V}_1 \qquad \text{(D-15)}$$

and

$$(C_4 T_{14} - C_1 - C_3 R_{13}) \bar{V}_1 = C_2 \bar{V}_2 \tag{D-16}$$

which will be used later when the momentum equations have been applied.

Axial Momentum Equation

This section proceeds along the same lines as the derivation above from the continuity equation. Equation D-2, in terms of steady and fluctuating components becomes

$$L \sin\alpha_m + (P_a + \tilde{p}_a) + (\rho_a + \tilde{\rho}_a)(U_a + \tilde{u}_a)^2 = (P_b + \tilde{p}_b) + (\rho_b + \tilde{\rho}_b)(U_b + \tilde{u}_b)^2 \tag{D-17}$$

After expanding this and eliminating the unsteady densities with $\rho = p / a^2$, the first order unsteady equation is found to be

$$(1 + M_a^2)\tilde{p}_a + 2\rho_a U_a \tilde{u}_a = (1 + M_b^2)\tilde{p}_b + 2\rho_b U_b \tilde{u}_b \tag{D-18}$$

As anticipated above, L has dropped out and need not be specified. (The *effects* of L are seen, however, through the mean flow parameters.) The same procedure followed above in arriving at equation D-11 lead to

$$F_4 \bar{V}_4 = F_1 \bar{V}_1 + F_2 \bar{V}_2 + F_3 \bar{V}_3 \tag{D-19}$$

$$\begin{aligned}
F_1 &= \rho_b a_b [(1 + M_b^2)(\Omega_{nk} + M_s \beta_{nk}) - (1 - M_b^2) M_b \alpha_{1nk}] \\
F_2 &= \rho_b a_b [(1 + M_b^2)(\Omega_{nk} + M_s \beta_{nk}) - (1 - M_b^2) M_b \alpha_{2nk}] \\
F_3 &= \rho_b a_b [2 M_b \beta_{nk}] \\
F_4 &= \rho_a a_a [(1 + M_a^2)\Omega_{nk} - (1 - M_a^2)\frac{a_a}{a_b} M_a \alpha_{4nk}]
\end{aligned} \tag{D-20}$$

The reflection and transmission coefficients of equation 16 produce the final results of this section.

$$F_4 \bar{V}_4 = (F_1 + F_2 R_{12} + F_3 R_{13}) \bar{V}_1 \tag{D-21}$$

and

$$(F_4 T_{14} - F_1 - F_3 R_{13}) \bar{V}_1 = F_2 \bar{V}_2 \tag{D-22}$$

These will be used to find the forms for R_{12}, R_{13}, and T_{14} at the end of the next section.

Transverse Momentum Equation

In terms of steady and fluctuating parts, equation D-3 becomes

$$-L\cos\alpha_m + (\rho_a + \tilde{\rho}_a)(U_a + \tilde{u}_a)(V_a + \tilde{v}_a) = (\rho_b + \tilde{\rho}_b)(U_b + \tilde{u}_b)(V_b + \tilde{v}_b) \tag{D-23}$$

Note that in the inlet region the transverse velocity $V_a = 0$ and in the swirl region $V_b = V_s$. Then, by the same procedures used above, the first order unsteady equation is found to be

$$\rho_a U_a \tilde{v}_a = \rho_b U_b \tilde{v}_b + \rho_b V_s \tilde{u}_b + M_b M_s \tilde{p}_b \tag{D-24}$$

With the same definitions used above, this becomes

$$G_4 \bar{V}_4 = G_1 \bar{V}_1 + G_2 \bar{V}_2 + G_3 \bar{V}_3 \tag{D-25}$$

with

$$\begin{aligned} G_1 &= \rho_b a_b[-M_b M_s(\Omega_{nk} + M_s\beta_{nk}) + M_b\beta_{nk} + (1 - M_b^2)M_s\alpha_{1nk}] \\ G_2 &= \rho_b a_b[-M_b M_s(\Omega_{nk} + M_s\beta_{nk}) + M_b\beta_{nk} + (1 - M_b^2)M_s\alpha_{2nk}] \\ G_3 &= \rho_b a_b[M_b\alpha_{3nk} - M_s\beta_{nk}] \\ G_4 &= \rho_a a_a[\frac{a_a}{a_b} M_a\beta_{nk}] \end{aligned} \tag{D-26}$$

In terms of the reflection and transmission coefficients

$$G_4 \bar{V}_4 = (G_1 + G_2 R_{12} + G_3 R_{13})\bar{V}_1 \tag{D-27}$$

and

$$(G_4 T_{14} - G_1 - G_3 R_{13})\bar{V}_1 = G_2 \bar{V}_2 \tag{D-28}$$

Coefficients for Inlet Disk

The preceeding equations have been derived in a form convenient for the elimination of the $\bar{V}$'s. For instance, division of equation D-15 by equation D-21 eliminates $\bar{V}_1$ and $\bar{V}_4$. Continuing this technique leads to equations that can be solved for the inlet transmission and reflection coefficients with the following results.

$$\begin{aligned} R_{12} &= \frac{E_2 E_3 - E_0 E_5}{E_1 E_5 - E_2 E_4} \\ R_{13} &= \frac{E_1 E_3 - E_0 E_4}{E_1 E_5 - E_2 E_4} \\ T_{14} &= \frac{E_7 E_8 - E_6 E_9}{E_4 E_9 - E_1 E_7} \end{aligned} \tag{D-29}$$

where the E coefficients are defined in terms of the previously defined C's, F's, and G's as follows.

$$
\begin{aligned}
E_0 &= C_4F_1 - C_1F_4 \\
E_1 &= C_4F_2 - C_2F_4 \\
E_2 &= C_3F_4 - C_4F_3 \\
E_3 &= C_4G_1 - C_1G_4 \\
E_4 &= C_4G_2 - C_2G_4 \\
E_5 &= C_3G_4 - C_4G_3 \\
E_6 &= C_2G_1 - C_1G_2 \\
E_7 &= C_3G_2 - C_2G_3 \\
E_8 &= C_2F_1 - C_1F_2 \\
E_9 &= C_3F_2 - C_2F_3
\end{aligned}
\qquad \text{(D-30)}
$$

Downstream-going Pressure Waves at Exit

For waves reflected at the stator exit actuator disk, the derivations are similar to that for the inlet. The major difference is that exponentials containing x do not vanish as they did at x=0. For later convenience, the exponentials are absorbed into the reflection and transmission coefficients, as will be seen below. As indicated by figure 7 for $x=x_e$, a downstream-going pressure wave ν_2 reflects an upstream-going pressure wave ν_1 and transmits a pressure wave ν_8 and a vorticity wave ν_9. Coefficients for these processes are derived next.

Continuity Equation

By analogy with equation D-6, the linearized continuity equation is

$$
\rho_b \tilde{u}_b + \frac{U_b}{a_b^2}\tilde{p}_b = \rho_c \tilde{u}_c + \frac{U_c}{a_c^2}\tilde{p}_c \qquad \text{(D-31)}
$$

Application of equations D-8 and similar equations for region c at $x=x_e$ leads to

$$
(\rho_b \bar{u}_1 + \frac{U_b}{a_b^2}\bar{p}_1)e^{i\alpha_1 x_e} + (\rho_b \bar{u}_2 + \frac{U_b}{a_b^2}\bar{p}_2)e^{i\alpha_2 x_e} = (\rho_c \bar{u}_8 + \frac{U_c}{a_c^2}\bar{p}_8)e^{i\alpha_8 x_e} + (\rho_c \bar{u}_9)e^{i\alpha_9 x_e} \qquad \text{(D-32)}
$$

As in the previous section, equations 7 and 8 from the main text are used to express this result entirely in terms of the transverse velocities. Then, with the same normalizations used above, we find

$$
C_1 \bar{V}_1 e^{i\alpha_{1nk}\bar{x}_e} + C_2 \bar{V}_2 e^{i\alpha_{2nk}\bar{x}_e} = C_8 \bar{V}_8 e^{i\alpha_{8nk}\bar{x}_e} + C_9 \bar{V}_9 e^{i\alpha_{9nk}\bar{x}_e} \qquad \text{(D-33)}
$$

where C_1 and C_2 have already been defined,

$$\bar{V}_8 = \bar{v}_8/(a_c \beta_{nk})$$
$$\bar{V}_9 = \bar{v}_9/(a_c \alpha_{9nk}) \tag{D-34}$$

and

$$C_8 = \rho_c a_c[(1 - M_c^2)\alpha_{8nk} - M_c \frac{a_b}{a_c} \Omega_{nk}]$$
$$C_9 = \rho_c a_c[-\beta_{nk}] \tag{D-35}$$

The transmission and reflection coefficients are defined with the axial exponential included

$$\bar{V}_1 e^{i\alpha_{1nk}\bar{x}_e} = R_{21} \bar{V}_2 e^{i\alpha_{2nk}\bar{x}_e}$$
$$\bar{V}_8 e^{i\alpha_{8nk}\bar{x}_e} = T_{28} \bar{V}_2 e^{i\alpha_{2nk}\bar{x}_e} \tag{D-36}$$
$$\bar{V}_9 e^{i\alpha_{9nk}\bar{x}_e} = T_{29} \bar{V}_2 e^{i\alpha_{2nk}\bar{x}_e}$$

When these definitions are applied to equation D-33, the following two equations can be derived

$$(C_1 R_{21} + C_2 - C_9 T_{29}) \bar{V}_2 e^{i\alpha_{2nk}\bar{x}_e} = C_8 \bar{V}_8 e^{i\alpha_{8nk}\bar{x}_e}$$
$$C_1 \bar{V}_1 e^{i\alpha_{1nk}\bar{x}_e} = (C_8 T_{28} + C_9 T_{29} - C_2) \bar{V}_2 e^{\alpha_{2nk}\bar{x}_e} \tag{D-37}$$

for use below.

Axial Momentum Equation

Proceeding along lines similar to the above derivations for the axial momentum equation, we define

$$F_8 = \rho_c a_c[(1 + M_c^2)\Omega_{nk} - (1 - M_c^2) \frac{a_c}{a_b} M_c \alpha_{8nk}]$$
$$F_9 = \rho_c a_c[2 \frac{a_c}{a_b} M_c \beta_{nk}] \tag{D-38}$$

and use the coefficients defined in equation D-35 to establish

$$F_1 \bar{V}_1 e^{i\alpha_{1nk}\bar{x}_e} = (F_8 T_{28} - F_2 + F_9 T_{29}) \bar{V}_2 e^{i\alpha_{2nk}\bar{x}_e}$$
$$(F_1 R_{21} + F_2 - F_9 T_{29}) \bar{V}_2 e^{i\alpha_{2nk}\bar{x}_e} = F_8 \bar{V}_8 e^{i\alpha_{8nk}\bar{x}_e} \tag{D-39}$$

which also will be used shortly.

Transverse Momentum Equation

Here we define

$$G_8 = \rho_c a_c \left[\frac{a_c}{a_b} M_c \beta_{nk} \right]$$
$$G_9 = \rho_c a_c \left[\frac{a_c}{a_b} M_c \alpha_{9nk} \right] \qquad \text{(D-40)}$$

From which it follows that

$$(G_1 R_{21} + G_2 - G_9 T_{29}) \bar{V}_2 e^{i\alpha_{2nk}\bar{x}_e} = G_8 \bar{V}_8 e^{i\alpha_{8nk}\bar{x}_e}$$
$$G_1 \bar{V}_1 e^{i\alpha_{1nk}\bar{x}_e} = (G_8 T_{28} + G_9 T_{29} - G_2) \bar{V}_2 e^{i\alpha_{2nk}\bar{x}_e} \qquad \text{(D-41)}$$

Now equations D-37, D-39, and D-41 can be manipulated to find the desired coefficients as follows

$$R_{21} = \frac{E_{15}E_{16} - E_{14}E_{17}}{E_{12}E_{15} - E_{10}E_{17}}$$
$$T_{28} = \frac{E_6 E_{11} - E_8 E_{13}}{E_{10}E_{13} - E_{11}E_{12}} \qquad \text{(D-42)}$$
$$T_{29} = \frac{E_6 E_{10} - E_8 E_{12}}{E_{10}E_{13} - E_{11}E_{12}}$$

where

$$E_{10} = C_1 F_8 - C_8 F_1$$
$$E_{11} = C_9 F_1 - C_1 F_9$$
$$E_{12} = C_1 G_8 - C_8 G_1$$
$$E_{13} = C_9 G_1 - C_1 G_9 \qquad \text{(D-43)}$$
$$E_{14} = C_8 F_2 - C_2 F_8$$
$$E_{15} = C_8 F_9 - C_9 F_8$$
$$E_{16} = C_8 G_2 - C_2 G_8$$
$$E_{17} = C_8 G_9 - C_9 G_8$$

Vorticity Waves at Exit

For this interaction, the derivation is the same as for the pressure wave at the inlet except the input wave is different. We quote only the results. The reflection and transmission coefficients are

$$R_{31} = \frac{E_{15}E_{19} - E_{17}E_{18}}{E_{12}E_{15} - E_{10}E_{17}}$$
$$T_{38} = \frac{E_{11}E_{21} - E_{13}E_{20}}{E_{11}E_{12} - E_{10}E_{13}} \qquad \text{(D-44)}$$
$$T_{39} = \frac{E_{10}E_{19} - E_{12}E_{18}}{E_{10}E_{17} - E_{12}E_{15}}$$

where

$$E_{18} = C_8F_3 - C_3F_8$$
$$E_{19} = C_8G_3 - C_3G_8 \qquad \text{(D-45)}$$
$$E_{20} = C_1F_3 - C_3F_1$$
$$E_{21} = C_1G_3 - C_3G_1$$

and where the C's, F's, and G's and the rest of the E's have already been defined.

This completes derivation of the reflection and transmission coefficients for waves impinging on the actuator disks. The coefficients are given in equations D-29, D-42 and D-44 in terms of coefficients defined by equations D-13, D-20, D-26, D-35, D-38, D-40, D-30, and D-43. These are all computed in subroutine RTCOEF in the code CUP2D.

APPENDIX E
FORMULAS FOR VISCOUS WAKES

In the main text, the method of inverting the matrix equations for the coupled loading was described in conjunction with equation 56. This equation requires a vector of upwash velocities *WWS(n,i)* at the stator caused by viscous wakes from the rotor. n denotes the harmonic order and i denotes the control point on the stator. This appendix derives the working form of these formulas for use in code CUP2D based on the viscous wake correlation of Silverstein, Katzoff, and Bullivant (ref. 13).

Figure E-1 shows the variables for the derivation. The objective is to start with a spatial description of the wake velocity defect fixed in the rotor frame, convert this to a waveform of upwash in the stator frame via coordinate transformation, and then Fourier analyze this to find the desired harmonics. From the sketch with the airfoil and wake in Figure E-1, the form of the defect is given by

$$\frac{w_v}{w_c} = \exp[-\pi\,(\bar{y}/Y)^2] \tag{E-1}$$

where the maximum defect is given by

$$\frac{w_c}{W_1} = \frac{1.21\sqrt{C_D}}{\hat{z}_1 - 0.70} \tag{E-2}$$

and the wake width parameter by

$$\frac{Y}{c_1} = 0.68\sqrt{C_D\,(\hat{z}_1 - 0.85)} \tag{E-3}$$

The last two formulas give the decay in magnitude and spread in width as a function of chordwise distance measured from the leading edge. $\hat{z}$ is normalized chordwise distance z_1/c_1 and C_D is the standard isolated airfoil drag coefficient defined by C_D = (drag/unit span)/(½ρU^2*chord).

Wake decay and spread are to be specified at the point where the wake is intercepted on the stator. This can be found by relating the chordwise positions to the x direction as follows

$$z_1 \cos\theta_1 = x_s + z_2 \cos\theta_2 \tag{E-4}$$

In terms of normalized quantities, this leads to

$$\hat{z}_1 = \frac{\bar{x}_s + \hat{z}_2\,\bar{c}_2 \cos\theta_2}{\bar{c}_1 \cos\theta_1} \tag{E-5}$$

To obtain the waveform in the stator frame, we note that the relative motion of the two blade rows can be specified in terms of y_1 and y_2, and then we locate the position in the wake $\bar{y}$ in terms of y_1 for a fixed x as follows

$$y_1 = x\tan\theta_1 + \bar{y}/\cos\theta_1 \tag{E-6}$$

And since

$$y_2 = y_1 + (\Omega_1 - \Omega_2)Rt = y_1 + \Omega Rt \tag{E-7}$$

it follows that

$$\bar{y} = y_2\cos\theta_1 - \cos\theta_1\,\Omega Rt - x\sin\theta_1 \tag{E-8}$$

By expressing x and y_2 in terms of z_2 and substituting into equation E-1, the wake waveform in the stator frame can now be written

$$w_v(t) = w_c\, f(t) \tag{E-9}$$

where

$$f(t) = \exp\left\{-\pi\left[\frac{\sin(\theta_2-\theta_1)\,z_2 - x_s\sin\theta_1 - \cos\theta_1\,\Omega Rt}{Y}\right]^2\right\} \tag{E-10}$$

If we recognize that this one pulse in a periodic waveform of period $2\pi/B_1\Omega$, it is a straightforward matter to express $f(t)$ in a Fourier series of the following form

$$f(t) = \sum_{n=1}^{\infty} F_n\, e^{inB_1\Omega t} \tag{E-11}$$

where, as usual, the real part is implied. The usual Fourier integral formulas lead to

$$F_n = \frac{2\sqrt{\pi}}{Q}\exp[-(\pi n/Q)^2]\; e^{inB_1[-\hat{z}_2\bar{c}_2\sin(\theta_2-\theta_1) + \bar{x}_s\sin\theta_1]/\cos\theta_1} \tag{E-12}$$

where

$$Q = \sqrt{\pi}\left(\frac{SC_1}{Y/c_1}\right)\cos\theta_1 \tag{E-13}$$

Now, we have only to find the component of w_v normal to the stator chord. This is given by $w_v \sin(\theta_2-\theta_1)$. Hence, the desired upwash harmonics can now be written

$$\left(\frac{w_{vs}}{W_2}\right)_n = \frac{w_c}{W_1}\frac{\cos\theta_2}{\cos\theta_1}\sin(\theta_2-\theta_1)\,F_n \tag{E-14}$$

where, for convenience, we have used $W_1/W_2 = \cos\theta_2/\cos\theta_1$. When w_c/W_1 and Y/c_1 are evaluated from equations E-2, E-3, and E-12 at values of $\hat{z}_2$ corresponding to the control points z_i used by Smith, the result is $WWS(n,i)$ as needed for inversion of the matrix equation.

The above formulas are equivalent to those used by Kaji and Okazaki except that we retain the absolute phase. In code CUP2D, the above formulas are coded in subroutine GTWAKE.

APPENDIX F
LIST OF SYMBOLS*

a = local speed of sound
c = blade chord
c_1, c_2 = rotor, stator chord
i = index to count control points on blades and vanes
j = index to count loading panels on blades and vanes
k = cascade index
m = nB_1-kB_2, circumferential mode order
n = loading harmonic index
p = disturbance (acoustic) pressure
u = axial component of disturbance velocity
v = transverse component of disturbance velocity
v' = Smith's basic solution for the transverse velocity, see appendix C
s = blade gap (spacing between blades or vanes in y direction
t = time
w_c = maximum velocity defect on viscous wake centerline
w_v = velocity profile in viscous wake definition
x = axial coordinate
x_e = axial distance from leading edge of rotor to trailing edge of stator
x_s = axial distance from leading edge of rotor to leading edge of stator
y = transverse coordinate
z_o, z_{oj} = source coordinate measured in chordwise direction (at angle θ to axial direction)

B_1 = number of blades on upsteam blade row (which is usually called the rotor)
B_2 = number of blades on downsteam blade row (which is usually called the stator)
BPF = blade passing frequency
L = discretized loading source
LR, LS = loading elements on rotor, stator
M = Mach number
M_r = Mach number relative to blade, W/a
M_s = Mach number of the mean flow in the swirl (y) direction
M_{y1} = rotational Mach number of upstream blade row (normally the rotor)
M_{y2} = rotational Mach number of downstream blade row (normally =0 for the stator)
N_h = number of loading harmonics included in coupling
N_p = number of panels on rotor (same as number of panels on stator)
PWL = sound power level in dB, see equation 114
R = effective radius of annulus, used to convert transverse linear coordinate to angle, $\phi=y/R$
R_{12},etc = modal reflection coefficient, see equation 16 and appendix D
SC = spacing to chord ratio, s/c
T_{14},etc = modal transmission coefficient, see equation 16 and appendix D
U = axial component of mean (background) flow
V = transverse component of mean (background) flow, relative to the blades
V_s = transverse component of the mean swirl flow, absolute frame
W = $[U^2+V^2]^{1/2}$ = mean flow speed
WR,WS= upwash velocity (normalized) on rotor, stator

* Note, the analysis of this report applies to counter rotation stages; however, for convenience, the upstream blade row is called the rotor and the downstream blade row is called the stator.

α = axial wavenumber
β = transverse wavenumber
β_{nk} = $-(nB_1-kB_2)$
θ = cascade angle (determined by U and V)
ω = angular frequency
ρ_a,ρ_b,ρ_c = mean density in regions A, B, C
ρ_o = local mean density
σ = interblade phase angle
ϕ = angle in cylindrical coordinates
ψ = kinematic phase, see equation 11
ψ_{nk} = see equations A-17 and A-18 (has different forms in different coordinate systems)

Γ = vorticity (loading source)
Ω = angular speed of rotor
Ω_{nk} = non-dimensional frequency, see equation B-2

Subscripts

1 denotes upstream-going pressure wave in region B, also denotes rotor
2 denotes downstream-going pressure wave in region B, also denotes stator
3 denotes vorticity pressure wave in region B
4 denotes upstream-going pressure wave in region A
5 denotes downstream-going pressure wave in region A
6 denotes vorticity pressure wave in region A
7 denotes upstream-going pressure wave in region C
8 denotes downstream-going pressure wave in region C
9 denotes vorticity pressure wave in region C
a denotes condition for region A (upstream of rotor leading edge)
b denotes condition for region B (between rotor leading edge and stator trailing edge)
c denotes condition for region C (downstream of stator trailing edge); also used in w_c, the maximum velocity defect on the wake centerline.
i = index to count control points on blades and vanes; also, imaginary unit
j = index to count loading panels on blades and vanes
k = cascade index
n = loading harmonic index
r denotes rotor
rr denotes effect of rotor on rotor
rs denotes effect of rotor on stator
sr denotes effect of stator on rotor
ss denotes effect of stator on stator
s denotes tangential (swirl) component, also denotes stator
x denotes axial component
R, I denote real and imaginary parts of a comlex quantity

overbar denotes normalization by effective radius, R for x's and c's
$(\,)^*$ denotes complex conjugate

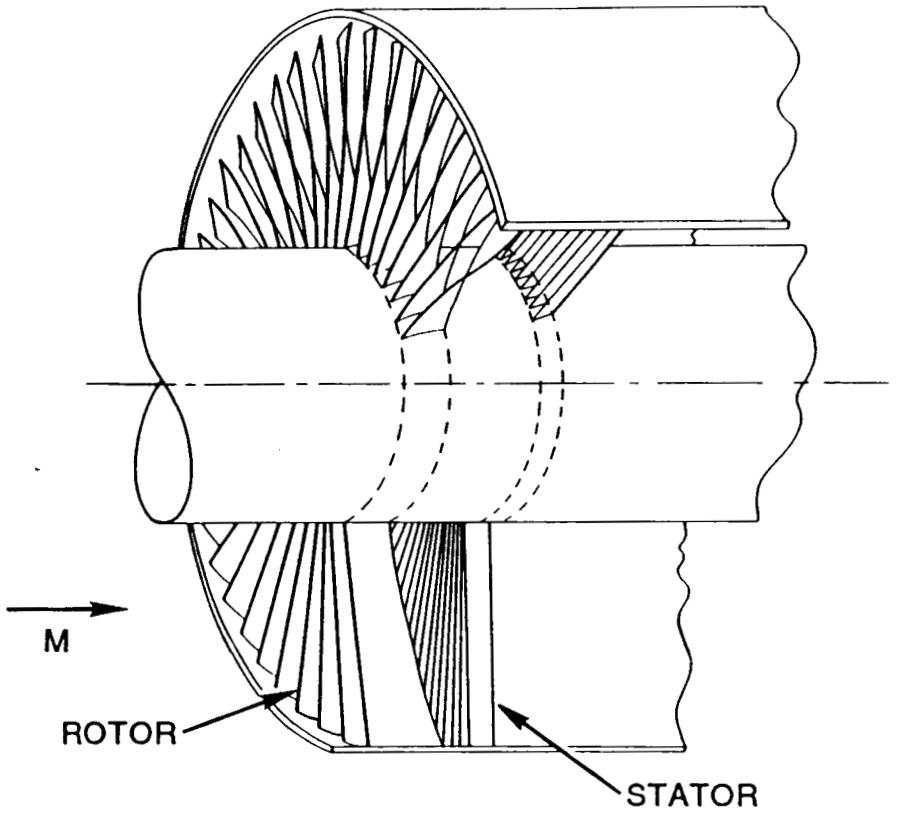

Figure 1. Three-dimensional rotor and stator geometry (ref. 3).

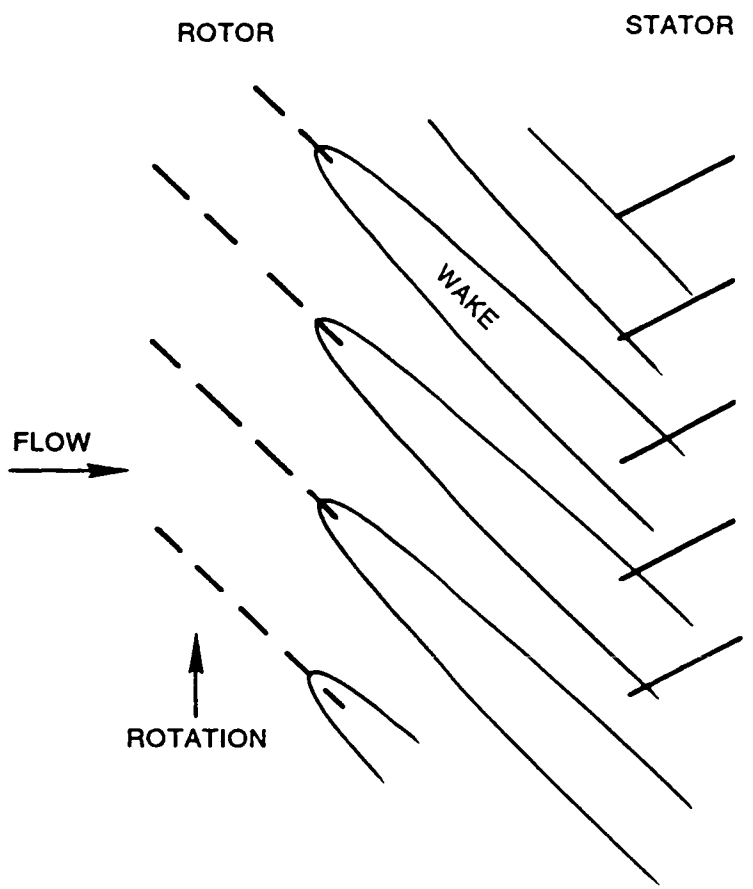

Figure 2. Simple rotor/stator interaction model. Dashed blades indicate that their role is only to generate wakes. They are transparent to acoustic waves.

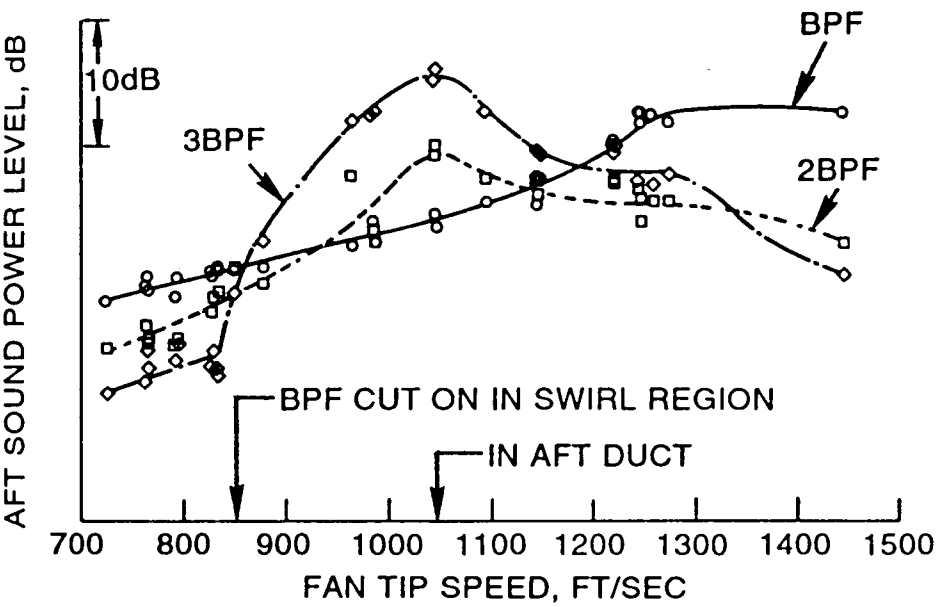

Figure 3. Aft radiated sound power levels from engine designed for BPF cut-off. (Topol, *et al.*, ref. 5).

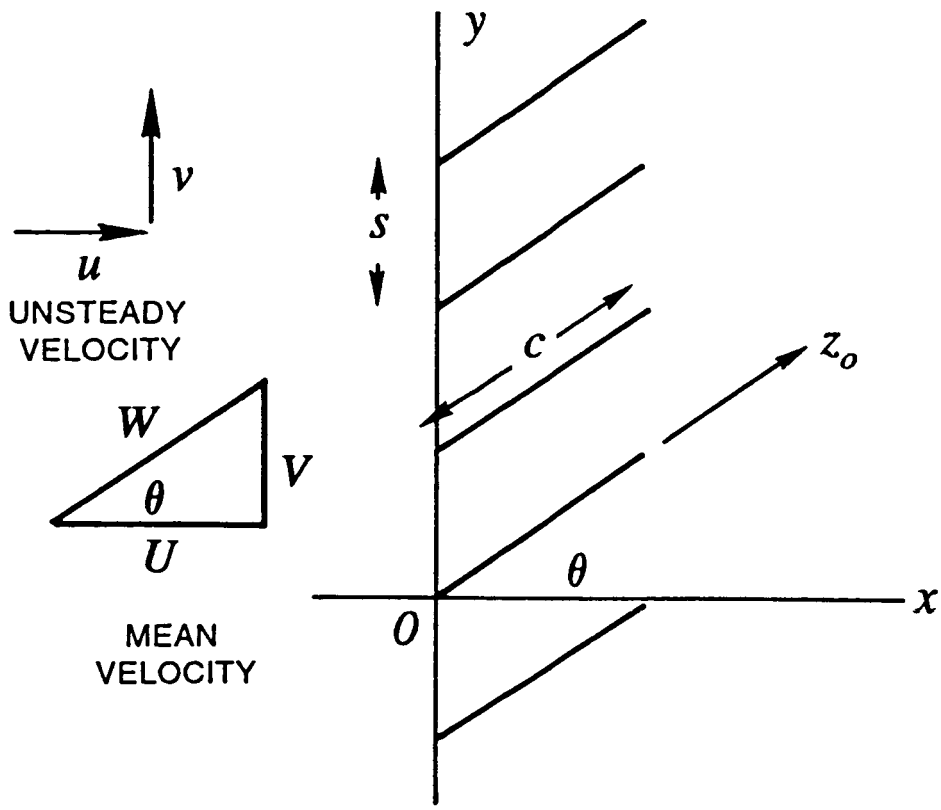

Figure 4. Two-dimensional geometry of Smith's theory (ref. 7).

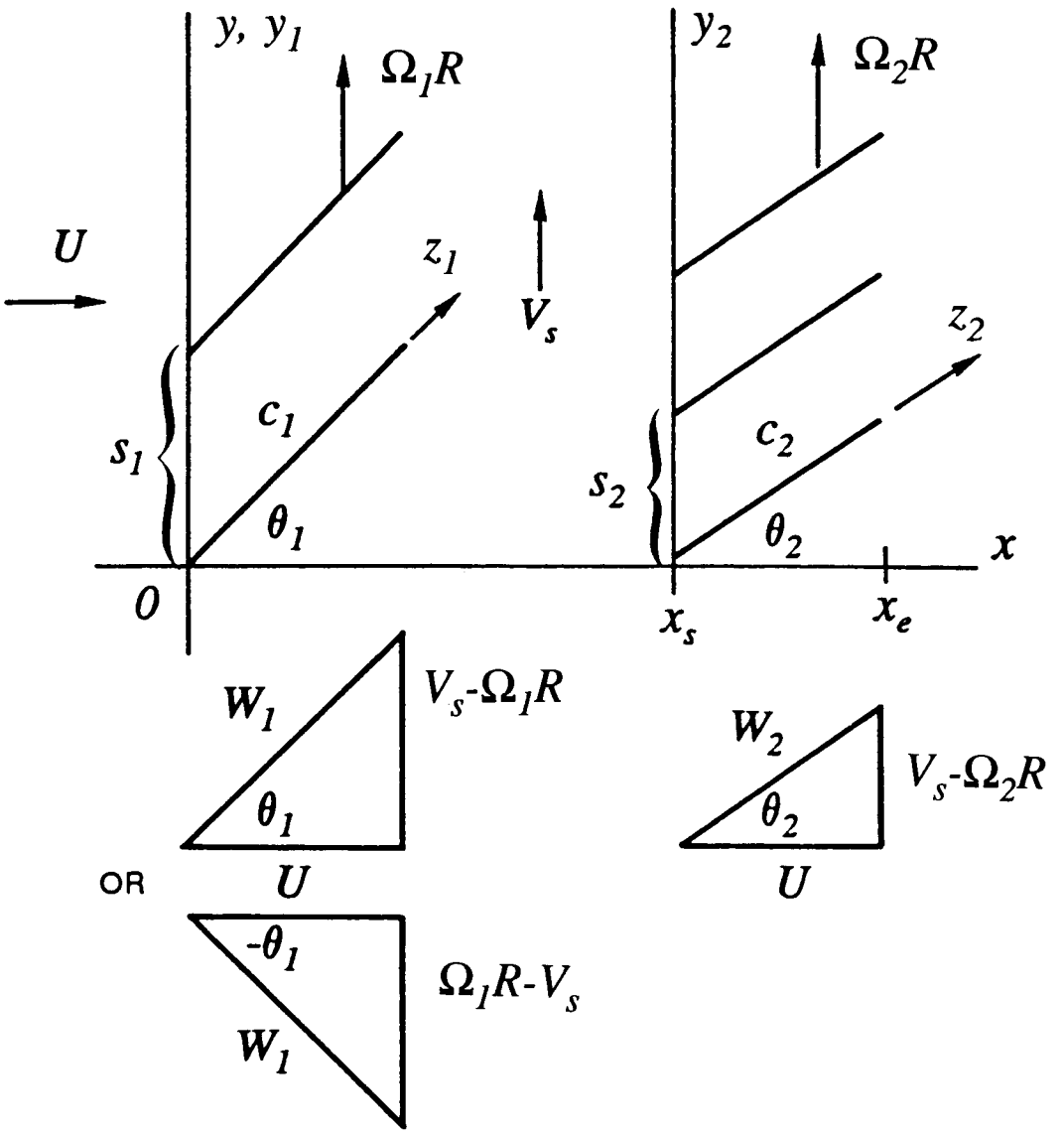

Figure 5. Geometry for coupled cascade analysis shown at t=0. Either blade row or both blade rows can rotate. Note that θ_1 is normally negative. Also, if the downstream blade row rotates, Ω_2 would be negative.

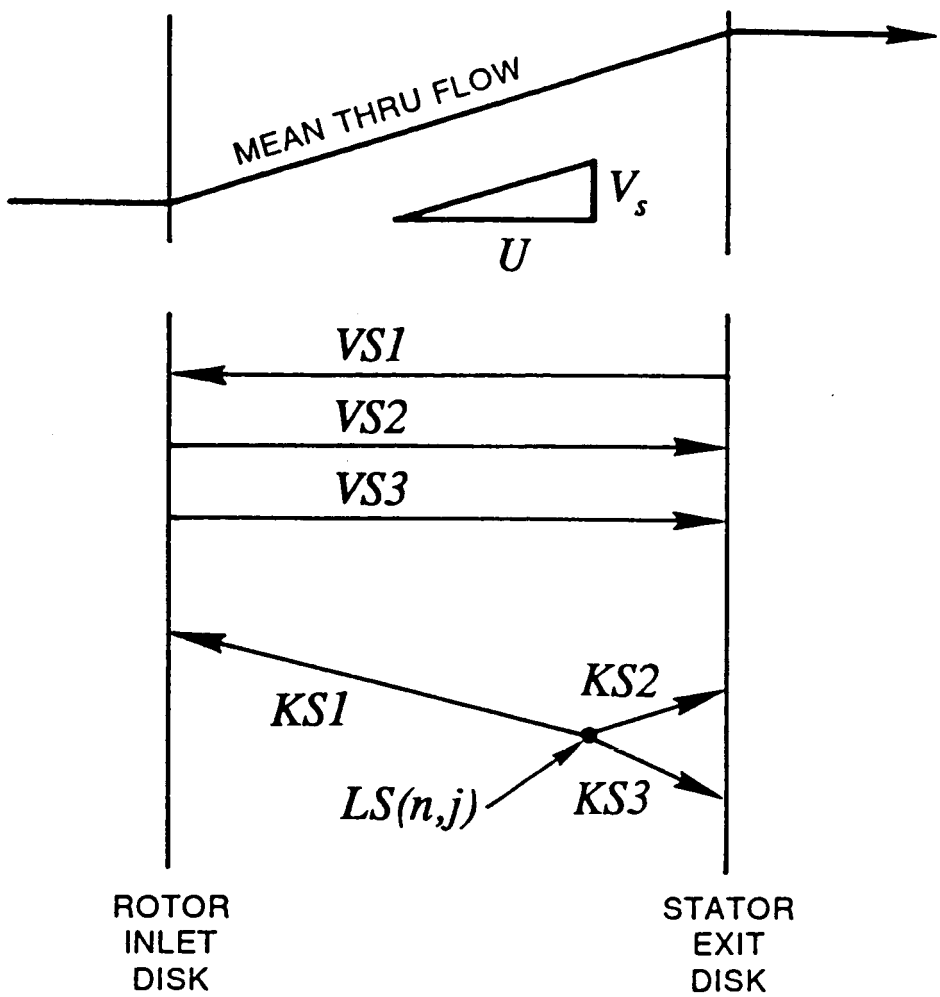

Figure 6. Direct waves (*KS1, KS2, KS3*) from load element *LS(n,j)* and waves reflected (*VS1, VS2, VS3*) from actuator disks. Note that the entire wave system is driven by *LS(n,j)*.

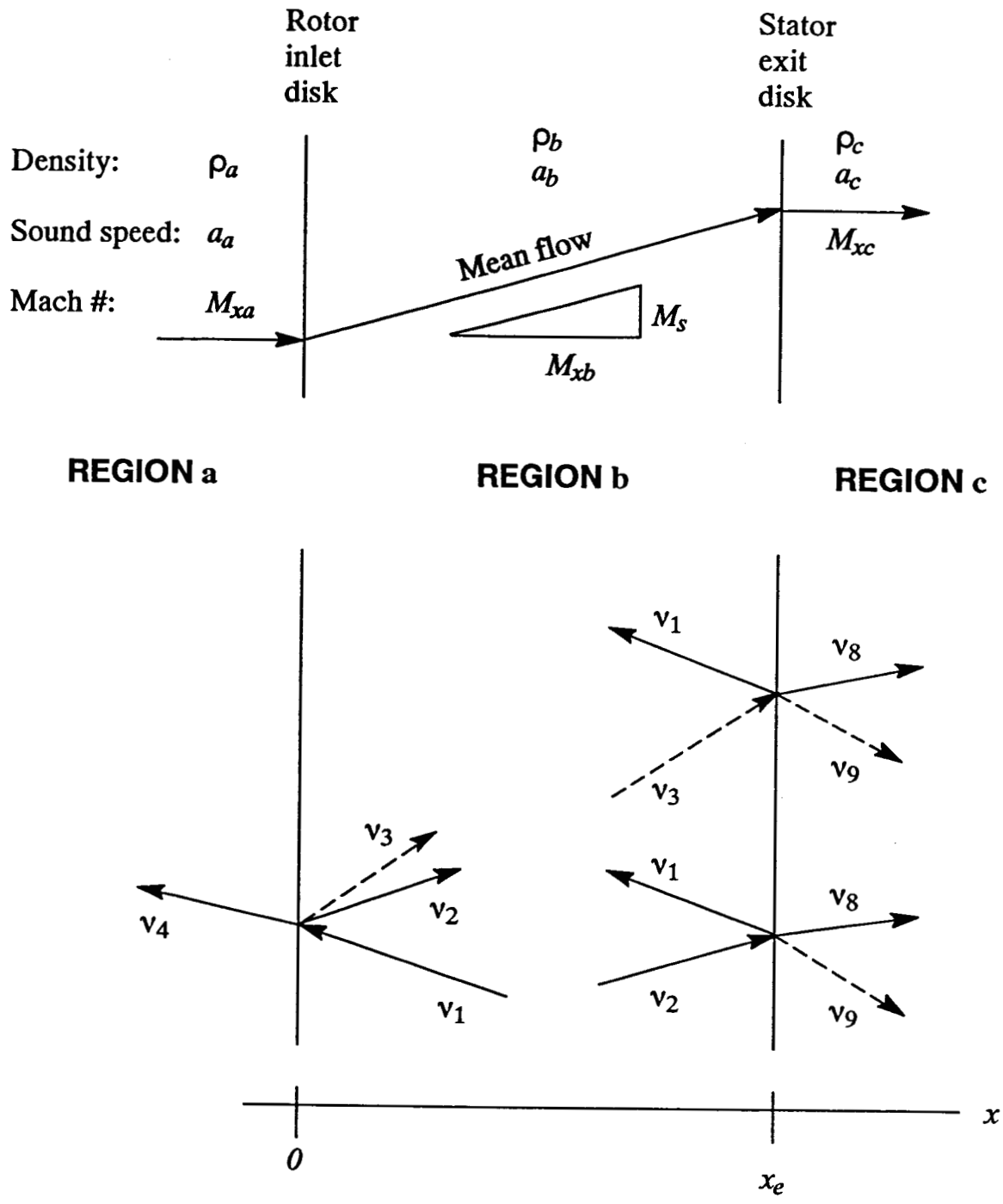

Figure 7. Three types of reflection/transmission included in the method. v_1, v_2, v_4, v_8 are the transverse velocity in the pressure waves (denoted by solid arrows). The dashed arrows denote vorticity waves with transverse velocity v_3 and v_9.

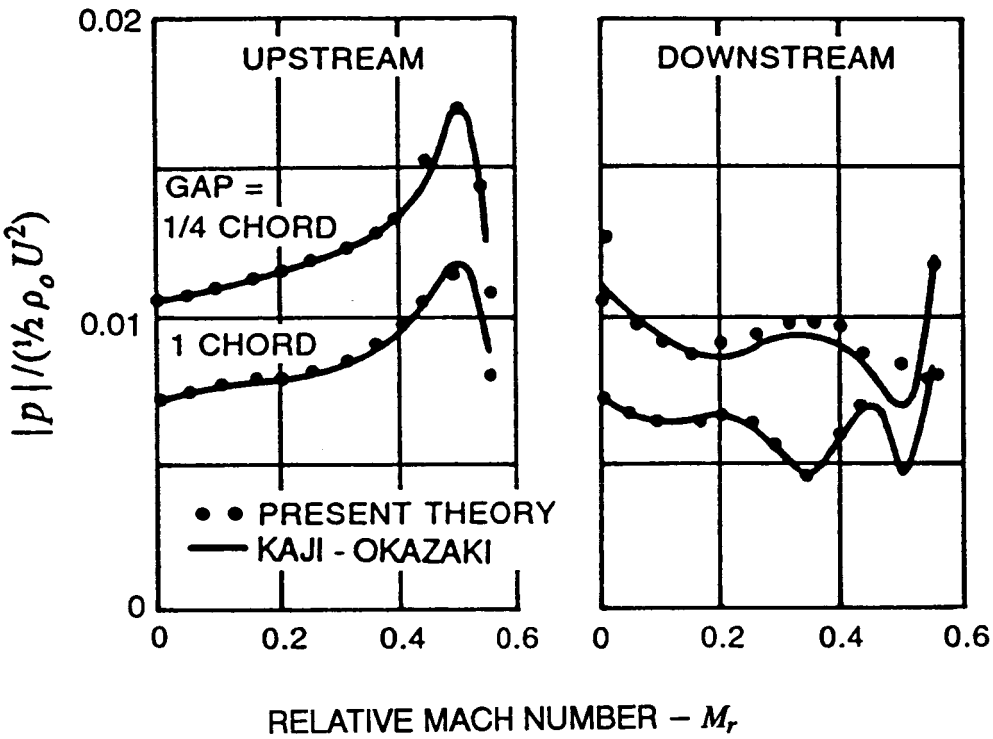

Figure 8. Comparison with Kaji and Okazaki theory for IGV/rotor interaction. Gap/chord ratio = 1.0 for both blade rows. Also, $B_1=B_2$. Drag coefficient = 0.02.

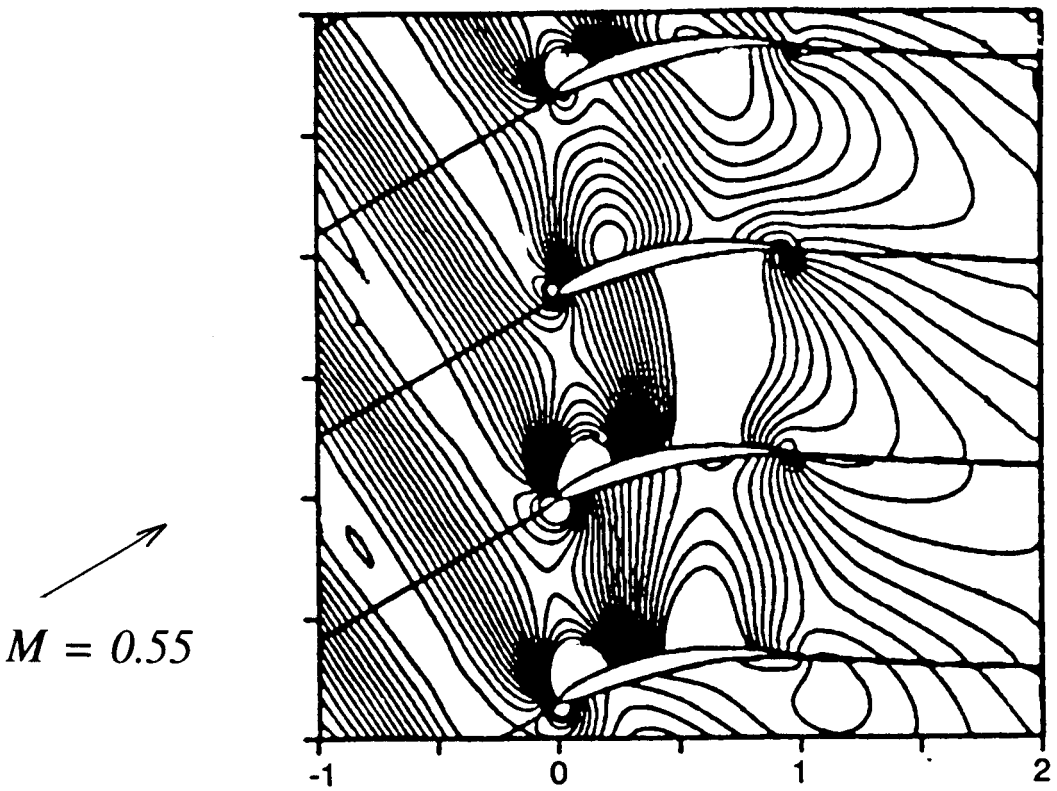

Figure 9. Computed results of Kousen and Verdon (ref. 11) using LINFLO for stator excited by vorticity wave. Plots shows the resulting pressure wave, which is cut on upstream and cut off downstream.

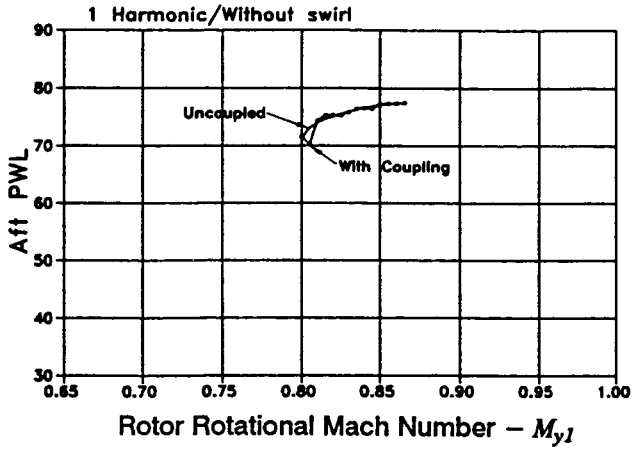

a) Effect of coupling for one harmonic only without swirl.

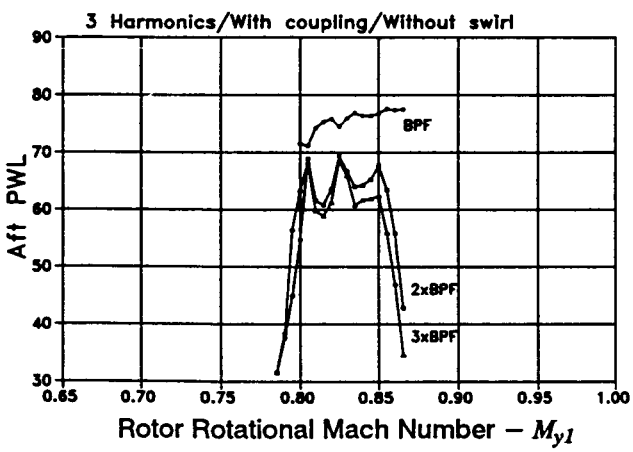

b) Effect of coupling (and frequency scattering) without swirl.

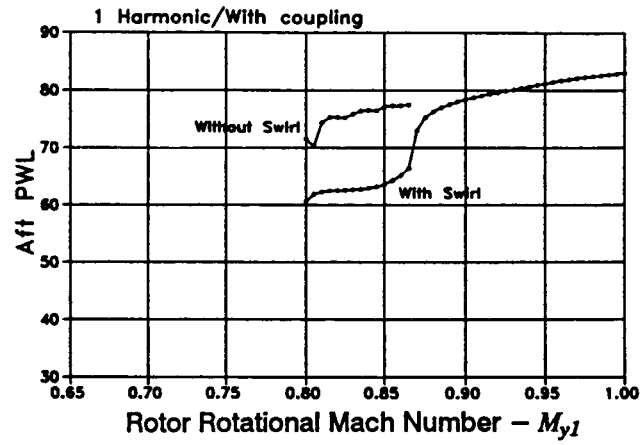

c) Effect of swirl for one harmonic with coupling. (Note: Major effect is that cascade angles change with swirl angle.)

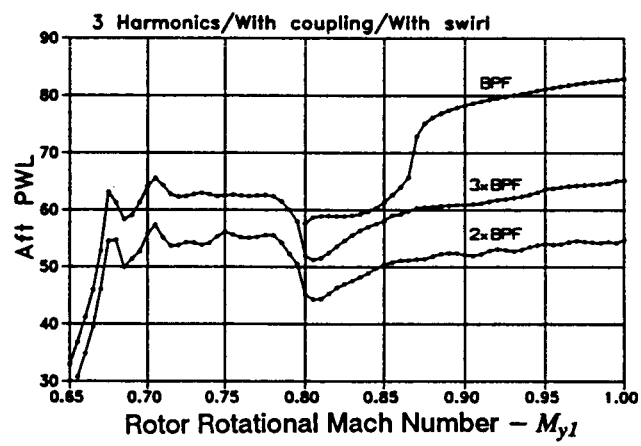

d) Effect of coupling with swirl. (All effects included.)

Figure 10. Computed results showing the effects of unsteady coupling, frequency scattering, and swirl on the harmonic power levels propagated downstream. B_1=38, B_2=72, N_p=30, $BVGAP$=2.0. Excitation by wake fundamental harmonic only. PWL defined in equation 114.

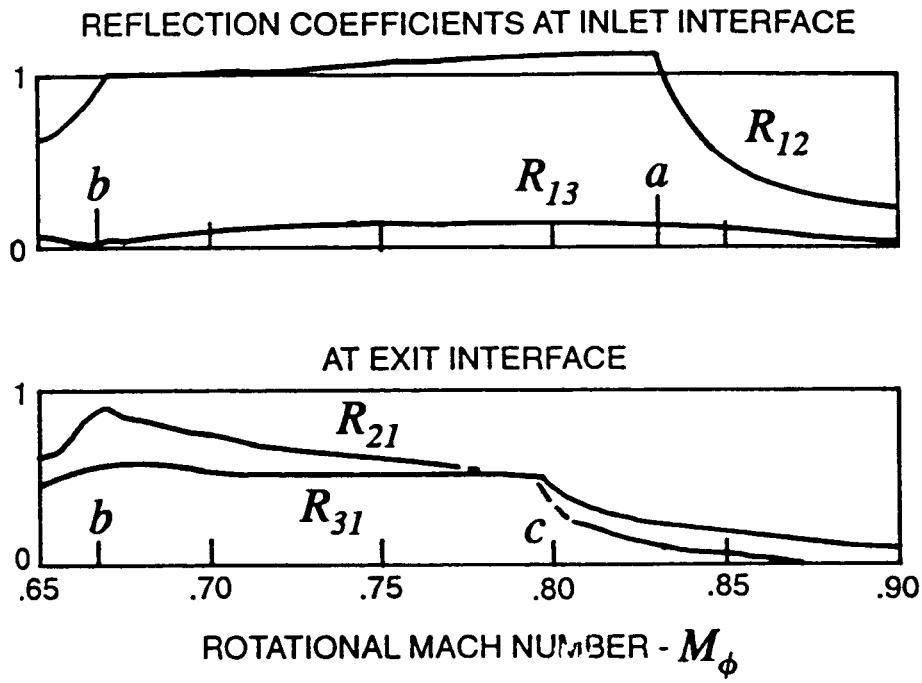

Figure 11. Absolute value of reflection coefficients for n,k mode. a,b,c denote cuton speeds for the mode in the upstream, interstage, and downstream regions.

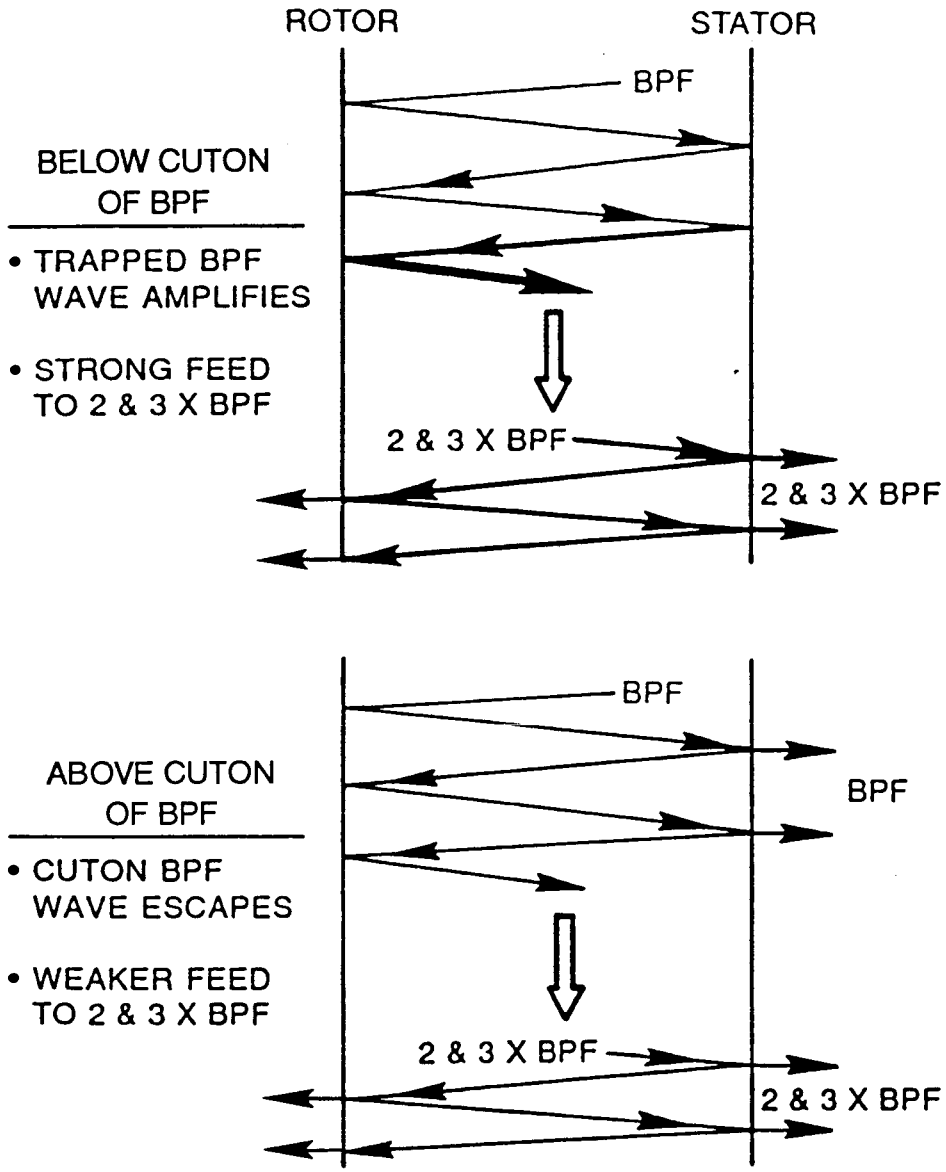

Figure 12. Physical model of mode trapping mechanism.

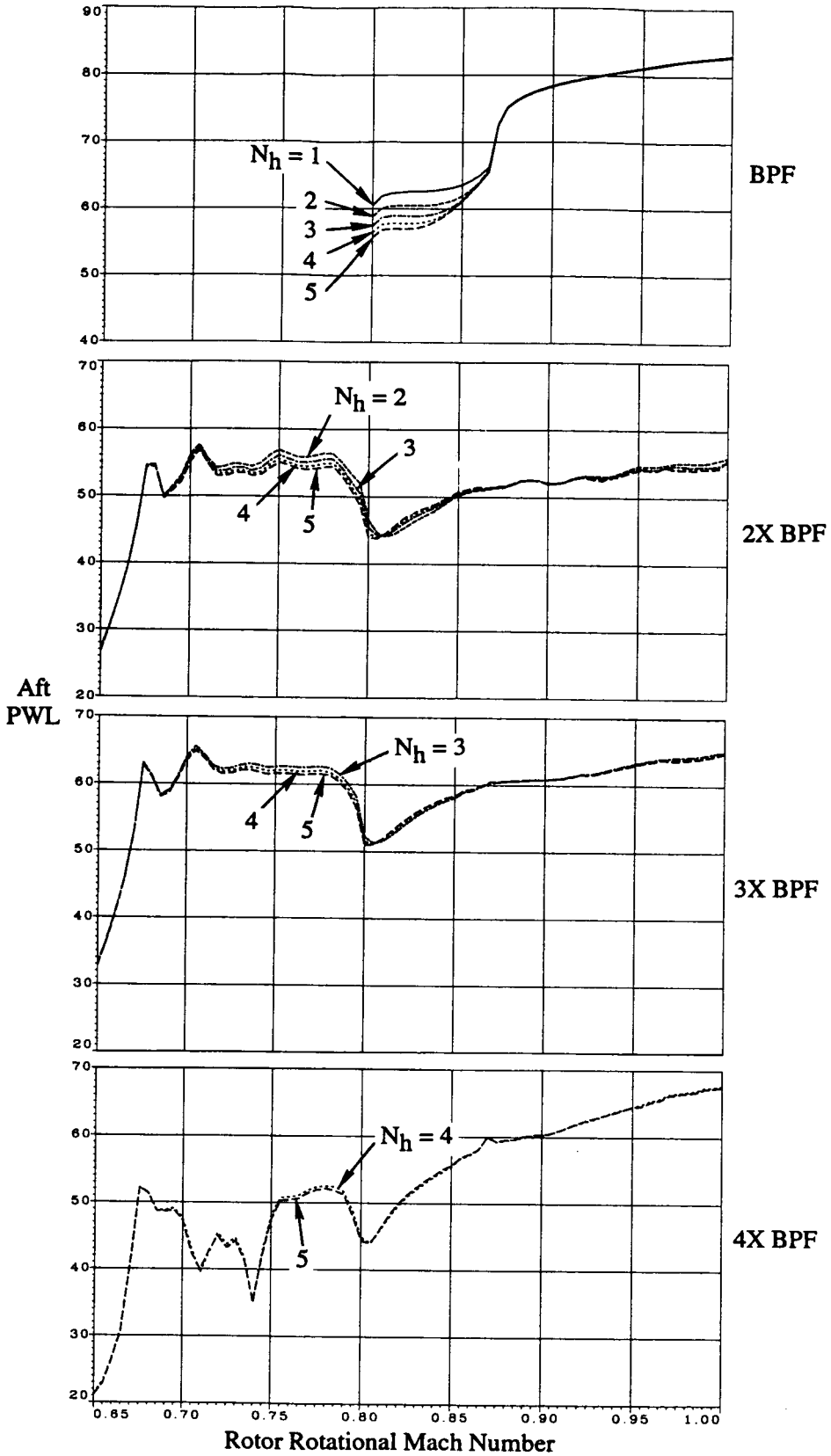

Figure 13. Influence on harmonic levels of N_h, the number of harmonics included in the analysis. B_1=38, B_2=72, N_p=50, *BVGAP*=2.0.

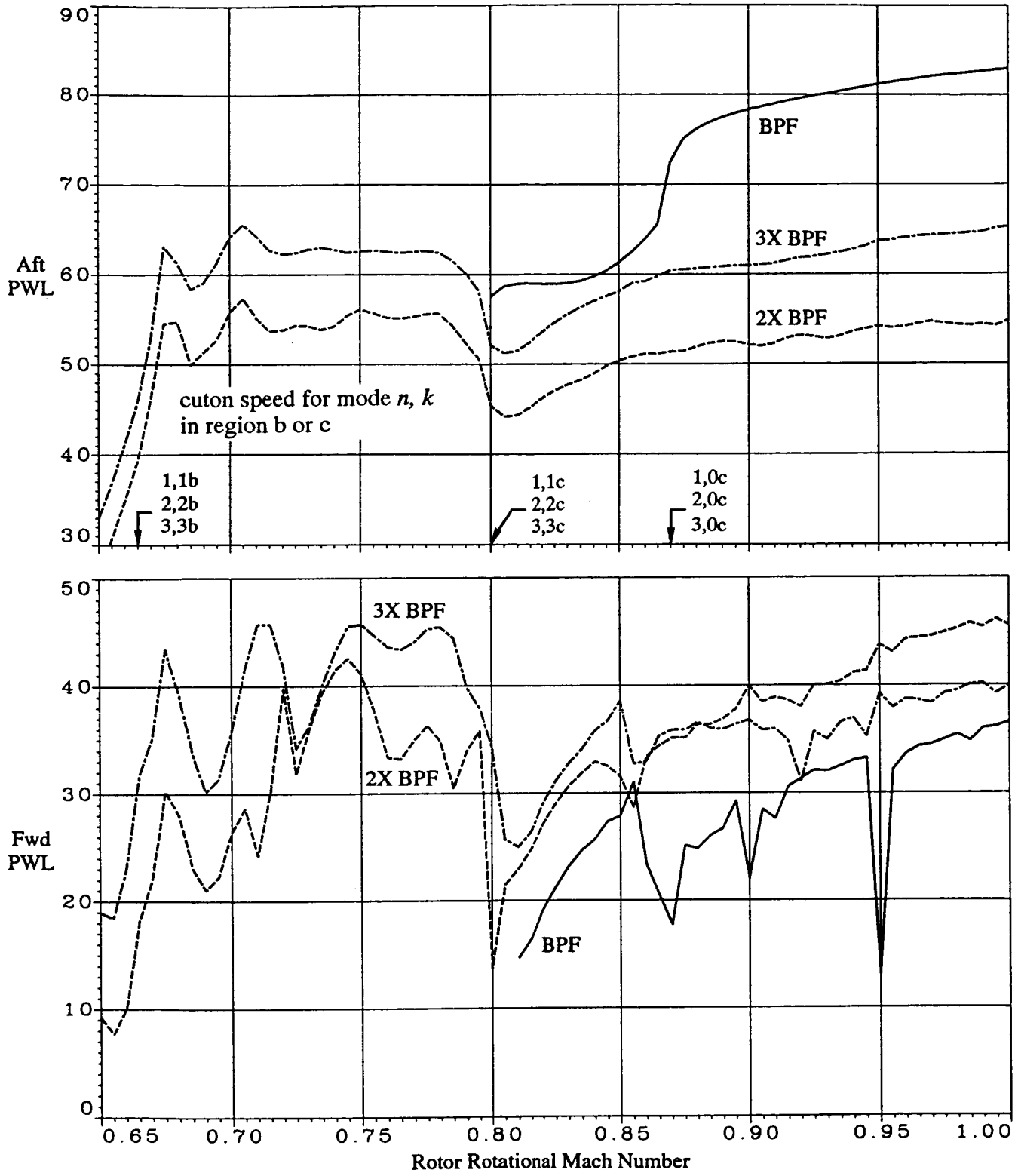

Figure 14. Comparison of harmonic power levels upstream and downstream. B_1=38, B_2=72, $BVGAP$=2.0, N_p=30, N_h=3. Arrows along abcissa indicate cuton speeds for relevant modes. Notation is n, k r where n, k indicates mode order and r is b or c denoting the region (inter-row, or downstream) as shown in figure 7.

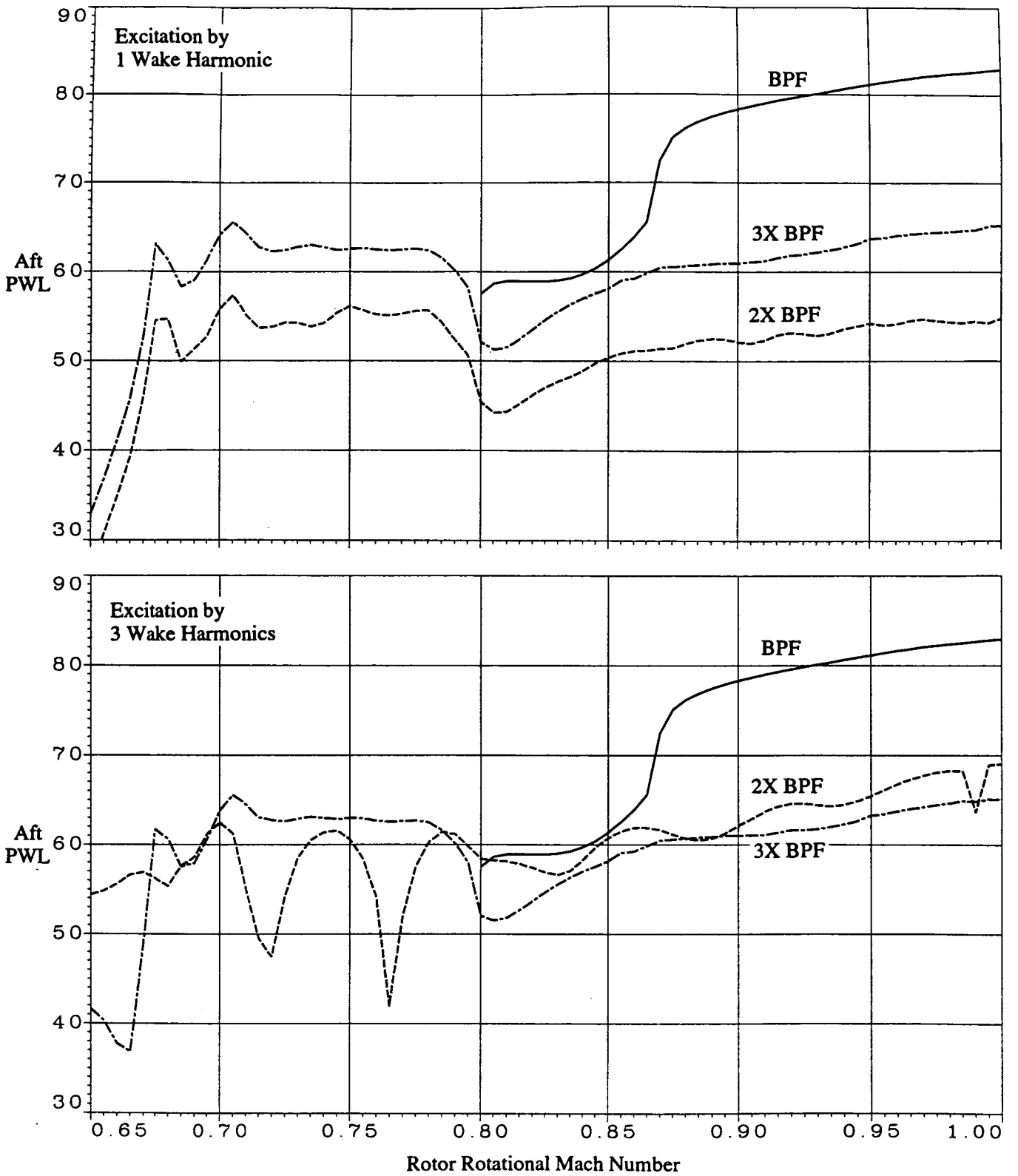

Figure 15. Predictions with and without wake upper harmonics set to 0. B_1=38, B_2=72, N_p=30, N_h=3, *BVGAP*=2.0

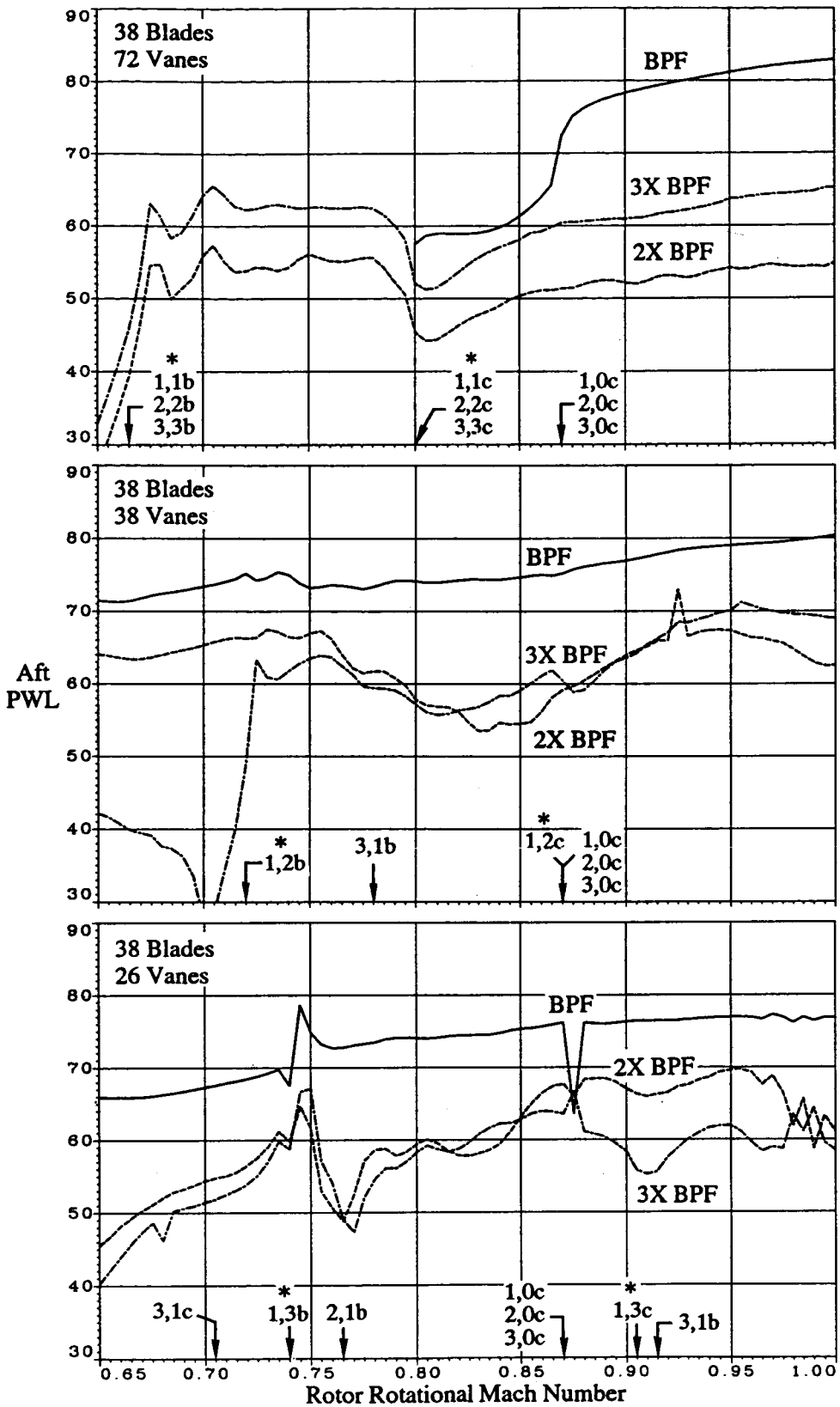

Figure 16. Effect of changing vane numbers at constant solidity. B_1=38, N_p=30, N_h=3, *BVGAP*=2.0. Notation on abcissas for mode cuton points same as in figure 14. The *'s indicate trapped modes.

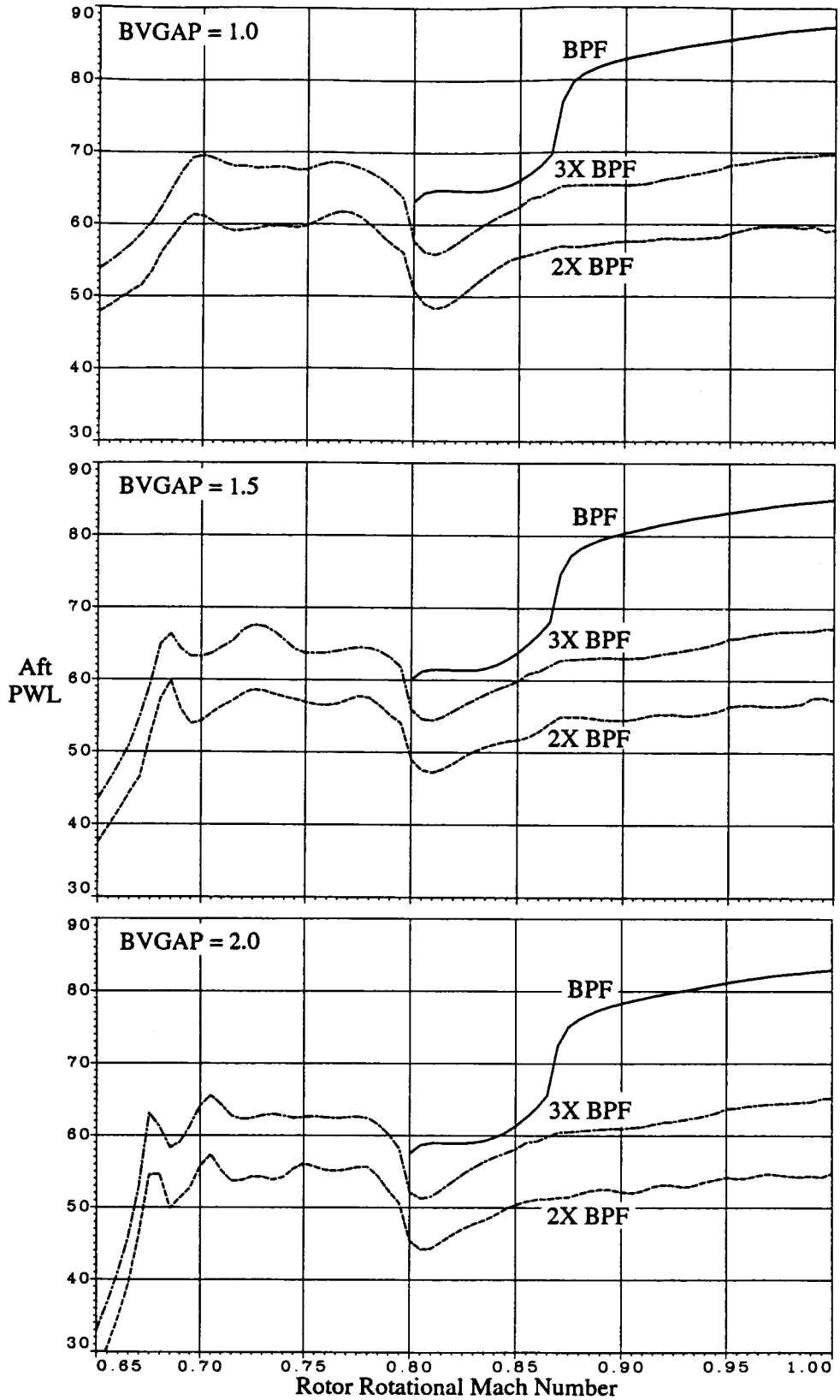

Figure 17. Effect of changing rotor/stator spacing. B_1=38, B_2=72,N_p=30, N_h=3. BVGAP=axial distance from rotor trailing edge to stator leading edge in rotor chords.

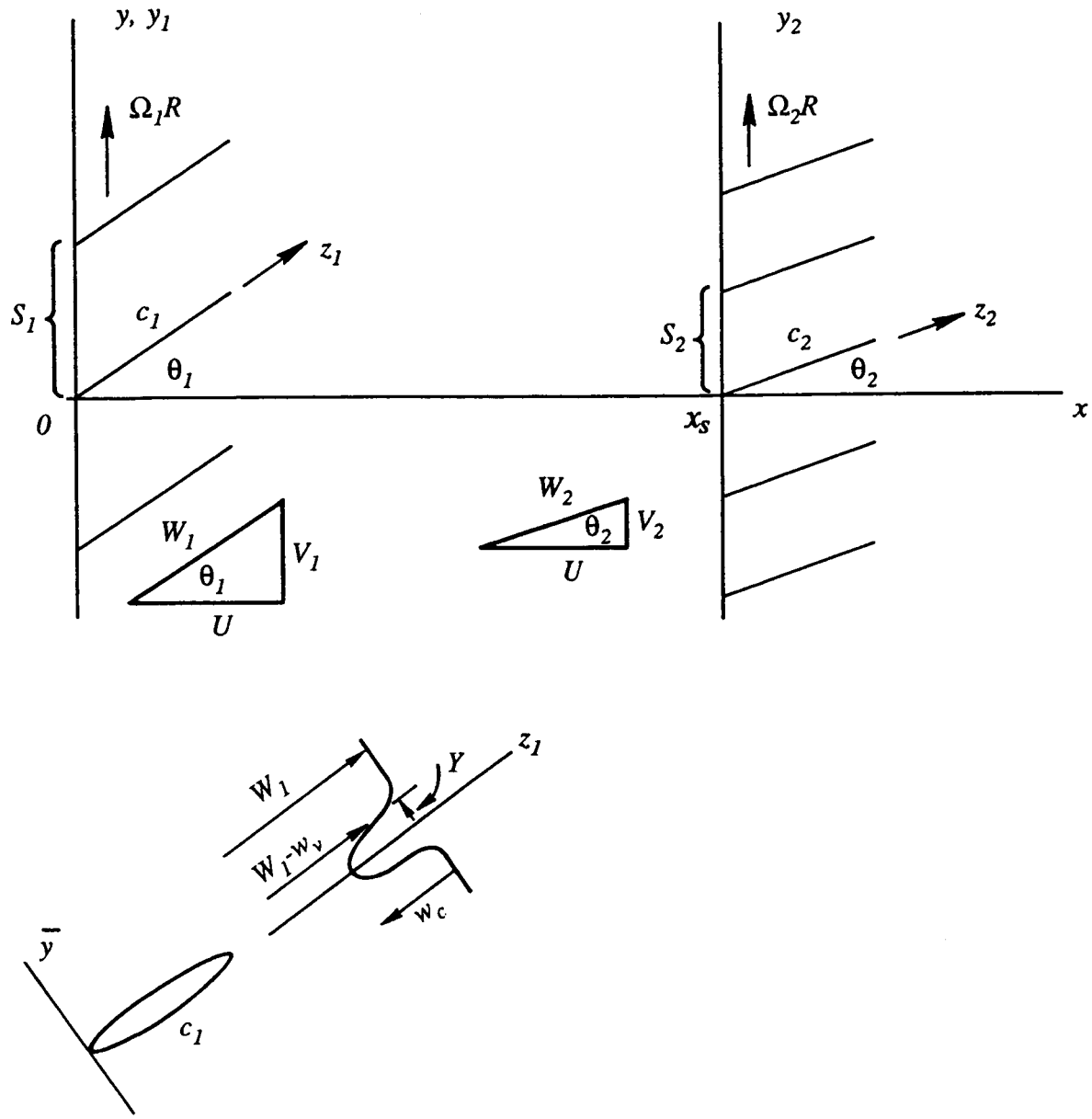

Figure 18. Sketches for derivation of wake harmonic formulas.

REPORT DOCUMENTATION PAGE

OMB No. 0704-0188

1. AGENCY USE ONLY (*Leave blank*)	2. REPORT DATE	3. REPORT TYPE AND DATES COVERED
	January 1994	Final Contractor Report

4. TITLE AND SUBTITLE

Coupled 2-Dimensional Cascade Theory for Noise and Unsteady Aerodynamics of Blade Row Interaction in Turbofans

Volume 1–Theory Development and Parametric Studies

5. FUNDING NUMBERS

WU–535–03–10
C–NAS3–25952

6. AUTHOR(S)

Donald B. Hanson

7. PERFORMING ORGANIZATION NAME(S) AND ADDRESS(ES)

United Technologies Corporation
Pratt and Whitney Division
400 Main Street
East Hartford, Connecticut 06096

8. PERFORMING ORGANIZATION REPORT NUMBER

E–7766

9. SPONSORING/MONITORING AGENCY NAME(S) AND ADDRESS(ES)

National Aeronautics and Space Administration
Lewis Research Center
Cleveland, Ohio 44135–3191

10. SPONSORING/MONITORING AGENCY REPORT NUMBER

NASA CR–4506

11. SUPPLEMENTARY NOTES

Project Manager, Dennis L. Huff, organization code 2770, (216) 433–3913.

12a. DISTRIBUTION/AVAILABILITY STATEMENT

Unclassified - Unlimited
Subject Category 07

12b. DISTRIBUTION CODE

13. ABSTRACT ***(Maximum 200 words)***

Typical analytical models for interaction between rotor and stator in a turbofan analyze the effect of wakes from the rotor impinging on the stator, producing unsteady loading, and thereby generating noise. Reflection/transmission characteristics of the rotor are sometimes added in a separate calculation. In those models, there is a one-to-one relationship between wake harmonics and noise harmonics; that is, the BPF (blade passing frequency) wake harmonic causes only the BPF noise harmonic, etc. This report presents a more complete model in which flow tangency boundary conditions are satisfied on 2 cascades in relative motion for several harmonics simultaneously. By an extension of S.N. Smith's code for 2D flat plate cascades, the noise generation/frequency scattering/blade row reflection problem is solved in a single matrix inversion. It is found that the BPF harmonic excitation of the stator scatters considerable energy in the higher BPF harmonics due to relative motion between the blade rows. Furthermore, when swirl between the rotor and stator is modeled, a "mode trapping" effect occurs which explains observations on fans operating at rotational speeds below BFP cuton: the BPF mode amplifies between blade rows by multiple reflections but cannot escape to the inlet and exit ducts. However, energy scattered into higher harmonics does propagate and dominates the spectrum at 2 and 3 times BPF. This report presents the complete derivation of the theory, comparison with a previous (more limited) coupled rotor/stator interaction theory due to Kaji and Okazaki, exploration of the mode trapping phenomenon, and parametric studies showing the effects of vane/blade ratio and rotor/stator interaction. For generality, the analysis applies to stages where the rotor is either upstream or downstream of the stator and to counter rotation stages. The theory has been coded in a FORTRAN program called CUP2D, documented in Volume 2 of this report. It is concluded that the new features of this analysis - unsteady coupling, frequency scattering, and flow turning between rotor and stator - have a profound effect on noise generation caused by rotor/stator interaction. Treating rotors and stators as isolated cascades is not adequate for noise analysis and prediction.

14. SUBJECT TERMS

Acoustics; Unsteady aerodynamics; Turbofan noise; Source noise modeling; Rotor/stator interaction

15. NUMBER OF PAGES

81

16. PRICE CODE

A05

17. SECURITY CLASSIFICATION OF REPORT	18. SECURITY CLASSIFICATION OF THIS PAGE	19. SECURITY CLASSIFICATION OF ABSTRACT	20. LIMITATION OF ABSTRACT
Unclassified	Unclassified	Unclassified	